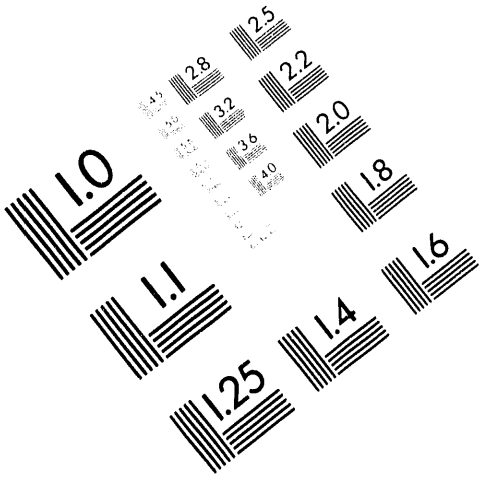

Association for Information and Image Management

1100 Wayne Avenue, Suite 1100
Silver Spring, Maryland 20910

301/587-8202

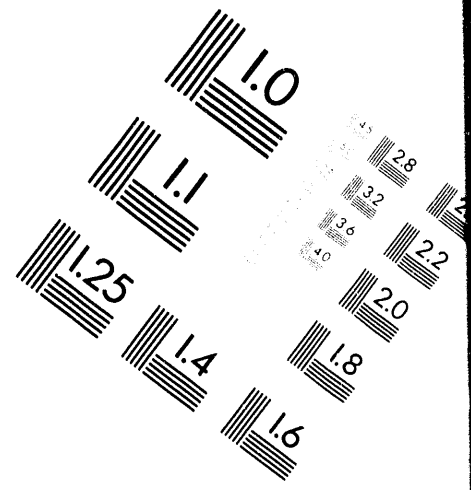

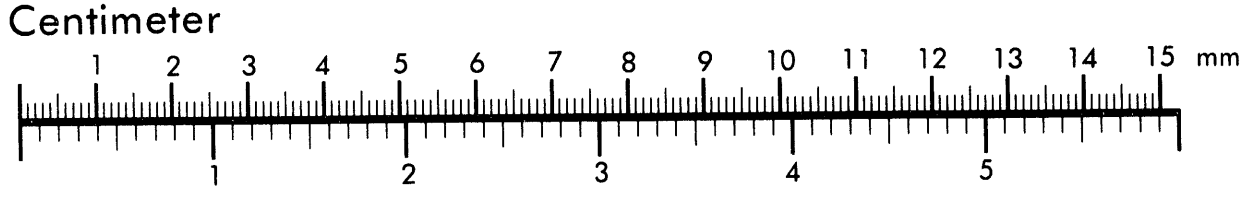

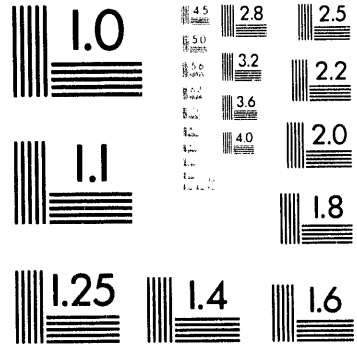

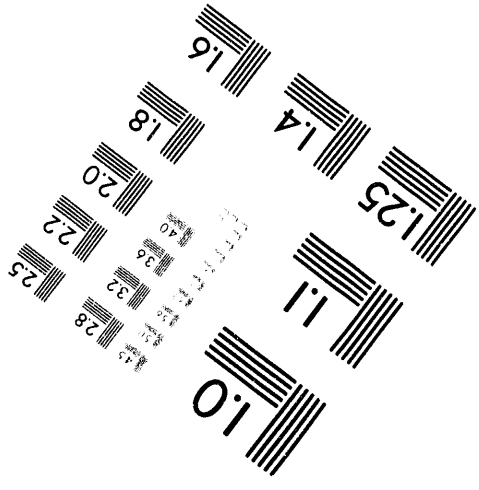

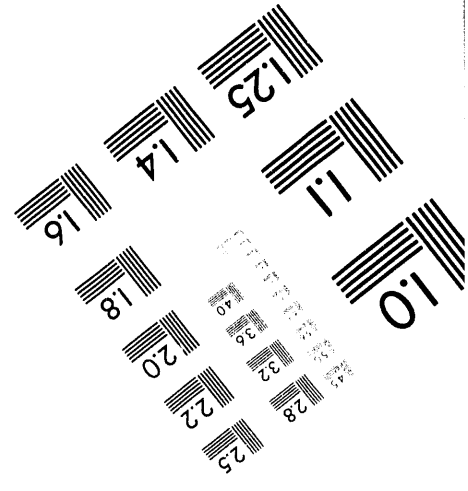

MANUFACTURED TO AIIM STANDARDS
BY APPLIED IMAGE, INC.

1 of 1

ANL/ESD-20

Study of Japanese Electrodynamic-Suspension Maglev Systems

Center for Transportation Research
Argonne National Laboratory

Operated by The University of Chicago,
under Contract W-31-109-Eng-38, for the
United States Department of Energy

Argonne National Laboratory

Argonne National Laboratory, with facilities in the states of Illinois and Idaho, is owned by the United States Government, and operated by the University of Chicago under the provisions of a contract with the Department of Energy.

This technical report is a product of Argonne's Energy Systems Division. For information on the division's scientific and engineering activities, contact:

Director, Energy Systems Division
Argonne National Laboratory
Argonne, Illinois 60439-4815
Telephone (708) 252-3724

Disclaimer

Reproduced directly from the best available copy.

Available to DOE and DOE contractors from the Office of Scientific and Technical Information, P.O. Box 62, Oak Ridge, TN 37831; prices available from (615) 576-8401.

Available to the public from the National Technical Information Service, U.S. Department of Commerce, 5285 Port Royal Road, Springfield, VA 22161.

Distribution
Category
UC-330

ANL/ESD-20

Study of Japanese Electrodynamic-Suspension Maglev Systems

by J.L. He, D.M. Rote, and H.T. Coffey

Center for Transportation Research, Energy Systems Division,
Argonne National Laboratory, 9700 South Cass Avenue, Argonne, Illinois 60439

April 1994

Work sponsored by United States Army Corps of Engineers and the Federal Railroad Administration through interagency agreements E8691R001 and DTFR 53-91-X-00018, respectively, with the United States Department of Energy and by Argonne National Laboratory

Contents

Contents (Cont.)

Figures

Figures (Cont.)

Figures (Cont.)

Tables

Acknowledgments

This report was sent to John Harding (Federal Railway Administration), Michael R. Coltman (Volpe National Transportation System Center), Rick Suever and John Potter (Army Corps of Engineers), Patrick L. Sutton (Department of Energy), John Hull (Argonne National Laboratory), Richard Thornton (Massachusetts Institute of Technology), S. Fujiwara (Railway Technical Research Institute, Japan), and E. Masada (University of Tokyo, Japan) for peer review. The authors wish to express their gratitude to the reviewers for their valuable comments.

The authors also wish to express their appreciation to the staffs of the RTRI and the Miyazaki Test Facility for serving as their hosts during several technical visits. Without their willingness to openly discuss their work, this report could not have been written. We also wish to express our thanks to E. Masada and his staff for many informative and worthwhile technical discussions.

The authors would also like to thank Robert Putnam (Argonne National Laboratory) for his technical editing.

Study of Japanese Electrodynamic-Suspension Maglev Systems

by

J.L. He, D.M. Rote, and H.T. Coffey

Abstract

This report presents the results of a study of the Japanese MLU magnetic-levitation (maglev) system. The development of the MLU system is reviewed, and the dynamic circuit model then is introduced and applied to the figure-eight-shaped null-flux coil suspension system. Three different types of figure-eight-shaped null-flux suspension systems are discussed in detail: (1) the figure-eight-shaped null-flux coil suspension system without cross-connection; (2) the combined suspension and guidance system; and (3) the combined propulsion, levitation, and guidance system. The electrodynamic-suspension maglev systems developed in Japan seem to be very promising and could result in a commercial application in the near future.

1 Introduction

Magnetic-levitation (maglev) technologies for high-speed transportation have received great attention in the United States (U.S.) for the past several years. U.S. maglev development efforts had stopped in 1975 but were restarted in 1990. Interest was restored in 1990 by the federal government, through sponsorship of the National Maglev Initiative. The final report of the National Maglev Initiative concludes that U.S. industry has the ability to develop an advanced U.S. maglev system. This would provide an opportunity to develop new technologies and industries and would, of course, result in direct benefits not only for the public, but also for U.S. businesses and the domestic work force.

Maglev systems can be classified into two major types, according to their suspension principle. One type, named for the electromagnetic-suspension (EMS) principle, utilizes the attractive magnetic force generated by the interaction between controlled electromagnets aboard the vehicle and the ferromagnetic rails on the guideway. The German Transrapid and Japanese HSST systems are of this type. The other type, named for the electrodynamic suspension (EDS) principle, employs the repulsive magnetic force generated by the interaction between magnets (mostly superconducting magnets) aboard the vehicle and the eddy currents induced in the nonferromagnetic conductors on the guideway. The Japanese MLU is an EDS-type maglev system.

Under the auspices of the System Concept Definition (SCD) Study sponsored by the National Maglev Initiative, four U.S maglev concepts (or SCD systems) were developed: the

Bechtel system, the Foster-Miller system, the Magneplane system, and the Grumman system. The first three of these are EDS-type systems. The Bechtel suspension concept, called flux-cancelling suspension, employs octupole superconducting magnets aboard the vehicle that interact with a ladder-shaped conductor (arranged on the box-shaped concrete guideway) to produce electrodynamic suspension. The Foster-Miller concept uses a U-shaped guideway and figure-eight-shaped null-flux coils mounted on the side-walls for levitation. This concept is similar to the Japanese MLU002 system. In addition, the Foster-Miller system uses a locally-commutated propulsion motor in combination with null-flux guidance to propel and guide the vehicle. The Magneplane system uses two curved sheet conductors (close to a semicircle) for suspension and guidance. The additional guidance forces are obtained from the edge effect between the propulsion magnets aboard the vehicle and the curved sheet conductor on the guideway. The Grumman maglev concept is the only one of the EMS type. It utilizes a Y-shaped guideway and combines conventional copper-wound magnets with a superconducting coil to achieve a large levitation gap. Each of these four systems appears to have unique features and potential advantages.

The Japanese have devoted a great amount of effort to developing an EDS maglev system that uses superconducting magnets aboard the vehicle to perform the three functions of propulsion, levitation, and guidance. Development of the EDS maglev system was begun in the 1960s by Japanese National Railways (JNR). At present, the Railway Technical Research Institute (RTRI) in Japan is responsible for the maglev program. The RTRI has nearly 100 people employed in the several laboratories associated with the maglev research and development program. These laboratories include the Maglev Development Laboratory, the Cryogenic Technology Laboratory, and the Power Supply Laboratory. In addition, the Miyazaki Test Center, which employs more than 20 staff members and has a 7-km-long test track, has been the principal facility for EDS maglev testing since about 1978. Recently, development started on a new 42-km-long test track, called the Yamanashi Test Line, in the Yamanashi Prefecture, west of Tokoyo.

Regardless which system is finally selected for further development in the United States, the experience acquired over the last two decades by foreign experts is invaluable. In particular, many similarities exist between the Japanese MLU and U.S. maglev concepts. It is important, therefore, to fully study and understand the MLU system and to apply the experience obtained by foreign experts to U.S. maglev concepts. It is also hoped that the material provided in this report may be beneficial for the further development of the MLU system in Japan.

2 Overview of the Electrodynamic Suspension Maglev Program in Japan

The Japanese National Railways tested an air-cored linear synchronous propulsion system, called LSM200, at the RTRI in 1972 . The first superconductive, magnetically-levitated vehicle, ML-100A, was tested in 1974 after the favorable results had been achieved with LSM200. The ML-100A used an inverted-T-shaped linear guideway, an air-cored linear-synchronous motor (LSM), and L-shaped cryostats that contained both the lift and propulsion magnets. A large-scale test facility was opened at Miyazaki on Kyushu Island in April 1977, and tests began on a 1.3-km section with the ML-500 test vehicle, which was supported by wheels. The testing of the magnetically suspended ML-500 test vehicle commenced on a 3.1-km section in December 1977. The full 7-km length of the test guideway was completed in August 1979, and in December 1979, the ML-500 reached a speed of 517 km/h on the completed guideway.

Testing began on the MLU001 and the MLU002 in 1980 and 1987, respectively. The MLU001 reached a speed of 400.8 km/h for a two-car train in February 1987, and the MLU002 (a single-unit car) was tested at 394.3 km/h in November 1989. The MLU002 test vehicle burned on October 3, 1991, in an accident at the Miyazaki Test Center. A new test vehicle, called MLU002N, was developed during 1992. Testing of the MLU002N test vehicle commenced in January 1993.[1-15]

2.1 ML-500 Test Vehicle

The EDS-type ML-500 test vehicle was the first vehicle to be tested at the Miyazaki test facility (Figure 2.1). Built in 1977, the ML-500 was a nonpassenger-carrying vehicle with the following dimensions: length, 13.5 m; width, 3.72 m; and height, 2.85 m, with a weight of 10 metric tons. The inverted-T-shaped guideway was utilized in the test. Aboard the vehicle were four L-shaped cryostats, each of which contained four superconducting magnets (two for propulsion and guidance and two for levitation). The helium refrigerator and compressor were installed on the ground, and liquid helium was supplied to the cryostats before each test run.

During the three-year test period, the maximum speed of the ML-500 increased gradually as the length of the guideway increased. The ML-500 attained 132 km/h on the 1.3-km-long guideway in 1977, 301 km/h on the 3.1-km-long guideway in 1978, and 517 km/h on the 7-km-long guideway in 1979. Three objectives were met by the ML-500 vehicle tests: (1) high-speed operation, up to 517 km/h in 1979; (2) measurement of vehicle dynamic response to guideway irregularities; and (3) operation with a simulated tunnel. From these experiments, the principles of operation and the design of the LSM propulsion system, electrodynamic suspension, superconducting magnet technology, and the power-supply system were verified.

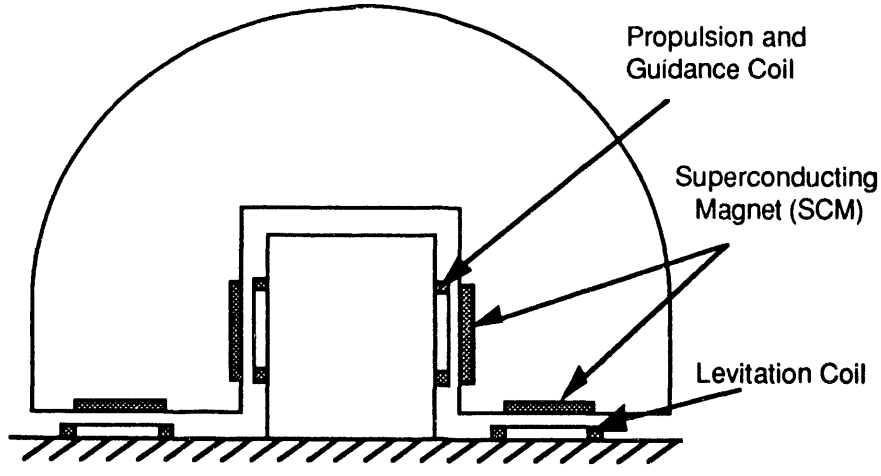

FIGURE 2.1 ML-500 Test Vehicle with Inverted-T-Shaped Guideway Configuration (cross section)

2.2 MLU001 Test Vehicle

The MLU001 test vehicle, a three-car train set with a total weight of about 30 metric tons and a total length of 28.8 m, was designed as a model of a practical passenger-carrying maglev train. The system used a U-shaped guideway configuration, in which the levitation forces were generated by the interaction between the levitation loop coils arranged horizontally on the guideway and the vertically oriented SCMs aboard the vehicle. The propulsion and guidance forces were generated by the interaction of these same SCMs with coils mounted vertically on both side walls of the guideway. The coils were excited by a three-phase external power source and were cross-connected to form a combined null-flux guidance and propulsion system (Figure 2.2).

The MLU001 began operation in December 1980. The test objective for this vehicle was to investigate the running characteristics of vehicles in coupled operation. The cars had about the same cross section as that of a commercial vehicle. The three cars together had a total of 32 seats. Superconducting magnets, each with a magnetomotive force of 700 kA, were distributed along the lengths of the cars under each side of each car body. Each car had eight coils in two rows, with four magnetic poles in each row. The I-shaped superconducting coils, installed vertically in the cars, performed three functions: propulsion, levitation, and guidance.

Various types of cryogenic systems were tested with this vehicle. The reliability of the on-board cryogenic system was verified; however, reliable on-board reliquefaction of vaporized helium was not achieved. Detailed technical parameters of the MLU001 vehicle are given in Table 2.1.

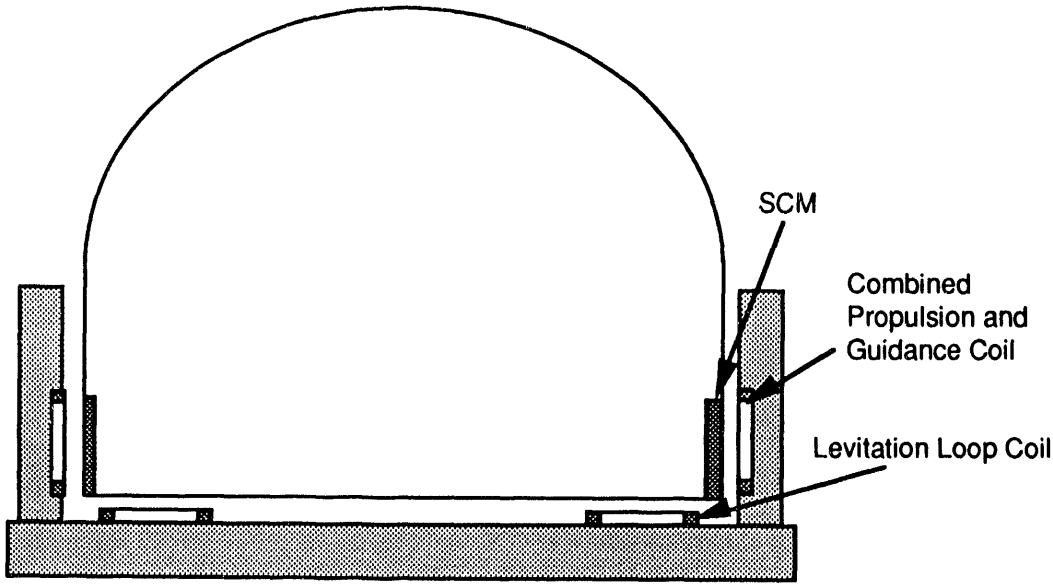

FIGURE 2.2 MLU001 Test Vehicle with a U-Shaped Guideway Configuration, Levitation Coils on the Ground, and Combined Propulsion and Guidance Coils on the Side Wall (cross section)

2.3 MLU002 Test Vehicle

The MLU002 test vehicle, constructed in 1987, was an application prototype vehicle with a weight of 17 metric tons and a length of 22 m. Table 2.2 lists the detailed parameters. The major difference between the MLU002 and the MLU001 was that the superconducting coils on the MLU002 were concentrated on separately-suspended bogies (support trucks similar to those used on conventional rolling stock), instead of being continuously distributed along the car bodies. In addition, the number of superconducting magnets was reduced, reflecting the greatly increased field strength of the magnets. This resulted in reduced vehicle weight and increased payload efficiency. The maximum speed of the MLU002 was designed to be 500 km/h; however, its actual speed was limited to 420 km/h because of the length of the test track. Both the MLU001 and the MLU002 used the U-shaped guideway configuration shown in Figure 2.2.

The MLU001 and MLU002 vehicles used the same guideway structure as the ML-500. At the present time, a section of the Miyazaki Test Track about 2-km long has been converted into a side-wall levitation system.[14] The center structure, which supported the LSM windings of the ML-500 system (the inverted-T-shaped guideway superstructure), was replaced by outside walls to support the LSM windings of the MLU001 and MLU002 vehicles (U-shaped guideway superstructure).

In 1989, the task of replacing the horizontal loop coils with vertically mounted, figure-eight-shaped null-flux lift coils was initiated. In addition, the later coils were cross-connected to form a combined figure-eight-shaped null-flux coil levitation and guidance system. As the

TABLE 2.1 Technical Parameters of MLU001 Test Vehicle

Parameter	Specification
Vehicle information	
Length (m)	
End car	10.1
Middle car	8.2
Width (m)	3.0
Height (m)	3.3
Weight per car (metric ton)	10
Total number of seats	32
Maximum speed (km/h)	
Three-vehicle-train	362.1
Two-vehicle-train	405
Single vehicle	400
Electrodynamic suspension	
Levitational force (kN)	98
Levitational height (cm)	24 (between coils)
Effective gap (cm)	10
No. of magnets per car	8 (two rows)
Magnetomotive force per magnet (kA)	700
Null-flux guidance	
Guidance force (kN)	49 (5-cm lateral displacement)
Distance between coils (cm)	32.5
Effective gap (cm)	19
LSM propulsion	
Propulsive force (kN)	51
Voltage/phase (kV)	3
Current/phase (kA)	1.1
No. of phases	3
Frequency (Hz)	0-27
Combined brake system	
Electrical brake (kN)	76 (per vehicle)
Mechanical brake (kN)	8
Power System	
Cycloconverter (MVA)	16
Motor (MW)	10
Generator (MW)	25
Motor-generator (MG) system weight (metric ton)	40
Magnetic field (T)	
On the floor	0.002
On the seat	0.001
At the center of the back	0.005
At the head rest	0.003

TABLE 2.2 Technical Parameters of MLU002 Test Vehicle

Parameter	Specification
Vehicle information	
Length (m)	22
Width (m)	3
Height (m)	3.7
Weight (metric ton)	17
Vehicle body	Al alloy
Seating capacity	44
Maximum speed (km/h)	
Designed	500
Actual test	420
Electrodynamic suspension	
Levitational force (kN)	196
Effective gap (cm)	11
No. of magnets/bogie	6
Magnetomotive force (kA)	700
Pole pitch (m)	2.1
Null-flux guidance	
Guidance force (kN)	83.3 (5-cm lateral displacement)
Distance between coils (kN)	29.5
Effective gap (cm)	20
LSM propulsion	
Thrust (kN)	79.4
Voltage/phase (kV)	5.8
Current/phase (kV)	0.9
No. of phases	3
Frequency (Hz)	0-28
Power system	
Cycloconverter (MVA)	16
Motor (MW)	10
Generator (MVA)	25
MG system weight (metric ton)	140

new coil system was installed, the cross connections between the LSM windings that were used to produce null-flux guidance were eliminated, and the single layer of propulsion coils was replaced by a double layer of propulsion coils. A cross-sectional view of the MLU 002 test vehicle side-wall null-flux levitation system is shown in Figure 2.3.

2.4 MLU002N Test Vehicle

The MLU002N test vehicle, developed during 1992 after the MLU002 burned, has been used in test runs since January 1993 (Figure 2.4). The MLU002N has the same basic configuration as the MLU002. However, it incorporated innovative features, including countermeasures against fire. The new test vehicle has the following features:[15] (1) aluminum alloy cabin; (2) hydraulically actuated aerodynamic brake panels; (3) 10 passenger seats, but no front window; (4) a two-stage secondary suspension system, used to connect the superconducting magnet support frame to a truck frame that is in turn connected to the car body;[16] (5) nonflammable aluminum alloy landing wheels, hydraulic oil, and heat-resistant piping; (6) pressure sensors for inner pressure of tires and guidance wheels; (7) front window replaced by forward-looking video cameras, one on the top and another near the bottom of the vehicle; and (8) newly designed superconducting magnet/cryostat systems with improved performance. The vehicle weighs 20 metric tons and is 22 m long, 3 m wide, and 3.7 m tall. Sixteen guidance wheels are used on the sides of the vehicle, half of which are steel wheels for emergency use. Twelve superconducting magnets (six on each side) are mounted at the vehicle ends, with three magnets in each group. Eight wheels are used to support the vehicle when landing or non levitated.

Recently, a combined propulsion, levitation, and guidance system was introduced in Japan. The new concept uses only one set of guideway coils to perform all three functions, as shown in Figure 2.5. The guideway coils, which are mounted on the two side walls, are cross-connected to provide null-flux suspension and guidance, and the coils on the same side are connected in a three-phase configuration and powered with a three-phase power source. In this system, the propulsive coils, as shown in Figure 2.3, were removed. (A detailed analysis of this new concept is provided in Chapter 6.)

2.5 Commercial-Type Vehicle

On the basis of the experience obtained from previous tests on the MLU001 and MLU002 vehicles, the Japanese engineers have designed a new commercial-type maglev vehicle. In this design, the superconducting magnets will be arranged on the bogies at the ends of each car, as shown in Figure 2.6. Because the passenger compartments will be located at a distance from the superconducting magnets, the magnetic flux density in these compartments will be considerably reduced. Table 2.3 gives the design specifications of the new commercial maglev vehicle.

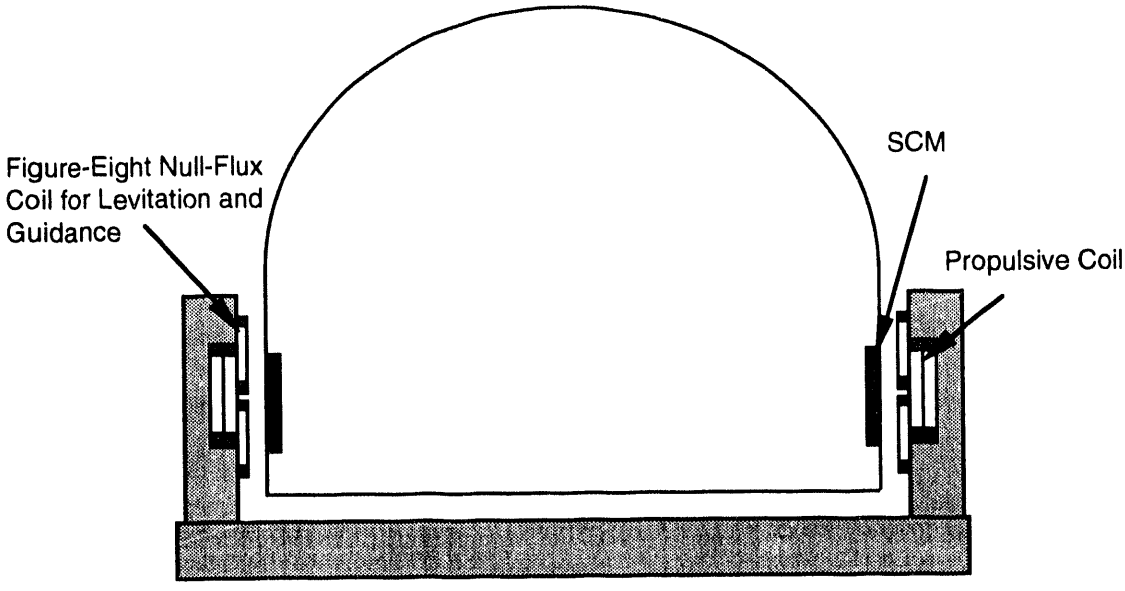

FIGURE 2.3 MLU002 Test Vehicle: Side-Wall Null-Flux Levitation System (cross section)

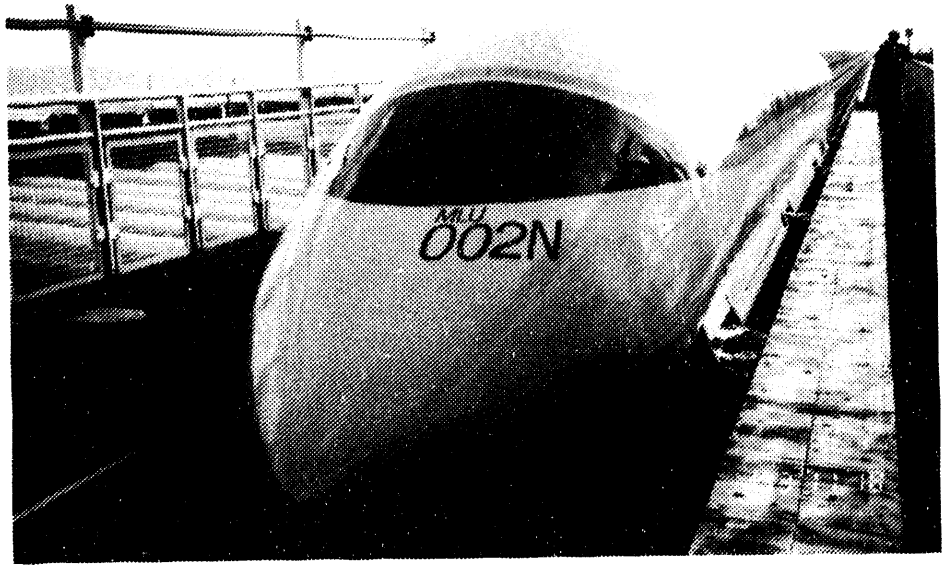

FIGURE 2.4 MLU002N Test Vehicle (photo taken by J.L. He)

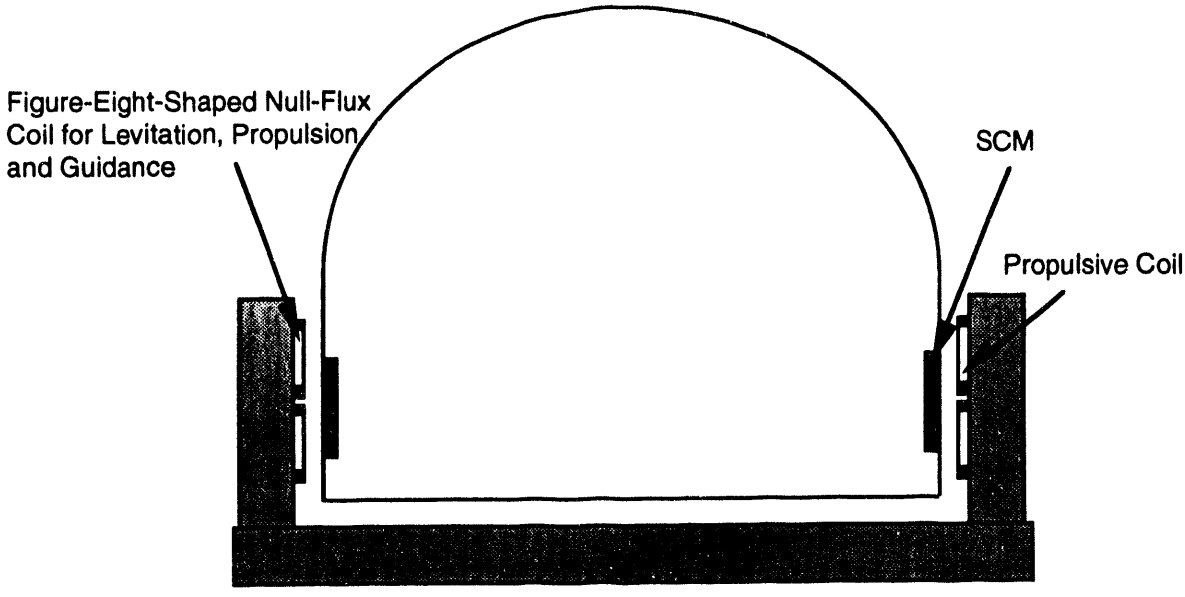

FIGURE 2.5 Combined Side-Wall Levitation, Propulsion, and Guidance Maglev Concept (cross section)

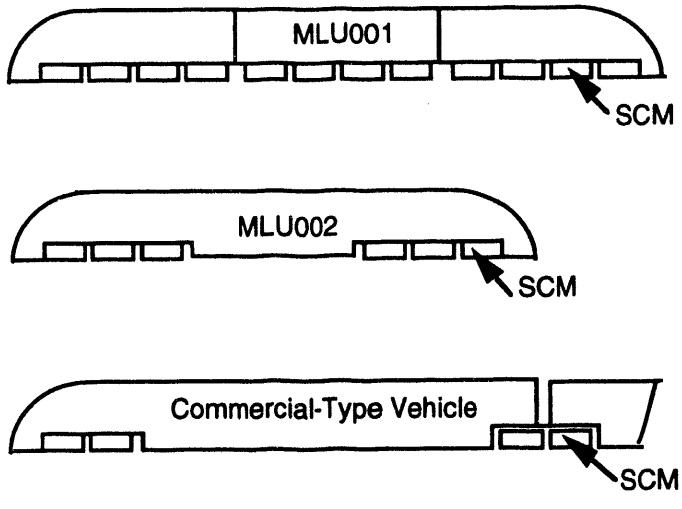

FIGURE 2.6 Arrangement of Superconducting Magnets for Various Test Cars (side view of test vehicle; vehicle not to scale)

TABLE 2.3 Design Specifications of Commercial Maglev System

Parameter	Specification
Vehicle information	
Length (m)	
End car	28
Middle car	21.6
Width (m)	2.8
Height (m)	2.65
Weight (metric tons)	
End car	27
Middle	18
Number of seats	
End car	67
Middle car	68
Train information	
Number of vehicles	14
Length (m)	315
Weight (metric ton)	270
Number of seats	950
Maximum speed (km/h)	500
Superconducting coil	
Dimensions (m)	2.2 × 0.5
Pole pitch (m)	2.7
Magnetomotive force (kA)	700
Ground coil	
Dimensions (m)	
Length	0.6
Width	0.3
Coil pitch	0.9
Propulsive coil	
Pole pitch (m)	1.8
Voltage (kV)	19
Levitation height (mm)	100
Midway between the tracks (m)	5.4
Curve radius	> 6000 m at 500 km/h
Gradient	6% with maximum of 10% (continuous operation, fixed speed)

2.6 Aerodynamic Braking

In normal and emergency service, the MLU002 vehicle used a regenerative braking system incorporated into the power-supply system of the linear synchronous motor. If the power supply system failed, three alternative braking systems were possible: dynamic braking, friction braking, and aerodynamic drag. A dynamic brake that fed electrical energy into a resistor bank was the first backup braking system. This system was operational over the entire vehicle speed range. In the lower speed range, below about 350 km/h, a mechanical friction brake could be used if the dynamic system failed. Above 350 km/h, however, mechanical friction brakes were not effective in the event of dynamic brake failure. Aerodynamic drag force, the dominant drag force at high speed, could be effectively used to provide safe, strong, reliable braking action at high speeds if both the regenerative and dynamic brakes failed.

Both scale-model tests in a wind tunnel and full-scale tests of aerodynamic braking systems have been conducted in Japan. The system tested on the MLU001 vehicle at the Miyazaki Test Track consisted of hydraulically-actuated panels that opened on the top and sides of each car in the train set. Tests conducted at speeds up to 350 km/h with the three-car MLU001 train set, in both the wheel-supported and levitated modes, yielded satisfactory results. No instabilities were observed, and the transition from the closed- to open-panel configurations did not result in abrupt jerking motions. The change in drag force was measured to occur over an interval of about one second. The accompanying small change in deceleration resulted in a smooth change in velocity. Tests included normal panel deployments in various combinations on the three cars and panel deployment failures in which only one of three panels opened (e.g., the right side opened while the top and left side panels remained closed). Time delays between opening panels on the first and last cars were also tested and found to have no adverse effects on the results.

Comparisons of field tests and wind-tunnel tests revealed that the braking forces were somewhat smaller than predicted from the wind-tunnel tests. Also, some interference that reduced the effectiveness of the rear aerodynamic brake panels was observed in the field tests, in contrast to the wind-tunnel tests, which indicated no interference. To date, no information has been released on tests of the aerodynamic braking system incorporated into the MLU002N vehicle.

2.7 Miyazaki Test Track

2.7.1 General Information

For the development of the EDS maglev system, JNR constructed a test track at Miyazaki. The first section, 1.3 km in length, was completed in 1977; the track was extended to a total length of 7 km in 1979. Track features include a downhill section with a gradient of 0.5% at about 1 km from the test center and a curve with a radius of 10 km. Operational tests began in July 1977 with the ML-500 vehicle on the inverted-T-shaped guideway. In 1980, the guideway was converted into a U-shaped configuration, with horizontally oriented ground-based coils for levitation and

vertically oriented side-wall coils for propulsion and guidance. The guideway contains about 20,000 suspension coils and 10,000 propulsion coils. The track was recently modified to include figure-eight-shaped null-flux coils mounted on the side wall for levitation and guidance. (To date, about one kilometer has been converted to this system.) The MLU001, MLU002, and MLU002N test vehicles were tested on the same U-shaped guideway, except that their suspension coils were arranged differently. In addition, a mechanical directional switch was installed in the test track in 1990.

Currently, the guideway has four coil arrangements as follows:

1. Horizontal ground coils for levitation with side-wall coils for propulsion and guidance. The first version of the U-shaped guideway was tested primarily during the 1980s. Only a short section of this version, near the control center, remains (Figure 2.7).

2. Figure-eight-shaped coils for levitation and guidance in combination with single-layer propulsion coils, which make up most of the guideway (Figure 2.8).

3. Figure-eight-shaped null-flux coil for levitation and guidance in combination with double-layer propulsive coils (Figure 2.9). The double-layer propulsion coils reduce harmonics and provides better propulsion performance.

FIGURE 2.7 Miyazaki Test Track: U-Shaped Guideway (Photo by J.L. He)

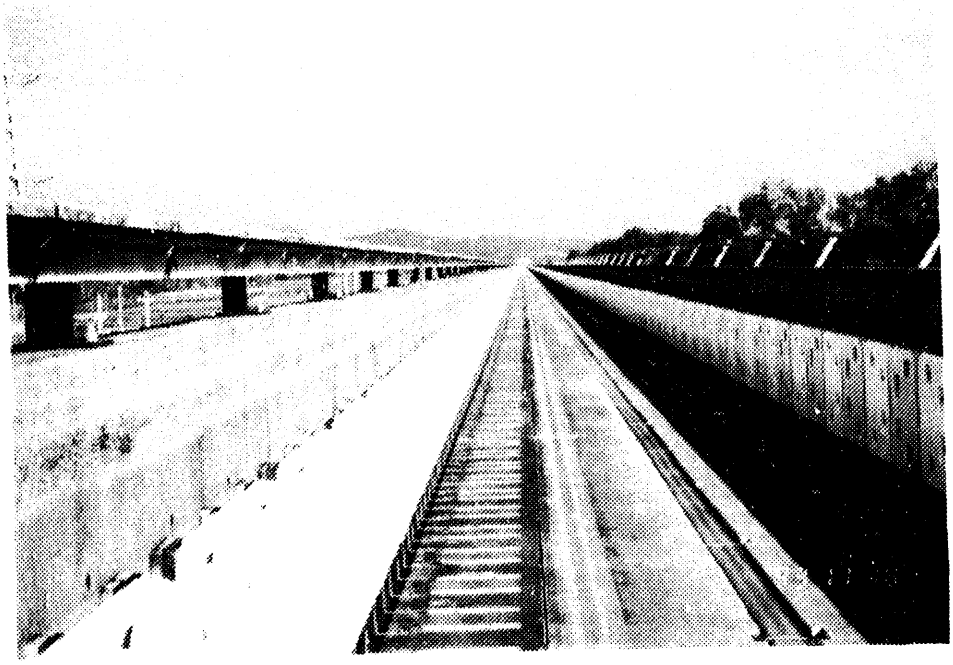

FIGURE 2.8 Miyazaki Test Track: Figure-Eight-Shaped Coils (for Levitation and Guidance) with Single-Layer Propulsion Coils (Photo by J.L. He)

FIGURE 2.9 Miyazaki Test Track: Figure-Eight-Shaped Coils (for Levitation and Guidance) with Double-Layer Propulsion Coils (Photo by J.L. He)

4. Figure-eight-shaped coils for combined functions of propulsion, levitation, and guidance (covered in Chapter 6). Coil arrangement 4 (approximately 100-m long section) is a new configuration recently developed in Japan. Running tests with the new type of guideway are expected to begin in 1994, after the high-speed test with the MLU002N vehicle is completed.

2.7.2 Propulsion and Power Supply

Prior to the conversion from the horizontal loop-coil suspension to a vertical side-to-side null-flux suspension, the propulsion system at the Miyazaki Test Track employed a long-stator LSM consisting of superconductive field coils aboard the vehicle and an array of stator windings on the track.[13] The interaction between the superconductive coils and the cross-connected armature coils on the guideway yields a null-flux guidance system. The power-supply system, a high-capacity cycloconverter, feeds only the active motor section of the vehicle. With this system an energized block length of about 42 m is achieved. (Chapter 6 discusses blocks.) A contact-free power collection system utilizing the reaction flux of the ground-based levitation coils supplies on-board power.

Prior to 1986, the Miyazaki power system included a motor-generator (MG) set, which converted the 60-Hz line power to 120 Hz, and a pair of cycloconverters, which produced variable-voltage, variable-frequency (0-34 Hz) output power for the LSM stator windings. In 1986, the power system was changed and the MG set was eliminated, and new, circulating-current-type cycloconverters were installed that were capable of converting the 60-Hz power into variable-voltage, variable-frequency output power at up to two-thirds of the line frequency.

The track propulsion-control system uses a central controller to transmit propulsion commands to the substation in accordance with vehicle information obtained through a leaky coaxial cable. In response to the propulsion commands, cycloconverters feed an alternating current to the propulsion coils in synchronization with the vehicle field phase, which is detected by cross-inductive wires strung along the guideway. Section changeover control for a pair of cycloconverters alternatively feeds a current to the propulsion coils along which the vehicle is passing. In emergencies, resistors for dynamic braking are applied, in addition to the normal regenerative braking.

The control system can be categorized in terms of current control, synchronization control, and speed control through thrust calculation.

2.8 New Test Track in Yamanashi

A new test-track site has been chosen in Yamanashi Prefecture, about 100 km west of Tokyo, and is now under construction. The new track will run about 42 km, part of which will be

double-tracked. It will include some gradient sections and a number of tunnel sections. The track is planned to permit 500-km/h running on the gradient sections and up to 550-km/h running on the flat straight sections. Two test vehicles will be able to pass each other on the double-tracked section. It is expected that the test results obtained from the new track will be immediately reflected in the commercial system design.

2.9 References

1. Nakao, H. et al., 1989, "New Type Superconducting Magnet for EDS System," Proceeding of the 11th International Conference on Magnetically Levitated Systems and Drives, Yokohama, Japan, July 7-11, published by Institute of Electrical Engineers of Japan, Tokyo, Japan, pp. 229-234.

2. Seki, A. and T. Simomae, 1989, "Electric Equipments of the Chuo Linear Express," Proceeding of the 11th International Conference on Magnetically Levitated Systems and Drives, Yokohama, Japan, July 7-11, published by Institute Electrical Engineers of Japan, Tokyo, Japan, pp. 135-139.

3. Seki, A., S. Kato, and T. Kawakami, 1989, "Concept of the Operational Safety System for the Chuo Linear Express," Proceeding of the 11th International Conference on Magnetically Levitated Systems and Drives, Yokohama, Japan, July 7-11, published by Institute of Electrical Engineering of Japan, Tokyo, Japan, pp. 287-290.

4. Fujie, J., 1989, "Current Status of EDS System in Japan," Proceeding of the 11th International Conference on Magnetically Levitated Systems and Drives, Yokohama, Japan, July 7-11, published by Institute of Electrical Engineering of Japan, Tokyo, Japan, pp. 81-83.

5. *Japanese Railway Information,* 1988, "Railway Systems and Components," No. 35, Jan., pp. 1-7.

6. Hara, Y., K. Terada, and K. Miyairi, 1988, "Structure of the MLU002 Maglev Vehicle," *Hitachi Review,* Vol. 37, No. 6, pp. 357-363.

7. Kyotani, Y., 1988, "Recent Progress by JNR on Maglev," Institute of Electrical and Electronics Engineers, New York, NY, *IEEE Transactions on Magnetics,* Vol. 24, No. 2, March, pp. 804-807.

8. Kyotani, Y. and H. Tanaka, 1986, "Present Status of JNR Maglev Development," Proceeding International Conference on Maglev and Linear Drives, May 14-16, Vancouver, B.C., Canada, published by Institute of Electrical and Electronics Engineers, New York, NY, 86CH2276-4, pp. 41-45.

9. Masada, E., 1985, "The Development of Maglev Transport and Related Systems in Japan," Proceedings of the International Conference on Maglev Transport '85, Sept. 17-19, Keidanren Kaikan, Tokyo, Japan, published by Institute of Electrical Engineers of Japan, Tokyo, Japan, pp. 21-28.

10. Jizo, Y., and Y. Furuta, 1985, "Superconducting Magnet for Maglev Train," Proceeding International Conference on Maglev Transport '85, Sept. 17-19, Keidanren Kaikan, Tokyo, Japan, published by Institute of Electrical Engineers of Japan, Tokyo, Japan, pp. 185-192.

11. Ohguma, H. et al., 1985, "On-board Refrigeration System of Magnetically Levitated High Speed Trains MLU001," Proceedings International Conference Maglev Transport '85, Sept. 17-19, Keidanren Kaikan, Tokyo, Japan, published by Institute of Electrical Engineers of Japan, Tokyo, Japan, pp. 193-198.

12. Tanaka, H., 1985, "Present Conditions of Maglev Test in JNR," *Japanese Railway Engineering*, No. 96, Dec., pp. 8-11.

13. Nakamura, K. et al., 1985, "LSM Propulsion of the Miyazaki Maglev Test Track," Proceedings of International Conference on Maglev Transport '85, Sept. 17-19, Keidanren Kaikan, Tokyo, Japan, Published by Institute of Electrical Engineers of Japan, Tokyo, Japan, pp. 91-98.

14. Fujiwara, S., and K. Sawada, 1993, "New Structure Electro-Magnetic Guideway for Maglev," Proceedings of the 13th International Conference on Magnetically Levitated Systems and Linear Drives, May 19-21, published by Argonne National Laboratory, Argonne, Ill., pp. 63-69.

15. Masada, E., 1993, "Development of Maglev Transportation in Japan: Present State and Future Prospects," Proceedings of the 13th International Conference on Magnetically Levitated Systems and Linear Drives, published by Argonne National Laboratory, Argonne, Ill., May, pp. 1-6.

16. Japan Railway, 1993, "The Linear Technology Guide."

3 Application of Dynamic Circuit Theory to the EDS Maglev System

3.1 Introduction

A maglev system uses magnetic forces to perform the functions of vehicle propulsion, levitation, guidance, and motion control (response to disturbances). The computation of these magnetic forces may differ somewhat from those in conventional electrical machines for three reasons. (1) Knowledge of three-dimensional time- and space-dependent magnetic forces is required to treat the basic six degrees of freedom of a maglev vehicle. The radial component of the force between the stator and rotor in a conventional machine is ignored. In a maglev system, that force component provides vehicle lift and may also serve as an important element in the control of the vehicle's motion. (2) Space harmonics, which result from the end-effects and the discontinuous distribution of the magnets aboard the vehicle, play a much more important role in the performance of a maglev vehicle than they do in conventional machines. Thus, the performance analysis based on a fundamental traveling wave, which is used in most conventional machines, is inadequate. (3) Time dependence of the magnetic forces (i.e., the transient as well as time-averaged characteristics of the forces) is important, because transient effects influence the noise and vibration of components, heat loads on superconductors, and vehicle motion and ride quality.

Several approaches are widely used for the computation of magnetic forces in maglev systems. The finite-element method is one of the more powerful numerical techniques for solving Maxwell's field equations. For given boundary conditions and specified system geometry, one is able to obtain sufficient information for a system by using two- and three-dimensional finite-element computer codes. However, when a system involves relative motions with space- and time-dependences, the finite-element method becomes difficult because considerable computing time is required to obtain the force-speed, or force-time, characteristics. In addition, most commercially available finite-element computer codes cannot solve the problems associated with moving conductors.[1]

Fourier transformation, or harmonic analysis, in combination with numerical techniques, is another powerful method that is applied to maglev problems, such as determining the lift and drag forces in a continuous-sheet guideway. Sometimes this also applies to the discrete coil guideway. The method, however, is usually limited to a two-dimensional steady-state analysis.[2-4]

Dynamic circuit theory, also called "general machinery theory" or "mesh-matrix method," is an approach suitable for maglev applications. It can overcome some of the limitations mentioned above and take both end-effects and edge-effects of the electromagnetic system into consideration. Dynamic circuit theory treats an electrodynamic system in terms of space- and time-dependent circuit parameters governed by a set of differential equations in matrix form. When plate or sheet conductors are considered, the method divides the conductors into many zones, each of which carries a different current. The circuit parameters for every conducting zone are then determined,

and the system of equations is formed. Once the system of equations is solved for the current distribution, the forces acting between the electrodynamic system components can be calculated in a straightforward manner. Because the equations are usually solved for the currents in the time domain, the method is well-suited for transient and dynamic analysis and for the computer simulation of electrodynamic systems, such as maglev trains, electromagnetic launchers, and other electrical machines.

Morgan discusses analyses of rotating electrical machines on the basis of general theory of electrical machines. Analyses of linear machines by means of the mesh-matrix method have been reported.[6-7] The use of dynamic circuit theory for electromagnetic launcher analysis and simulation has been discussed in several publications,[8-9] with emphasis on the transient and the dynamic performance. In launcher analyses, a relatively short time period (a fraction of a second) is considered because of the hypervelocity of the projectile. In addition, a capacitor bank or a pulsed generator is used as the power source for electromagnetic launchers.

The use of dynamic circuit theory for the computation of a continuous-sheet suspension in a maglev system was discussed by a Canadian maglev group.[10-11] In their model, the dynamic circuit theory was combined with a harmonic analysis. The superconducting magnets aboard the vehicle were replaced by a current sheet that was expressed in terms of a Fourier series. A d-q transformation, which is usually used in rotating-machine theory to transform a rotating machine into a stationary primitive machine, was applied to the direction of motion for all harmonics. The performance of the continuous-sheet guideway was determined on the basis of the circuit solutions in combination with the superposition theorem.

Applications of the dynamic circuit theory to various maglev suspension and propulsion systems involving nonsteady-state forces or discrete coils (as opposed to continuous-sheet conductors) have been discussed in previous papers.[12-13] In particular, the use of dynamic circuit theory to simulate the performance of a maglev system (including suspension and propulsion forces) has been discussed in detail. In this document, we summarize the dynamic circuit and apply the theory to several electrodynamic-suspension systems, including a loop-shaped coil suspension and a figure-eight-shaped null-flux suspension. The emphasis is on direct solution and direct computation of forces, without using Fourier and d-q transformations or postcomputation processing. Mathematical models are provided for various suspension systems, and their similarities and differences are considered on the basis of dynamic circuit theory. An attempt is also made to provide some physical insight into the relationships between system parameters and the nature of the resulting forces. This insight, in turn, provides some guidance for the design of discrete-coil maglev systems. The mathematical models can be used for the development of the computer codes that are necessary for the design, analysis, and simulation of large-scale maglev systems. Indeed, work is currently in progress at Argonne on the development of maglev-system-simulating computer codes to account for both the electrodynamics and mechanical dynamics of vehicles interacting with guideways.

3.2 General Model

3.2.1 Energy Conservation and Magnetic Forces in a Maglev System

A maglev system can be represented by the dynamic circuit model, in which the system energy, power, and forces, as well as other quantities, are expressed in terms of their equivalent circuit parameters. In general, those circuit parameters are functions of time and space. Thus, the dynamic and transient performance of a maglev system can be determined on the basis of the solution of the dynamic circuit model.

In general, we may consider a maglev system in which m vehicle coils or conductors interact with n guideway coils or conductors to produce propulsive, levitational, and guidance forces. All these coils are assumed to be connected to individual power sources. Thus, the superconducting coils aboard the vehicle can be represented by letting the terminal voltages and resistances of the vehicle coils vanish; the passive guideway conductors can be represented by letting their terminal voltages vanish; and the propulsion system can be represented by connecting a polyphase power source to the guideway stator coils. Assuming [i] and [e] to be column $(m + n)$ matrices made up of the individual currents and voltages associated with the vehicle and guideway coils or conductors, respectively; [L] to be a square $(m + n) \times (m + n)$ matrix, each element of which represents either the self-inductance of a vehicle or guideway coil or the mutual inductance between any two coils; and [R] to be a diagonal ($m + n$ elements) matrix made up of the individual vehicle coil and guideway coil resistances, the system voltage equations can be written in matrix form on the basis of Kirchhoff's voltage law:

$$[\,e\,] = [\,R\,][\,i\,] + \frac{d}{dt}\{[\,L\,][\,i\,]\}\,. \tag{3.1}$$

In general, a maglev vehicle (or a vehicle-borne coil) undergoes motions in three dimensions. Letting v_x, v_y, and v_z be the velocities of the vehicle in the x, y, and z directions, respectively, Equation 3.1 can be rewritten in terms of speed voltages (i.e., voltages induced by relative motions):

$$[\,e\,] = [\,R\,][\,i\,] + v_x[G_x][\,i\,] + v_y[G_y][\,i\,] + v_z[G_z][\,i\,] + [\,L\,]\frac{d}{dt}[\,i\,]\,, \tag{3.2}$$

where

$$[G_x] = \partial[L]/\partial x,$$

$$[G_y] = \partial[L]/\partial y,$$

and

$$[G_z] = \partial[L]/\partial z.$$

The total time-dependent electrical power input, P, to a maglev system is

$$P = [\,i\,]^T[\,R\,][\,i\,] + [\,i\,]^T[\,L\,]\frac{d}{dt}[\,i\,] + v_x[\,i\,]^T[G_x][\,i\,] + v_y[\,i\,]^T[G_y][\,i\,]$$

$$+ v_z[\,i\,]^T[G_z][\,i\,], \tag{3.3}$$

where the superscript T stands for the matrix transpose. Rearranging the right-hand side of Equation 3.3, one obtains

$$P = [\,i\,]^T[\,R\,][\,i\,] + \frac{d}{dt}\left\{\frac{1}{2}[\,i\,]^T[\,L\,][\,i\,]\right\} + \frac{1}{2}v_x[\,i\,]^T[G_x][\,i\,]$$

$$+ \frac{1}{2}v_y[\,i\,]^T[G_y][\,i\,] + \frac{1}{2}v_z[\,i\,]^T[G_z][\,i\,]. \tag{3.4}$$

Equation 3.4 shows the power balance of a maglev system. We note in this equation that the term on the left represents the total electrical power input to the system, which may include the power from a stationary power system and the power from the batteries aboard the vehicle. The first term on the right-hand side represents the dissipated power of the system, which may include the power losses both in the guideway coils or conductors and in the vehicle coils, if superconducting magnets are not used aboard the vehicle. Even if superconducting coils are used, some power losses may arise, and they can be represented by the first term. In addition, if damping plates or coils are used on board the vehicle, losses therein would be represented by the first term. The second term represents the time rate of change of the magnetic energy stored in the system, and the last three terms on the right-hand side represent the converted mechanical power due to the three-dimensional motion of the vehicle. Finally, the three force components acting on the vehicle, f_x, f_y, and f_z, can be obtained from Equation 3.4 by dividing the terms for the converted mechanical power by their corresponding velocity components, v_x, v_y, and v_z, respectively:

$$f_x = \frac{1}{2}[\,i\,]^T[G_x][\,i\,], \tag{3.5}$$

$$f_y = \frac{1}{2}[\,i\,]^T[G_y][\,i\,], \tag{3.6}$$

and

$$f_z = \frac{1}{2}[\,i\,]^T[G_z][\,i\,]. \tag{3.7}$$

According to the conventional notation, f_x refers to the force component in the direction of motion, f_y is the force component in the horizontal direction, and f_z is the force component in the vertical

direction. Time-averaged magnetic forces can be obtained by integrating Equations 3.5 through 3.7 over any desired time period. Note that, in general, one must also consider the power dissipated in overcoming aerodynamic drag forces. That power term is not represented in Equation 3.4.

When the model is applied to an EDS maglev system in which no electric power is supplied to either the guideway or vehicle coils, the input electrical power term in the left-hand side of Equation 3.4 is set to zero. In this case, the third term on the right-hand side may represent the mechanical power required by the system to overcome the electromagnetic drag losses of the system. Thus, the force balance equation is obtained from Equations 3.4 through 3.7 as

$$f_x = -\frac{1}{v_x}[i]^T[R][i] - \frac{\partial}{\partial x}\left\{\frac{1}{2}[i]^T[L][i]\right\} - \frac{v_y}{v_x}f_y - \frac{v_z}{v_x}f_z \quad . \tag{3.8}$$

Equation 3.8 shows that the applied longitudinal force is balanced by four terms. The first term stands for dissipative energy, representing a drag due to the ohmic loss. The second term reflects the change of the magnetic energy stored, which is considered to be a nondissipative or conservative force and may be negative or positive, depending on the change of the magnetic energy stored in the system in the direction of motion. The last two terms of Equation 3.8 represent the magnetic force coupling due to transverse motions; the transverse velocity components, v_y and v_z, may produce a force coupling to the longitudinal motion because of the spatial dependences of mutual inductances. In general, the last two terms contain both dissipative and nondissipative parts.

Assuming that a vehicle is moving in the x direction at a speed v_x and neglecting the transverse motions v_y and v_z, one can simplify Equation 3.8 to

$$f_x = -\frac{1}{v_x}[i]^T[R][i] - \frac{\partial}{\partial x}\left\{\frac{1}{2}[i]^T[L][i]\right\}. \tag{3.9}$$

Equation 3.9 shows that the longitudinal time-dependent magnetic force in a maglev system consists of two terms: the dissipative term and the nondissipative term. In time-averaged calculations, the first term yields a well-known magnetic drag, and the second term vanishes.

3.2.2 Transformation for the Coil Connections

A maglev system usually involves many coils that may logically be connected in several different groups to perform such different functions as propulsion, levitation, and guidance. For instance, a figure-eight-shaped null-flux coil can be viewed as two loop-shaped coils connected in reverse direction. Propulsion coils, in general, are connected into three groups to form three-phase armature windings. Other maglev systems are expected to have even more complicated coil

connections to perform integrated maglev functions. The dynamic circuit model can be applied to many maglev systems, if the approximate transformations of the coil connections are made.

General transformations for solving electrical machine problems were thoroughly discussed by Morgan.[2] The transformation for the coil connections is particularly useful for maglev simulation and analysis on the basis of the dynamic circuit model. Because the vehicle and guideway coils are usually connected in different configurations that may need different transformations, it is necessary to partition all the matrices by rows or columns to form submatrices. Thus, the previously defined current and voltage matrices, expressed in terms of submatrices, are

$$[\,i\,] = \begin{bmatrix} \mathbf{I_v} \\ \mathbf{I_g} \end{bmatrix} \tag{3.10}$$

and

$$[\,e\,] = \begin{bmatrix} \mathbf{E_v} \\ \mathbf{E_g} \end{bmatrix}, \tag{3.11}$$

where the boldface letters $\mathbf{I_v}$, $\mathbf{E_v}$ and $\mathbf{I_g}$, $\mathbf{E_g}$ are the current and voltage submatrices of the vehicle coils and guideway coils, respectively. The subscripts v and g stand for the vehicle and guideway, respectively. The inductance matrix becomes

$$[\,L\,] = \begin{bmatrix} \mathbf{L_v} & \mathbf{L_{vg}} \\ \mathbf{L_{gv}} & \mathbf{L_g} \end{bmatrix}, \tag{3.12}$$

where $\mathbf{L_v}$ and $\mathbf{L_g}$ are the inductance submatrices of the vehicle coils and guideway coils, respectively. Thus, $\mathbf{L_{vg}} = \mathbf{L_{gv}}$ are the submatrices that represent the coupling between the vehicle coils and guideway coils. They are the most important part of the system because all magnetic forces are generated from this coupling. Similarly, the resistance matrix in the system may be partitioned into submatrices $\mathbf{R_v}$ and $\mathbf{R_g}$:

$$[\,R\,] = \begin{bmatrix} \mathbf{R_v} & 0 \\ 0 & \mathbf{R_g} \end{bmatrix}. \tag{3.13}$$

The $\mathbf{R_v}$ becomes a zero submatrix when superconducting coils (assumed to have no losses) are used aboard the vehicle. One can define a transformation matrix [T] as

$$[\,T\,] = \begin{bmatrix} \mathbf{T_v} & 0 \\ 0 & \mathbf{T_g} \end{bmatrix} \tag{3.14}$$

where $\mathbf{T_v}$ and $\mathbf{T_g}$ are the transformation submatrices for the vehicle coils and the guideway coils, respectively, which depend on the connection of the coils. The term $\mathbf{T_v}$ may be a unit submatrix if the transformation is only applied to the guideway coils. If the primed quantities are introduced as a new system after transformation, then, on the basis of power invariance, one can obtain for the current I

$$[\,I\,] = [\,T\,][\,I\,] \tag{3.15}$$

and for the voltage V

$$[\,V\,]' = [\,T\,]^T [\,V\,]. \tag{3.16}$$

The inductance matrix, the derivative of the inductance matrix, and the resistance matrix for the new system are

$$[\,L\,]' = [\,T\,]^T [\,L\,][\,T\,], \tag{3.17}$$

$$[\,G\,]' = [\,T\,]^T [\,G\,][\,T\,], \tag{3.18}$$

and

$$[\,R\,]' = [\,T\,]^T [\,R\,][\,T\,]. \tag{3.19}$$

By substituting the primed quantities in Equations 3.15 to 3.19 into Equations 3.1 to 3.9, one can obtain the power balance and force equations for the new system.

3.3 References

1. Wang, Z., S. Chen, and D. Rote, 1991, "Present Status of Computational Tools for Maglev Development," Argonne National Laboratory Report ANL/ESD/TM-24, published by Argonne National Laboratory, Argonne, Ill., Oct.

2. Reitz, J.R., and L.C. Davis, 1972, "Force on Rectangular Coil Moving above a Conducting Slab," *J. Applied Physics*, 43(4):1547-53, April.

3. Lee, S.W., and R. Menendez, 1975, "Force at Low- and High-Speed Limits in Magnetic Levitations," *J. Applied Physics*, Vol. 4b, No. 1, Jan., pp. 422-425.

4. Coffey, H.T., F. Chilton, and L.O. Hoppie, 1972, *The Feasibility of Magnetically Levitating High Speed Ground Vehicles*, prepared by Stanford Research Institute for U.S. Department of Transportation, Federal Railroad Administration Report FRA-10001, Feb.

5. Morgan, A.T., 1979, *General Theory of Electrical Machines,* Heyden and Son Ltd., London, England.

6. Elliott, D.G., 1975, "Matrix Analysis of Linear Induction Machines," Federal Railroad Administration Report FRA-OR&D-75-77, Federal Railroad Administration, Washington, D.C. 20590, Sept.

7. Ooi, B.T., 1973, "A Generalized Machine Theory for the Linear Motor," Institute of Electrical and Electronics Engineers, New York, NY, *Transactions on Power Apparatus and Systems,* Vol. PAS-92, No. 5, July/Aug., pp. 1252-1259.

8. He, J.L., E. Levi, Z. Zabar, and L. Birenbaum, 1989, "Concerning the Design of Capacitively Driven Induction Coil Guns," Institute of Electrical and Electronics Engineers, New York, NY, *Transactions on Plasma Science,* Vol. 17, No. 3, June, pp. 429-438.

9. Elliott, D.G., 1989, "Mesh-Matrix Analysis Method for Electromagnetic Launchers," Institute of Electrical and Electronics Engineers, New York, NY, *Transactions on Magnetics,* Vol. 25, No. 1, Jan., pp. 164-169.

10. Ooi, B.T., 1977, "A Dynamic Circuit Theory of the Repulsive Magnetic Levitation System," Institute of Electrical and Electronics Engineers, New York, NY, *Transactions on Power Apparatus and Systems,* Vol. PAS-96, No. 4, July/Aug., pp. 1094-1100.

11. Jain, O.P., 1978, *Further Applications of the Dynamic Circuit Theory to the Electrodynamic Repulsive Magnetic Levitation Systems,* Ph.D. Dissertation, Department of Electrical Engineering, McGill University, Montreal, Canada, July.

12 He, J.L., D.M. Rote, and H.T. Coffey, 1993, "Applications of the Dynamic Circuit Theory to Maglev Suspension Systems," Institute of Electrical and Electronics Engineers, New York, NY, Transactions on Magnetics, Vol. 29, No. 6, Nov., pp. 4153-4164.

13. Andriollo, M., G. Martinelli, and A. Morini, 1992, "General Expressions for Forces Acting in EDS-MAGLEV Systems Driven by Linear Synchronous Motors," proceedings of International Conference on Electrical Machines and Power Electronics, May 27-29, Kusadasi, Turkey, pp. 580-587.

4 Analysis of the Figure-Eight-Shaped Null-Flux Coil Suspension System

4.1 Introduction

Null-flux coil arrangements are an important class of guideway conductor configuration for maglev designs incorporating EDS systems. The concept of using flat and folded figure-eight-shaped null-flux coils in conjunction with EDS systems was originated by Powell and Danby in the late 1960s.[1] A maglev design concept utilizing a separate set of horizontal null-flux loops for lateral guidance was put forward by the Canadian maglev design group in the late 1970s. Subsequently, they replaced the separate null-flux loops with cross-connected propulsion windings mounted vertically on the guideway to improve the guidance forces.[2]

The MLU001 and MLU002 maglev vehicles built by the Japanese were tested at Miyazaki in the 1980s. The Miyazaki Test Track incorporated cross-connected propulsion windings for lateral guidance (Figure 2.2). In 1988 and 1989, Japanese engineers reported on analytical studies and the first test of the MLU002 vehicle utilizing side-wall-mounted figure-eight-shaped null-flux coils for both suspension and lateral guidance (Figure 2.3).[3-7] A similar side-wall-mounted null-flux system is planned for the new 42-km test track in the Yamanashi Prefecture. The major features of the null-flux suspension system are its simple configuration and its capacity to provide both suspension and guidance forces with a high lift-to-drag ratio. In particular, the system can provide zero magnetic drag at the null-flux equilibrium point, making the start-up of the maglev vehicle more efficient.

A maglev vehicle uses magnetic forces for propulsion, levitation, and guidance. Two commonly used approaches for the computation of magnetic forces are the electromagnetic field approach and the electrical circuit approach, as discussed in the preceding chapter. The dynamic circuit model is a circuit approach in which the circuit components are chosen to represent components and their relative motions in a real system, and the circuit parameters are functions of position and time. The main advantage of the dynamic circuit model over other methods is that it can simulate the transient and dynamic performance of an electromagnetic or electromechanical system in a relatively simple manner. The model is especially well-suited for EDS-type maglev systems involving coil-shaped components. In dynamic circuit theory, all of the flux links between any two coils in the system are represented by the time-varying, position-dependent mutual inductances of the two coils. For instance, the flux cancellation between the upper and the lower loops of the figure-eight-shaped null-flux coil is represented by two mutual inductances connected in opposite polarity. Furthermore, all magnetic forces in the system are considered to be generated as a result of the changes in the magnetic energies stored in the system or the changes in mutual inductances between the coils.

The computation of magnetic forces using dynamic circuit theory for various suspension systems has been discussed in a previous paper.[8] This chapter addresses the computation of the figure-eight-shaped null-flux coil suspension system without cross-connection. The computer

model for the null-flux suspension is described on the basis of dynamic circuit theory. Numerical examples are presented to demonstrate the capabilities of the model and to predict the performance of the null-flux suspension system.

4.2 Dynamic Circuit Model of the Figure-Eight-Shaped Null-Flux Coil Suspension

The two most commonly discussed null-flux suspension configurations are the flat figure-eight-shaped null-flux coil configuration and the folded figure-eight-shaped null-flux coil configuration. These are shown in Figures 4.1 and 4.2, respectively. Both geometries follow the same principle of operation: the flux produced by the upper loop coil always opposes that produced by the lower loop coil. Thus, taking into account the forced gravity when a moving superconducting magnet (SCM) is displaced from the balanced force or equilibrium position, the null-flux magnetic lift forces automatically act to restore it to equilibrium position. One can describe both flat and folded null-flux coil suspensions by the dynamic circuit model shown in Figure 4.3, where it is assumed, for general purposes, that m moving superconducting coils interact with n null-flux coils consisting of $2n$ loops. In this model, each superconducting coil is

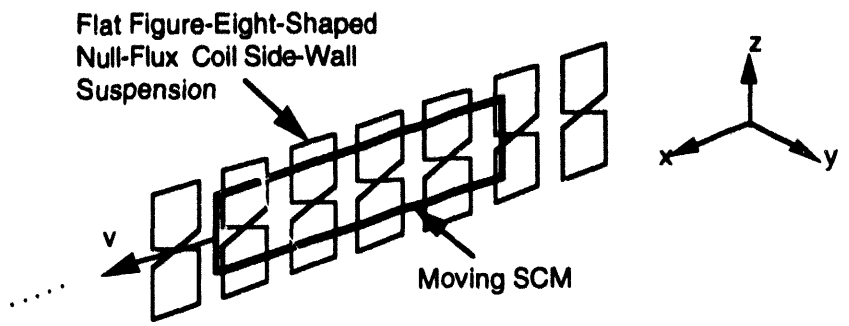

FIGURE 4.1 Superconducting Coil Moving along a Flat Figure-Eight-Shaped Null-Flux Coil Guideway (side-wall suspension)

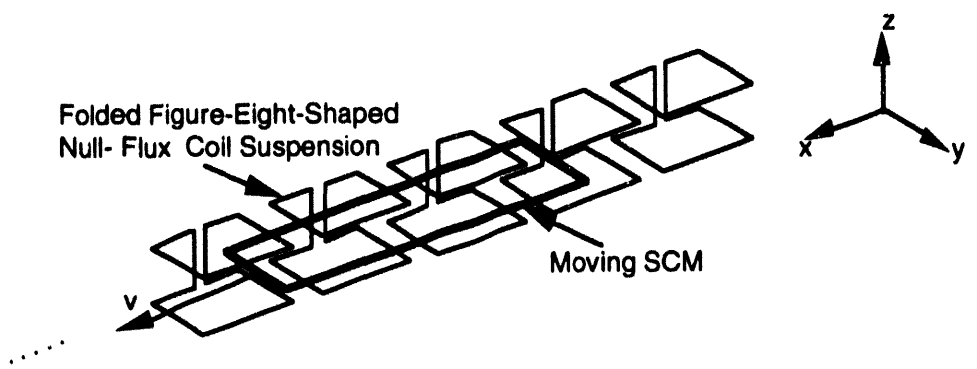

FIGURE 4.2 Superconducting Coil Moving above a Folded Figure-Eight-Shaped Null-Flux Coil Guideway

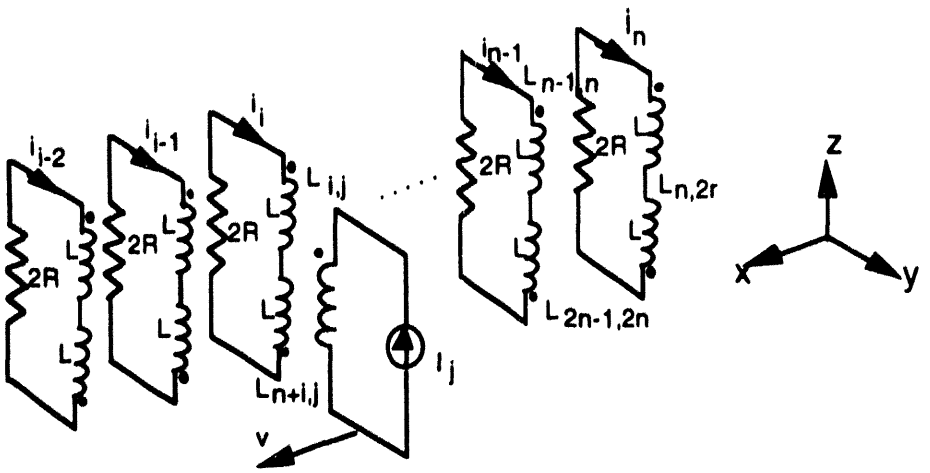

FIGURE 4.3 Dynamic Circuit Representation of the Flat and Folded Figure-Eight-Shaped Null-Flux Coil Suspensions (only one SCM shown)

represented by a constant current source, mutual inductances exist between any two loops, and the polarity of each inductor is indicated by a dot at its end. It should be noted that Figure 4.3 can represent the configuration in either Figure 4.1 or Figure 4.2; however, the dynamic circuit parameters in Figure 4.3 are different for the two configurations.

Consider the general case in which m SCMs aboard a vehicle interact with n short-circuited guideway coils to produce either levitation or guidance forces, the n figure-eight-shaped null-flux coils comprise $2n$ loops, and the upper loop coils are numbered from 1 to n and the lower loop coils from $n+1$ to $2n$. Applying Equations 3.2 through 3.7 to the null-flux system as shown in Figure 4.3 and neglecting the vertical and lateral speeds v_z and v_y, respectively, one obtains for the voltage equations:

$$\begin{bmatrix} R & & \\ & R & \\ & \cdots & \\ & & R \end{bmatrix}\begin{bmatrix} i_1 \\ i_2 \\ \cdots \\ i_n \end{bmatrix} + \begin{bmatrix} L_{1,1}-L_{1,n+1} & L_{1,2}-L_{1,n+2} & \cdots & L_{1,n}-L_{1,2n} \\ L_{2,1}-L_{2,n+1} & L_{2,2}-L_{2,n+2} & & L_{2,n}-L_{2,2n} \\ \cdots & \cdots & \cdots & \cdots \\ L_{n,1}-L_{n,n+1} & \cdots & \cdots & L_{n,n}-L_{n,2n} \end{bmatrix}\frac{d}{dt}\begin{bmatrix} i_1 \\ i_2 \\ \cdots \\ i_n \end{bmatrix} =$$

$$-\frac{v_x}{2}\begin{bmatrix} G_{1,1}-G_{n+1,1} & G_{1,2}-G_{n+1,2} & \cdots & G_{1,m}-G_{n+1,m} \\ G_{2,1}-G_{n+2,1} & G_{2,2}-G_{n+2,2} & & G_{2,m}-G_{n+2,m} \\ \cdots & \cdots & \cdots & \cdots \\ G_{n,1}-G_{2n,1} & \cdots & \cdots & G_{n,m}-G_{2n,m} \end{bmatrix}\begin{bmatrix} I_1 \\ I_2 \\ \cdots \\ I_m \end{bmatrix}. \qquad (4.1)$$

For the time-varying magnetic forces, one obtains:

$$f_x = \sum_{i=1}^{n} \sum_{j=1}^{m} i_i I_j \left[\frac{\partial L_{i,j}}{\partial x} - \frac{\partial L_{n+i,j}}{\partial x} \right], \tag{4.2}$$

$$f_y = \sum_{i=1}^{n} \sum_{j=1}^{m} i_i I_j \left[\frac{\partial L_{i,j}}{\partial y} - \frac{\partial L_{n+i,j}}{\partial y} \right], \tag{4.3}$$

and

$$f_z = \sum_{i=1}^{n} \sum_{j=1}^{m} i_i I_j \left[\frac{\partial L_{i,j}}{\partial z} - \frac{\partial L_{n+i,j}}{\partial z} \right]. \tag{4.4}$$

where R is the resistance of a single loop coil, L_{ij} (i=1,n and j=1,n) are the self-inductances of the loops or the mutual inductances between the loops, and G_{ij} (i=1,n and j=1,m) are the derivatives of the mutual inductances between the loops and the moving superconducting coils.

Several important points should be noted about Equations 4.1 through 4.4. First, the currents induced in the null-flux coils are due to the speed voltages in the right-hand side of Equation 4.1. The speed voltages are given by the product of the vehicle speed v_x, the superconducting coil current I_j (j=1,m), and the derivative of the mutual inductance between the moving vehicle coils and the stationary guideway coils. This means that the suspension forces depend upon the product of the above three factors. Second, the currents in the null-flux coils are reduced substantially (when compared with the currents induced in a normal-flux, single loop-shaped coil guideway) because of the flux cancellation between the upper and lower loops. This is also seen from Equation 4.1, where the inductance matrix elements are generally large because the $L_{i,n+i}$ (i=1,n) are negative, and the induced speed voltages in the right-hand side of the equation are reduced by half. For the best situation, assuming the superconducting coils to be far away from the null-flux equilibrium point ($G_{ij} >> G_{n+i,j}$), the current induced in the null-flux coil guideway is only about one-half of that in the loop-shaped coil guideway. From the viewpoint of the lumped circuit parameters, the resistance and the self-inductance in each null-flux coil are two times larger than those in a single loop coil. Equations 4.2 through 4.4 show that the time-varying magnetic forces depend on the products of the currents in the null-flux coils and superconducting coils and on the difference of the derivatives of the mutual inductances between the upper and lower loops. Thus, it can be concluded that the forces in the null-flux coil guideway, in general, are smaller than in the single loop-shaped coil suspension. Because the lift force must equal the vehicle weight, the relatively smaller force produced by the null-flux suspension system must be compensated by greater ampere-turns in the SCM or improved coupling between the SCM and the guideway coils. However, it should be noted that the figure-eight-shaped null-flux coil suspension can produce both null-flux lift and guidance forces, whereas a single set of loop-shaped guideway coils cannot generate both forces. Furthermore, the lift-to-drag ratio of the null-flux suspension can be several

times higher than that of other EDS suspensions. Detailed performance of the null-flux suspension is discussed in the next section.

4.3 Computer Simulation Results and Discussion

To demonstrate the capability of the dynamic circuit model and to understand the performance of a maglev system using the null-flux suspension concept, a maglev system using side-wall null-flux suspension but lacking cross-connections is chosen (see Figure 4.1). Dimensions similar to those in the Japanese MLU002 test vehicle are used in a numerical example. Table 4.1 gives the corresponding dimensions used for the computer simulation. A number of computations were conducted with various parameter ranges; for example, the three-dimensional magnetic forces were computed as functions of air gap, vertical displacement, lateral displacement, vehicle speed, and other parameters. Figures 4.4 through 4.13 illustrate the performance predictions for the null-flux-shaped suspension system under the various conditions. The dependence of magnetic forces on the dimensions of the figure-eight-shaped null-flux coils is also discussed. The simulation results show that the maglev system that uses figure-eight-shaped null-flux suspension has many potential advantages over other systems, including high vertical stiffness and a very high lift-to-drag ratio.

TABLE 4.1 Data Used for Computer Simulation

Parameter	Specification
Vehicle	
Total weight (metric ton)	17
Maximum velocity (km/h)	500
Height (m)	3.7
Width (m)	3
Number of SCMs	12
Superconducting magnet	
Length (x-direction) (m)	1.7
Width (z-direction) (m)	0.5
Gap between magnets (m)	0.4
Current (kA)	700
Ground null-flux coil	
Length (m)	0.55
Width (m)	0.31
Distance between upper and lower loops (m)	0.12
Distance between null-flux coils (m)	0.15
Number of turns (m)	36
Al conductor cross-section (cm^2)	1

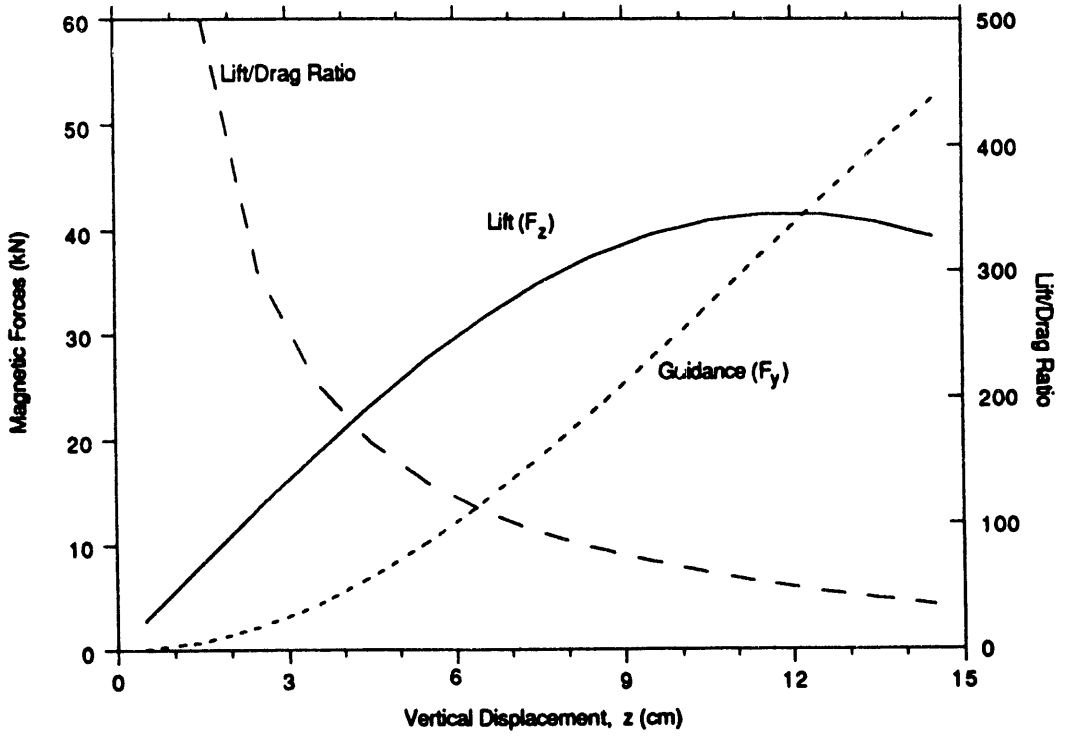

FIGURE 4.4 Null-Flux Lift, Lateral Guidance, and Lift-to-Drag Ratio per SCM as a Function of Vertical Displacement (Air Gap: 20 cm; Velocity: 500 km/h)

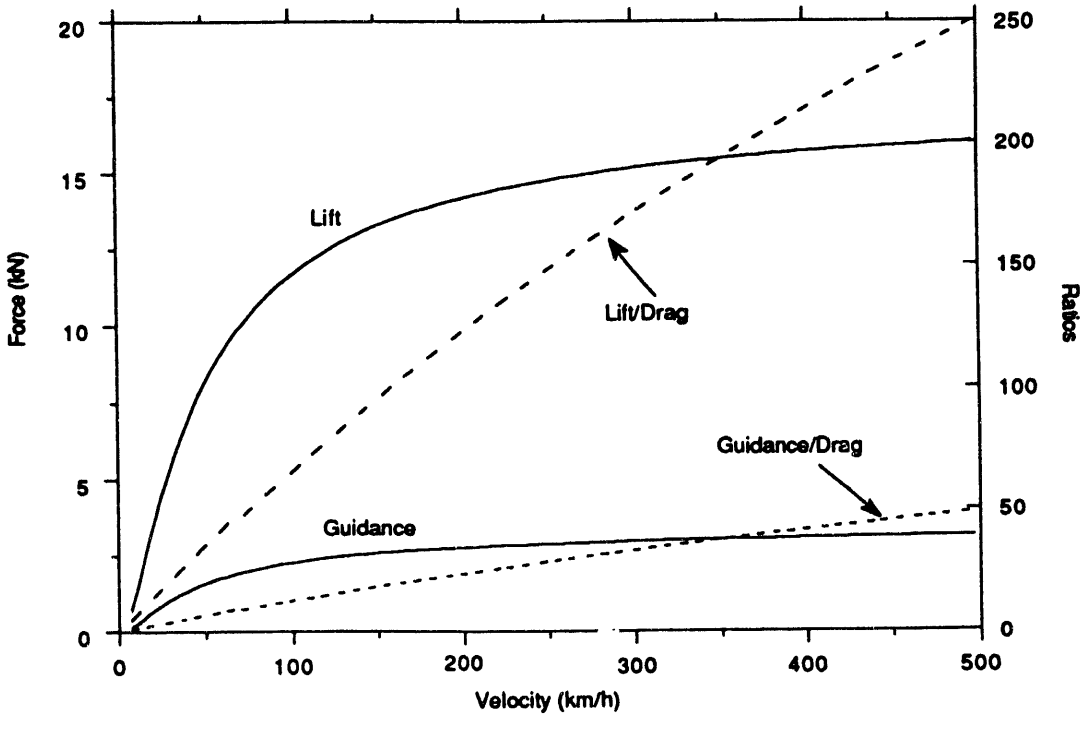

FIGURE 4.5 Lift, Guidance, Lift-to-Drag Ratio, and Guidance-to-Drag Ratio as a Function of Vertical Speed (Air Gap: 20 cm; Vertical Displacement 3 cm)

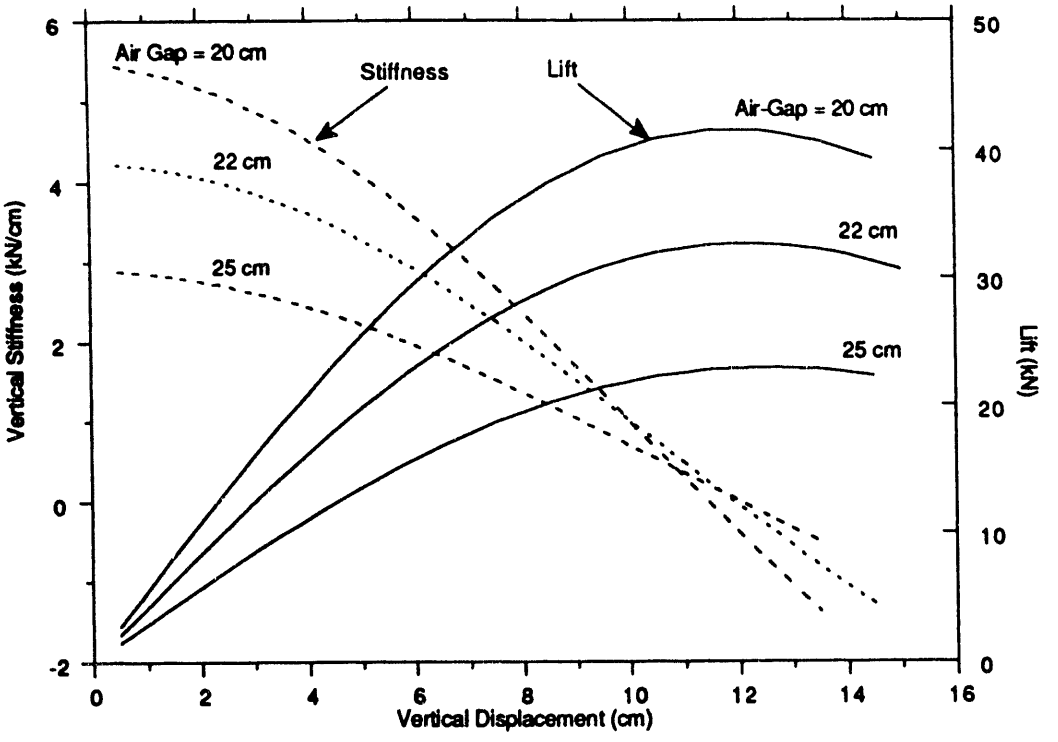

FIGURE 4.6 Null-Flux Lift and Vertical Stiffness per SCM as a Function of Vertical Displacement with Air Gap as a Parameter (Velocity: 500 km/h)

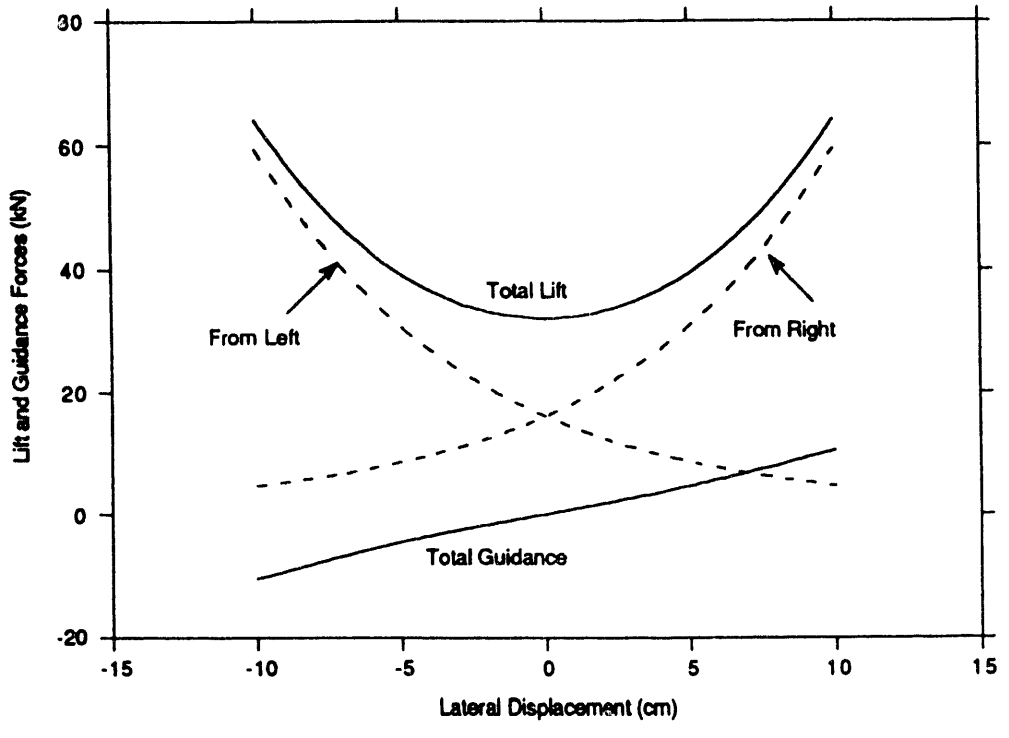

FIGURE 4.7 Magnetic Forces Acting on a Pair of SCMs as a Function of Lateral Displacement (Velocity: 500 km/h; Air Gap: 20 cm; Vertical Displacement: 3 cm)

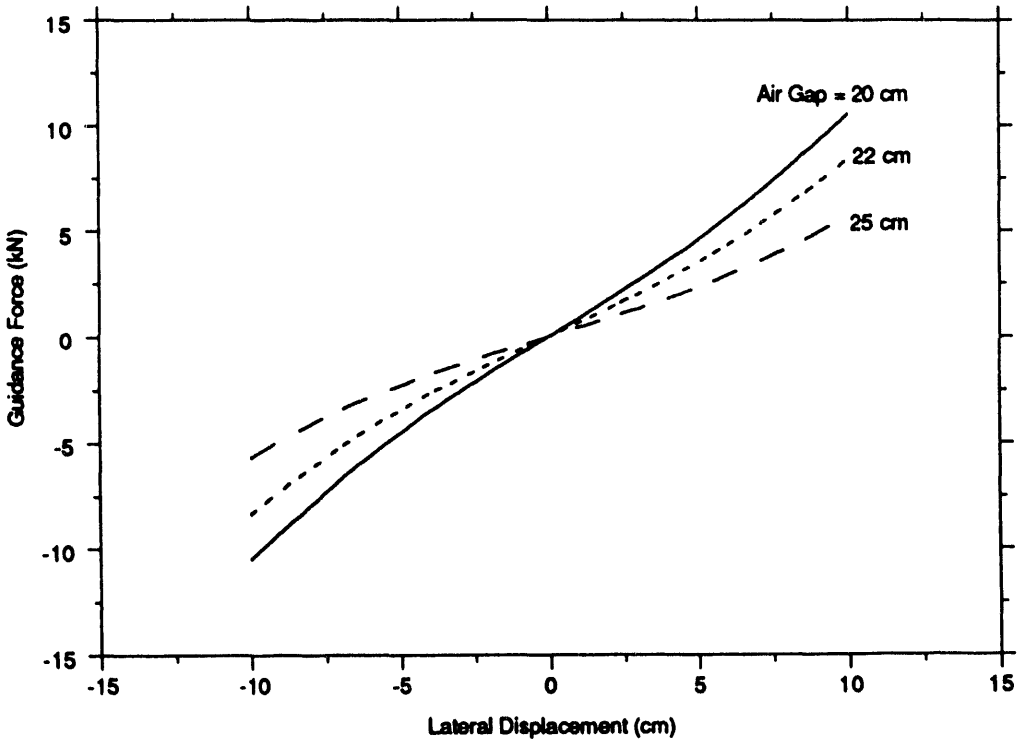

FIGURE 4.8 Guidance Force on SCM Pair as a Function of Lateral Displacement with Air Gap as a Parameter (Velocity: 500 km/h; Vertical Displacement: 7 cm)

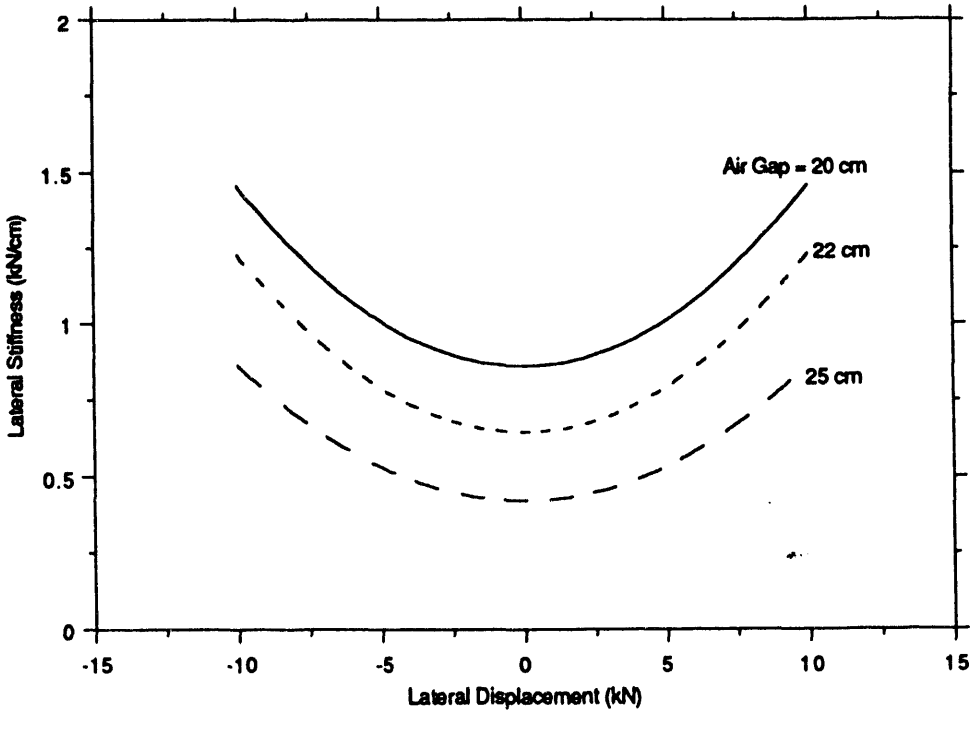

FIGURE 4.9 Lateral Stiffness as a Function of Lateral Displacement with Air Gap as a Parameter (Velocity: 500 km/h; Vertical Displacement: 3 cm)

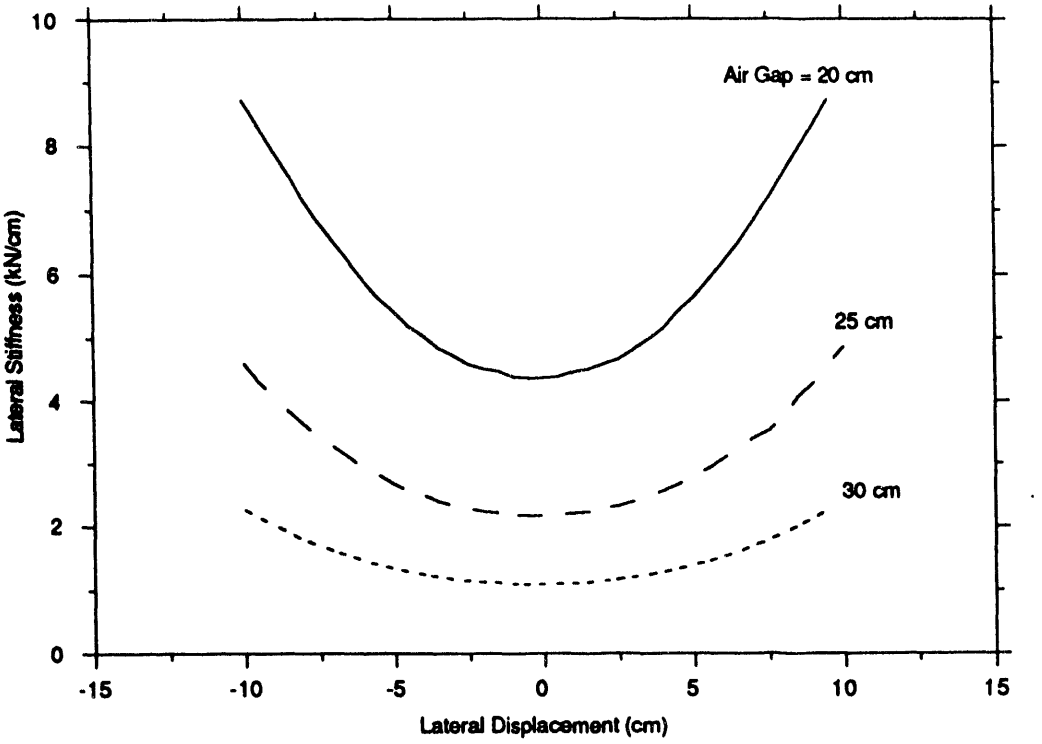

FIGURE 4.10 Lateral Stiffness as a Function of Lateral Displacement with Air Gap as a Parameter (Velocity: 500 km/h; Vertical Displacement: 7 cm)

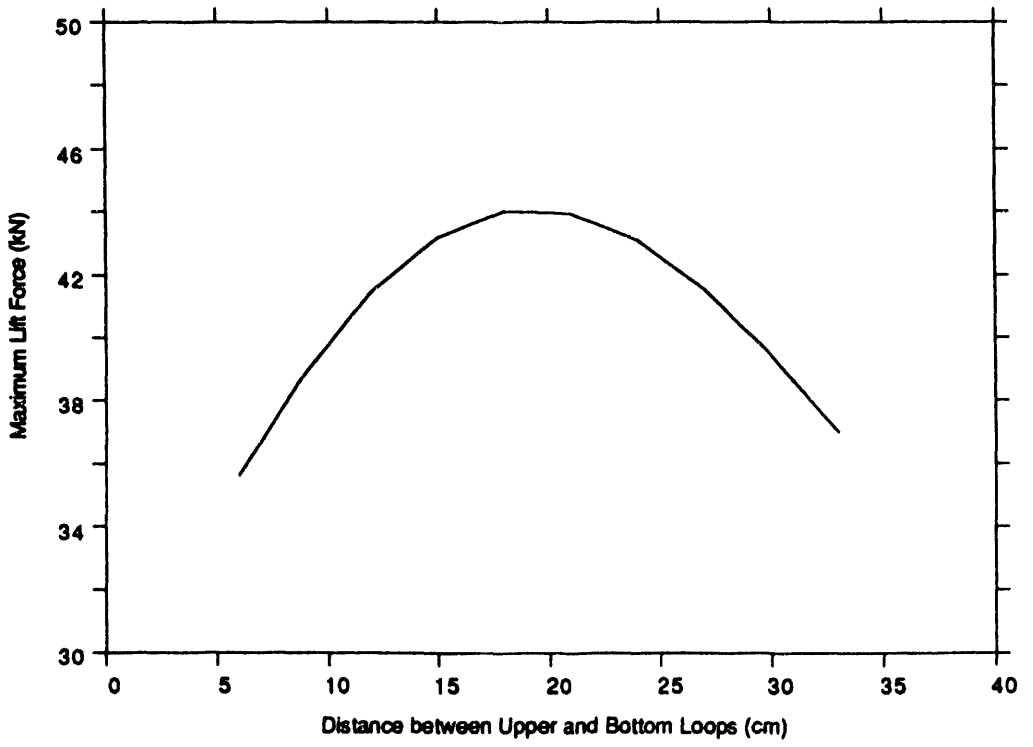

FIGURE 4.11 Maximum Lift Force as a Function of the Distance between Upper and Lower Loops (Air Gap: 20 cm; Velocity: 500 km/h)

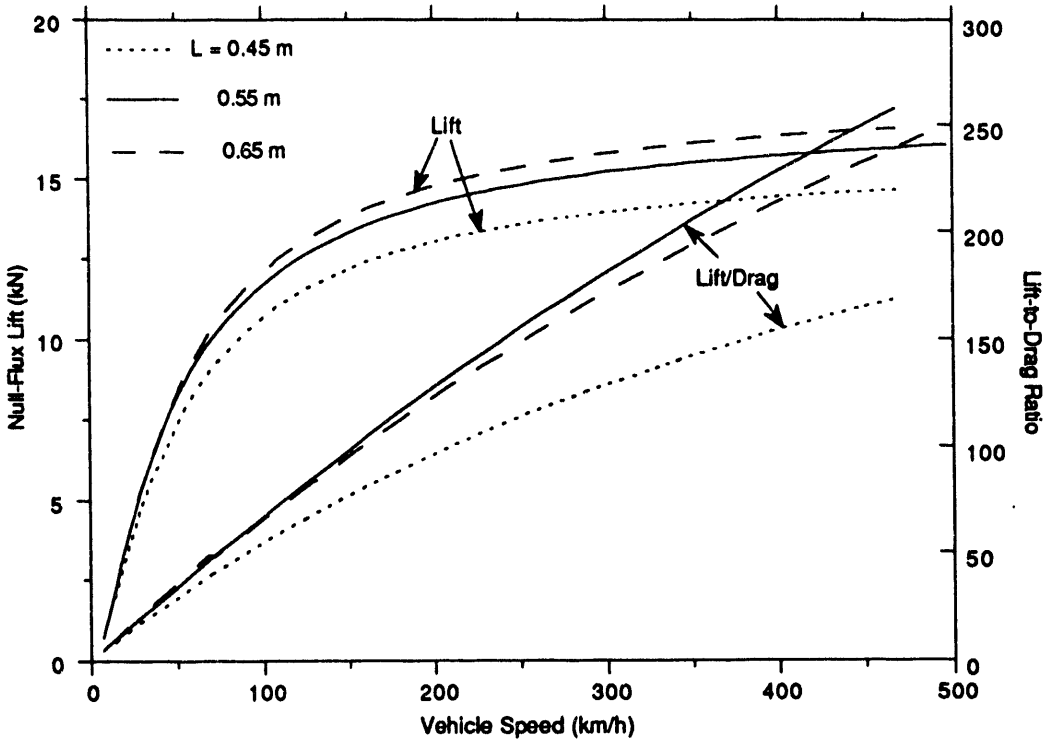

FIGURE 4.12 Dependence on Velocity of Null-Flux Lift per SCM and Lift-to-Drag Ratio with the Length of Figure-Eight-Shaped Null-Flux Coil (L) as a Parameter

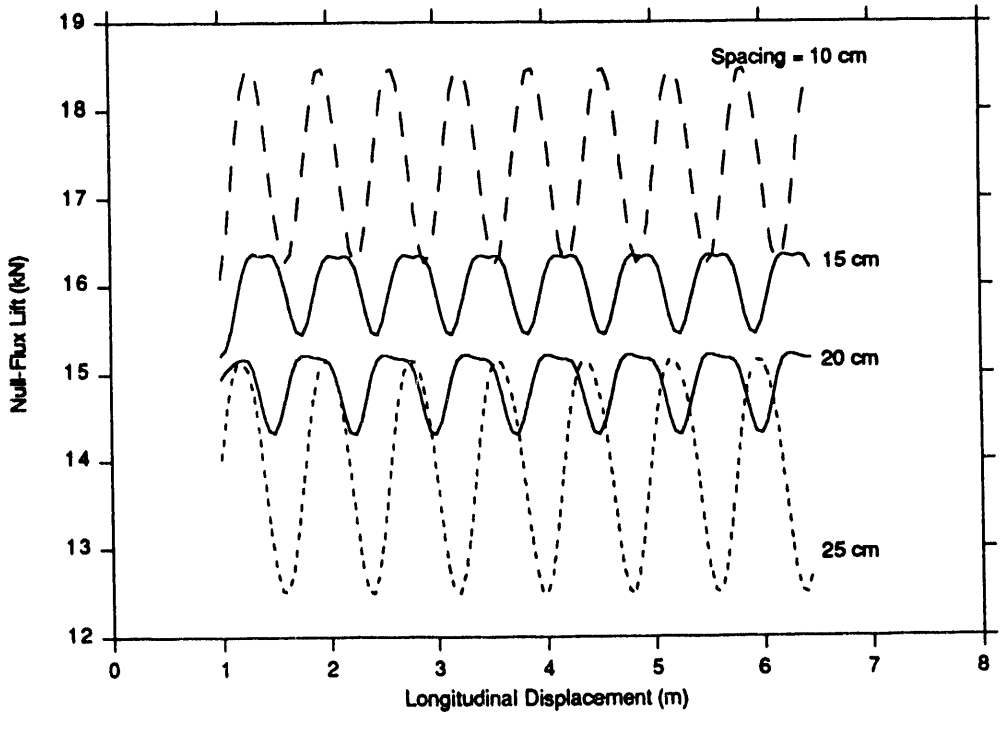

FIGURE 4.13 Null-Flux Lift Force as a Function of Longitudinal Displacement of the SCM with the Spacing between the Figure-Eight-Shaped Coils as a Parameter (Coil Length 55 cm, Vehicle Speed 500 km/h)

4.3.1 Force Characteristics of Null-Flux Suspension

Figure 4.4 shows the dependence of the null-flux lift and guidance forces per superconducting magnet (SCM) and of the lift-to-drag ratio on vehicle speed. The null-flux levitation system can achieve very high lift-to-drag ratios, typically about 250 at 500 km/h with a vertical displacement of 3 cm. However, the ratio drops sharply as the vertical displacement increases. This implies that it is necessary for the null-flux suspension to operate at a small value of the vertical displacement in order to show its major advantage over other systems and to achieve a high system efficiency. The magnetic lift force at this normal operation point (3 cm) is about 15 kN/magnet, or 180 kN for a 12-magnet vehicle. This is sufficient to lift a vehicle of 17 to 18 metric tons.

Figure 4.4 also shows that the lift force approaches a maximum value of 42 kN/SCM at about 10- to 12-cm vertical displacement, or maximum vertical displacement. Beyond a 12-cm displacement the lift force decreases, meaning that the suspension system becomes unstable. However, the lateral guidance force of the system is much smaller than the lift force for vertical displacements of less than about 6 cm. This means that in the range where the lift-to-drag ratio is large, the guidance force is relatively small.

Figure 4.5 illustrates force-speed characteristics for the null-flux suspension. As expected, these characteristics are similar to those for any other EDS system. Both lift and guidance forces increase as the speed increases. The lift-to-drag and guidance-to-drag ratios are proportional to the vehicle speed. However, their slopes are very different; at a speed of 500 km/h, the lift-to-drag ratio is 250 and the guidance-to-drag ratio is only 50. High lift-to-drag ratio is a unique feature of null-flux suspension. It is important to note that the guidance-to-drag ratio of 50 for a null-flux suspension is similar to the lift-to-drag ratio in a loop-shaped coil suspension system.

Another important feature of figure-eight-shaped null-flux coil suspension is its large vertical stiffness. Figure 4.6 illustrates the null-flux lift and vertical stiffness per SCM as a function of vertical displacement, with the equivalent air gap as a parameter. For a vehicle having an air gap of 20 cm and a speed of 500 km/h, the vertical stiffness is about 5 kN/cm per SCM at 2- to 3-cm vertical displacement. If a vehicle can carry 40 passengers, each weighing 80 kg, it will only sink by 5 mm in going from the empty to the fully loaded state.

Computations were made on a pair of SCMs aboard the vehicle, one SCM interacting with the right side-wall and the other interacting with the left side-wall. From this simulation, one is able to see the performance of the system under lateral disturbances. Figure 4.7 demonstrates the dependence on lateral displacement of the magnetic forces acting on the pair of SCMs. The total lift force (i.e., the sum of the lift forces on the two SCMs) is minimized when the vehicle is centered. In addition, the lift force on each individual SCM varies strongly with lateral displacement, whereas the total guidance force varies only weakly with displacement. In fact, the lift force per SCM almost doubles as the lateral displacement increases or decreases by 5 cm from 0.

The large imbalance in the lift forces on the left and right sides of the vehicle under large lateral displacements will lead to a rolling motion of the vehicle. In addition, because of the increase in total lift with lateral displacement, the center of mass of the vehicle will also move upward with lateral displacement. The extent of the rolling motion depends not only on the lateral displacement but also on the vertical stiffness of the lift force (see Figure 4.6). For example, a lateral displacement of 2 cm (from 0) increases the lift of one SCM from 14 to 20 kN, and reduces the lift on the other SCM from 14 to 12 kN. Figure 4.6 shows that reducing the air gap from 20 to 18 cm (i.e., a 2-cm lateral displacement) would give a decrease in vertical displacement of about 1.1 cm. An increase in air gap from 20 to 22 cm would result in an increase in vertical displacement of about 0.5 cm. For a 3-m-wide vehicle, the angle of rotation would be about 0.31° along longitudinal axis. Hence, provided that the vertical stiffness is very large, even if the lateral displacement is relatively large, the angle of rotation will remain relatively small (on the order of one or two degrees at most).

The lateral guidance acting on a pair of SCMs is relatively small, as shown in Figures 4.7 and 4.8. As a consequence, the lateral stiffness is relatively small, as shown in Figure 4.9 for a vertical displacement of 3 cm. As the vertical displacement increases to 7 cm, the lateral stiffness increases substantially, as shown in Figure 4.10. Such large vertical displacements result in substantially reduced lift-to-drag ratios (from about 260 at 3 cm to 100 at 7 cm, according to Figure 4.4). Hence, if large lift-to-drag ratios are desired, and at the same time only small lateral displacements and associated rolling motions caused by perturbing lateral forces can be tolerated, alternative means of enhancing the lateral stiffness must be sought.

4.3.2 Enhancement of Lateral Stiffness

The second generation of Canadian maglev design, as well as the Japanese MLU001 and MLU002 systems, incorporated cross-connected propulsion windings to achieve a type of null-flux guidance. Such a scheme can be combined with the vertically mounted figure-eight-shaped null-flux suspension coils to achieve enhanced lateral guidance. Alternatively, as shown by Fujiwara and Fujimoto,[4-5] it is also possible to cross-connect the figure-eight-shaped null-flux coils themselves to achieve null-flux operation for both the lift and guidance functions. In fact, by using this type of cross coupling, the lateral stiffness can be increased by a factor of 5 to 10. In addition to cross-connections, changing the coil parameters may also result in improved null-flux coil performance, as indicated below.

4.3.3 Effects of Figure-Eight-Shaped Coil Dimensions

Dimensions of the figure-eight-shaped null-flux coils can optimize system performance. Sensitivity studies were conducted on several key dimensions of the null-flux coils. Figure 4.11 illustrates the dependence of maximum lift force on the distance between the upper and lower loops of the figure-eight-shaped coil. It can be seen that the maximum lift force varies as the distance between the two loops increases; and this force approaches a peak of about 44 kN at a distance of

about 20 cm. This means that the previous computation, based on a 12-cm distance between the loops that corresponds to a 42-kN maximum lift force, is not optimal. Furthermore, since the vertical stiffness is closely related to the maximum lift force, one may control the vertical stiffness by varying the distance between two loops of the figure-eight-shaped null-flux coils.

Figure 4.12 shows the null-flux lift per SCM and the lift-to-drag ratio as functions of vehicle speed, with the length (longitudinal direction) of the figure-eight-shaped null-flux coil (L) as a parameter. Although the null-flux lift force increases by only about 10% as the length of the figure-eight-shaped coil increases from 0.45 to 0.65 m, the lift-to-drag ratio increases by about 50%. It seems that relatively longer coils can have better lift-to-drag ratio. However, if the null-flux coil is too long, the resistance of the coil increases, and the lift-to-drag ratio is also reduced. In addition, the cost of a guideway is closely related to the dimensions of the figure-eight-shaped null-flux coils. Proper selection of the null-flux coil length can improve the suspension performance and reduce the guideway cost. Numerical studies show that the length of the coil plus the space between the two adjacent coils should be about one-third of the length of the SCMs.

4.3.4 Time Dependence of Magnetic Forces

All of the magnetic forces in the null-flux suspension system fluctuate as the vehicle moves along the guideway. The amplitude of the fluctuation depends strongly upon the coil length and the spacing between coils. The pole-pitch of the null-flux coil is one of the major factors. Figure 4.13 shows the dependence of the null-flux lift on the longitudinal position of the SCM, with the distance between two figure-eight-shaped coils as a parameter. The length of the coil is 55 cm and the vehicle speed is 500 km/h for all four conditions. The figure-eight-shaped coil suspensions having 10- and 25-cm coil spacings are observed to suffer from large force fluctuations, while those having 15- and 20-cm coil spacings have small force fluctuations. There seems to be an optimal spacing at about 17 cm that minimizes the force fluctuations. However, the average force always increases as the spacing decreases. The frequency of the force fluctuation is given by the vehicle speed divided by the length of the figure-eight-shaped coil plus the spacing between two neighboring coils. The frequencies of the force fluctuations are 214 Hz for the 10-cm spacing, 198 Hz for the 15-cm spacing, 185 Hz for the 20-cm spacing, and 174 Hz for the 25-cm spacing.

4.4 Conclusions

The dynamic circuit model is a useful tool for studying a maglev system that incorporates moving conducting coils. The model can simulate the dynamic performance of the system and, in particular, can be used to calculate the spatial and temporal variations in magnetic forces.

The figure-eight-shaped null-flux side-wall suspension system has many advantages over other suspension systems. In particular, it has a simple configuration and can provide very high lift-to-drag ratios. The null-flux lift force depends strongly on both vertical and lateral

displacement. The lateral guidance force of the side-wall suspension system is relatively weak and must be enhanced to provide stability against excessively large lateral displacements that could lead to roll instability. Additional configurations are needed to increase the lateral guidance force in the system, which is discussed in detail in Chapter 5.

4.5 References

1. Danby, G.T., and J.R. Powell, 1988, Design Approaches and Parameters for Magnetically Levitated Transport Systems, Superconductivity and Its Applications. Elsevier Science Publishing Co., Inc., pp. 318-342.

2. Hayes, W.F., and H.G. Tucker, 1984, "Design Concept and Comparative Performance of an Electrodynamic Maglev Transportation System for Toronto-Montreal Corridor of Canada," Institute of Mechanical Engineers, c400/84, pp. 137-148.

3. Fujiwara, S., 1988, "Characteristics of EDS Maglev Having Levitation Coils on the Side-Wall of the Guideway," *Quarterly Report, Railway Technical Research Institute*, Japan, Vol. 29, No. 4, Nov., pp. 157-163.

4. Fujiwara, S., and T. Fujimoto, 1989, "Characteristics of the Combined Levitation and Guidance System Using Ground Coils on the Side-Wall of the Guideway," Proceedings of the International Conference on Maglev '89, July, pp. 241-244.

5. Fujimoto, T., and S. Fujiwara, 1991, "Electrodynamic Characteristics of MLU002," Quarterly Report, Railway Technical Research Institute, Japan, Vol. 32, No. 2, June, pp. 50-58.

6. Tanaka, H., 1991, "Change in the Coil Distribution of Electrodynamic Suspension System," Proceedings of the International Symposium on Magnetic Suspension Technology, NASA Langley Research Center, Hampton, Va., Aug. 19-23, pp. 813-825.

7. Saitoh, T., K. Miyashita, and H. Kiwaki, 1989, "Study for Harmonic Ripple of Electromagnetic Force in Superconducting Magnetically Levitated Vehicle with Non-Rectangular Ground Coils," Proceedings of International Conference on Maglev '89, July, pp. 245-250.

8. He, J.L., D.M. Rote, and H.T. Coffey, 1991, "Computation of Magnetic Suspension of Maglev Systems Using Dynamic Circuit Theory," Proceedings of the International Symposium on Magnetic Suspension Technology," Hampton, Va., Aug. 19-23, NASA Publication 3152, pp. 919-938.

5 Analysis of the Combined Figure-Eight-Shaped Null-Flux Coil Levitation and Guidance System

5.1 Introduction

The cross-connected, null-flux coil suspension system has been under development in Japan for several years.[1-3] The system consists of two arrays of figure-eight-shaped null-flux coils mounted on the side walls of the guideway, each coil on the left side wall being cross-connected with another one on the right side wall to form a combined levitation and guidance system. Both the null-flux levitation and the null-flux guidance forces are generated by the interaction between two rows of SCMs aboard the vehicle and two rows of null-flux coils on the guideway. The concept has become very popular in the world maglev community because of the high lift-to-drag and guidance-to-drag ratios, the high suspension stiffness, and the very low magnetic drag at low speed associated with this system.

This chapter discusses the electrodynamic performance of the cross-connected, null-flux coil suspension system on the basis of the dynamic circuit model. The equivalent circuits of the system are presented, and general expressions are derived for the determination of magnetic forces acting on the SCMs and the current induced in the null-flux coils. Closed-form formulas for the magnetic forces are derived by using a harmonic approximation. These formulas are valuable for the design of maglev systems and for studies of vehicle dynamics.

5.2 The Equivalent-Circuit Model

5.2.1 Equivalent Circuit for an SCM Interacting with a Null-Flux Coil

The simplest model for a figure-eight-shaped null-flux coil interacting with an SCM is an equivalent circuit containing one mesh with two branches, as shown in Figure 5.1. Each branch,

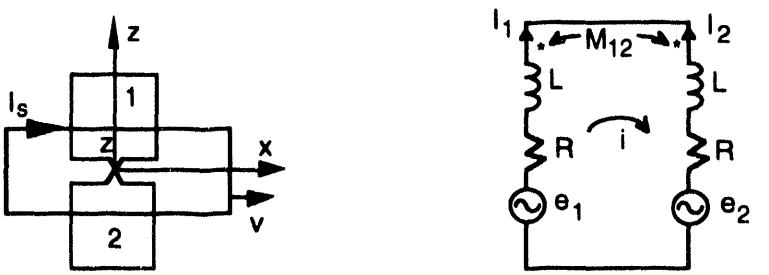

FIGURE 5.1 Equivalent Circuit of a Single SCM Interacting with a Null-Flux Coil

having a resistance R and an inductance L, represents a single loop of the null-flux coil. The coupling between the upper and lower loops is described by the mutual inductance M_{12}, and the couplings between the moving SCM and the upper and lower loops of the null-flux coil are modeled by two time- and space-dependent voltage sources e_1 and e_2, respectively. In Figure 5.1, I_1 and I_2 stand for the currents flowing in the upper and lower loops, and i ($= I_1 = -I_2$) is the current circulating in the null-flux coil.

Let I_s and v be the current and speed of the SCM, and let M_{s1} and M_{s2} be the mutual inductances between the SCM and the upper and lower loops of the null-flux coil, respectively. One can express e_1 and e_2 as follows:

$$e_1 = -I_s v \frac{\partial M_{s1}}{\partial x} \tag{5.1}$$

and

$$e_2 = -I_s v \frac{\partial M_{s2}}{\partial x} \tag{5.2}$$

The voltage equation for the system is

$$2Ri + 2(L - M_{12}) \frac{di}{dt} = e_1 - e_2 \,. \tag{5.3}$$

The three components of time-dependent magnetic forces f_x, f_y, and f_z existing between the moving SCM and the null-flux coil are

$$f_x = I_s I_1 \frac{\partial M_{s1}}{\partial x} + I_s I_2 \frac{\partial M_{s2}}{\partial x} = I_s i \left(\frac{\partial M_{s1}}{\partial x} - \frac{\partial M_{s2}}{\partial x} \right), \tag{5.4}$$

$$f_y = I_s I_1 \frac{\partial M_{s1}}{\partial y} + I_s I_2 \frac{\partial M_{s2}}{\partial y} = I_s i \left(\frac{\partial M_{s1}}{\partial y} - \frac{\partial M_{s2}}{\partial y} \right), \tag{5.5}$$

and

$$f_z = I_s I_1 \frac{\partial M_{s1}}{\partial z} + I_s I_2 \frac{\partial M_{s2}}{\partial z} = I_s i \left(\frac{\partial M_{s1}}{\partial z} - \frac{\partial M_{s2}}{\partial z} \right). \tag{5.6}$$

Equations 5.1 through 5.6 can only be solved step by step numerically, because M_{si} (i = 1,2) is time- and space-dependent. The electrodynamic performance of the system is then predicted on the basis of the system solution. Equations 5.3 through 5.6 indicate that the three components of magnetic force are proportional to the product of the circulating current i, the SCM current I_s, and the difference of the mutual-inductance derivatives between the SCM and the upper and lower loops. The magnetic forces vanish as the SCM moves to the equilibrium position (z = 0).

5.2.2 Equivalent Circuit Model for the Cross-Connected, Null-Flux Coil Suspension

A pair of SCMs aboard the vehicle, interacting with cross-connected, figure-eight-shaped null-flux coils that are mounted on the two sides of the guideway (see Figure 5.2), can be modeled by the equivalent circuit shown in Figure 5.3. Each branch (with resistance R, inductance L, and voltage source e) represents a single loop of the null-flux coil. The mutual inductance between loops 1 and 2 equals the mutual inductance between loops 3 and 4, both being M_{12}.

I_i (i = 1,4) and e_i (i = 1,4) are the currents flowing in the loops and the voltages induced in the loops, respectively. The mesh currents flowing in the circuit are i_1, i_2, and i_3. In particular, i_2 represents the current flowing in the cross-connecting cable across the guideway, and it contributes to the null-flux guidance. The resistance and inductance of the cross-connected cables are neglected in Figure 5.3. In parallel with the derivation of Equations 5.1 and 5.2, the voltages induced in loops 3 and 4 can be expressed in terms of the mutual inductances M_{s3} and M_{s4} between the SCM and loops 3 and 4, respectively:

$$e_3 = -I_s v \frac{\partial M_{s3}}{\partial x} \tag{5.7}$$

and

$$e_4 = -I_s v \frac{\partial M_{s4}}{\partial x} . \tag{5.8}$$

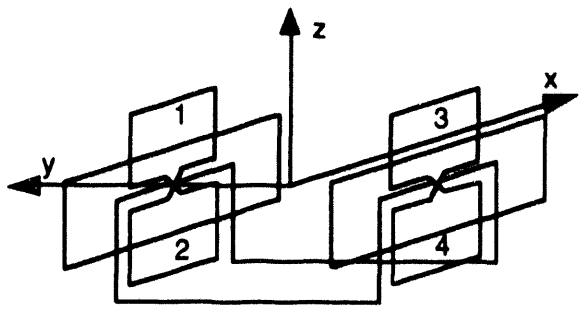

FIGURE 5.2 Cross-Connected, Figure-Eight-Shaped Null-Flux Coils for Maglev Levitation and Guidance

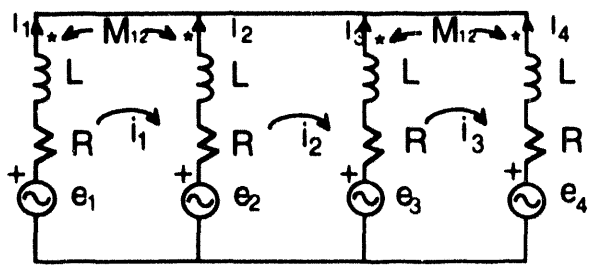

FIGURE 5.3 Equivalent Circuit for the Cross-Connected, Null-Flux Coil Suspension System

Figure 5.3 can be simplified by eliminating the mutual inductances, M_{12}, between the upper and lower loops. Using Kirchhoff's voltage law, one can write voltage equations in terms of mesh currents, as follows:

$$2Ri_1 + 2(L - M_{12})\frac{di_1}{dt} - Ri_2 - (L - M_{12})\frac{di_2}{dt} = e_1 - e_2, \tag{5.9}$$

$$-Ri_1 - (L - M_{12})\frac{di_1}{dt} + 2Ri_2 + 2L\frac{di_2}{dt} - Ri_3 - (L - M_{12})\frac{di_3}{dt} = e_2 - e_3, \tag{5.10}$$

and

$$-Ri_2 - (L - M_{12})\frac{di_2}{dt} + 2Ri_3 + 2(L - M_{12})\frac{di_3}{dt} = e_3 - e_4. \tag{5.11}$$

After solving for the mesh currents from Equations 5.9 through 5.11, one can determine the three components of magnetic forces acting on the moving SCM:

$$f_x = \sum_{j=1}^{4} I_s I_j \frac{\partial M_{sj}}{\partial x} = I_s \left\{ i_1 \left(\frac{\partial M_{s1}}{\partial x} - \frac{\partial M_{s2}}{\partial x} \right) + i_2 \left(\frac{\partial M_{s2}}{\partial x} - \frac{\partial M_{s3}}{\partial x} \right) + i_3 \left(\frac{\partial M_{s3}}{\partial x} - \frac{\partial M_{s4}}{\partial x} \right) \right\}, \tag{5.12}$$

$$f_y = \sum_{j=1}^{4} I_s I_j \frac{\partial M_{sj}}{\partial y} = I_s \left\{ i_1 \left(\frac{\partial M_{s1}}{\partial y_1} - \frac{\partial M_{s2}}{\partial y_1} \right) + i_2 \left(\frac{\partial M_{s2}}{\partial y_1} - \frac{\partial M_{s3}}{\partial y_2} \right) + i_3 \left(\frac{\partial M_{s3}}{\partial y_2} - \frac{\partial M_{s4}}{\partial y_2} \right) \right\}, \tag{5.13}$$

and

$$f_z = \sum_{j=1}^{4} I_s I_j \frac{\partial M_{sj}}{\partial z} = I_s \left\{ i_1 \left(\frac{\partial M_{s1}}{\partial z} - \frac{\partial M_{s2}}{\partial z} \right) + i_2 \left(\frac{\partial M_{s2}}{\partial z} - \frac{\partial M_{s3}}{\partial z} \right) + i_3 \left(\frac{\partial M_{s3}}{\partial z} - \frac{\partial M_{s4}}{\partial z} \right) \right\}, \tag{5.14}$$

where the relations between the mesh and branch currents ($I_1 = i_1$, $I_2 = i_3 - i_1$, $I_3 = i_3 - i_2$, and $I_4 = -i_3$) are used. Two different lateral coordinates, needed for the two lateral air gaps, are specified by y_1 and y_2 in Equation 5.13. Comparing Equations 5.12 through 5.14 with Equations 5.4 through 5.6, one notes that the three components of magnetic force in the cross-connected null-flux coil suspension system depend upon the current i_2 flowing between the two figure-eight-shaped null-flux coils. At the lateral equilibrium position, no current flows between the two figure-eight-shaped null-flux coils. In this case, the cross-connected, null-flux coil suspension system becomes two independent, conventional null-flux coil suspension systems. The guidance force of the cross-connected, null-flux coil suspension system consists of two parts.

One part is due to cross-connection, which follows the null-flux suspension principle, and the other part is due to the individual null-flux coils and the air gap difference. The latter part can be determined from Equations 5.4 through 5.6. To obtain the guidance force resulting from the cross-connection, one can (1) simplify Figure 5.3 by eliminating the mutual inductances between the upper and lower loops, and (2) find a Thevenin equivalent circuit by eliminating meshes 1 and 3, as shown in Figure 5.4.

Figure 5.4 shows that the voltage e_1 has the same polarity as e_2, and e_3 has the same polarity as e_4. The null-flux guidance force will be generated when the condition $e_1 + e_2 \neq e_3 + e_4$, or $I_1 + I_2 \neq I_3 + I_4$, is true. The current flowing in the cross-connecting cable between the two null-flux coils can be determined from the simplified equivalent circuit shown in Figure 5.4 in terms of the voltage equation:

$$Ri_2 + (L - M)\frac{di_2}{dt} = \frac{1}{2}[(e_1 + e_2) - (e_3 + e_4)] . \tag{5.15}$$

The cross-connection part of the null-flux guidance force is

$$f_y = \frac{1}{2} i_2 I_s \left[\left(\frac{\partial M_{s1}}{\partial y_1} + \frac{\partial M_{s2}}{\partial y_1}\right) - \left(\frac{\partial M_{s3}}{\partial y_2} + \frac{\partial M_{s4}}{\partial y_2}\right)\right] . \tag{5.16}$$

Because the null-flux suspension system usually operates near vertical equilibrium, it is a good approximation to assume that the derivative of the mutual inductance M_{s1} with respect to y_1 is equal to that of M_{s2} with respect to y_1. Similarly, one may assume that the derivatives of mutual inductances M_{s3} and M_{s4} with respect to y_2 are also equal. Thus, Equation 5.16 is simplified:

$$f_y = i_2 I_s \left[\frac{\partial M_{s1}}{\partial y_1} - \frac{\partial M_{s3}}{\partial y_2}\right] . \tag{5.17}$$

Equations 5.16 and 5.17 represent only the guidance force resulting from the current flowing in the cross-connecting cable (i_2), while Equation 5.13 gives a total guidance force.

Equations 5.9 to 5.15 can be numerically solved, by using an approach similar to that discussed previously, to obtain the transient currents induced in the null-flux coils and the time-dependent magnetic forces acting on the SCMs.[4-5]

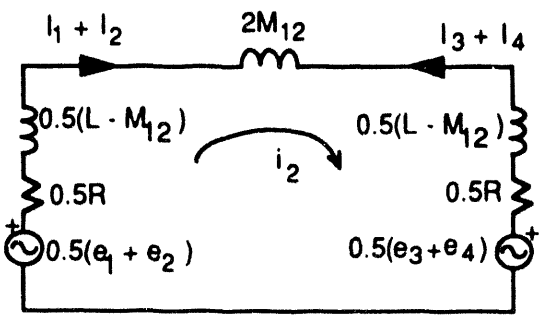

FIGURE 5.4 Simplified Equivalent Circuit for Determining Null-Flux Guidance Force

5.3 Harmonic Approximation

Exact solutions of Equations 5.9 through 5.14 require a numerical approach because of the time- and space-dependence of the mutual inductances between the moving SCMs and the null-flux coils. It is difficult to gain physical insight and to conduct vehicle dynamic stability studies with numerical solutions. Thus, Equations 5.9 through 5.14 are further developed on the basis of a harmonic approximation to obtain simplified analytical expressions useful for preliminary system design. Because a maglev vehicle usually consists of several groups of SCMs, each group comprising several SCMs arranged in one row with alternating polarities, the flux linkage through the null-flux coils varies its direction as the SCM row moves forward. It is a good approximation to express the mutual inductance between a group of SCMs and a null-flux coil by a harmonic function, the fundamental wave of which is

$$M_{sj} = M_{pj}(y,z) \cos \frac{\pi}{\tau} x = M_{pj}(y,z) \cos \omega t \qquad j=1,4, \qquad (5.18)$$

where M_{pj} is the peak value of the mutual inductance between one SCM and the jth loop of the null-flux coil. The M_{pj} depends upon only displacements in the vertical (z-axis) and lateral (y-axis) directions. The pole pitch of the SCMs is τ, and $\omega = \pi v/\tau$ is the angular frequency. Note that Equation 5.18 is only an approximation; higher-order harmonics may be added to this expression to obtain greater accuracy.

Substituting Equations 5.1, 5.2, 5.7, 5.8, and 5.18 into Equations 5.9 through 5.11, one can solve for the sinusoidal current i_2 flowing in the cross-connecting cable:

$$i_2 = \frac{(E_1 + E_2) - (E_3 + E_4)}{2\sqrt{R^2 + \omega^2 (L + M_{12})^2}} \sin(\omega t - \phi_2) \qquad (5.19)$$

where

$$\phi_2 = \tan^{-1} \frac{\omega t (L + M_{12})}{R} \qquad (5.20)$$

and

$$E_j = \omega I_s M_{pj} . \qquad (5.21)$$

The current will flow through the cross-connecting cable as long as (E_1+E_2) is not equal to (E_3+E_4), or so long as there exists a lateral displacement. Mesh currents i_1 and i_3 are found to be

$$i_1 = \frac{E_1 - E_2}{2\sqrt{R^2 + \omega^2(L - M_{12})^2}} \sin(\omega t - \phi_1) + \frac{1}{2} i_2 \tag{5.22}$$

and

$$i_3 = \frac{E_3 - E_4}{2\sqrt{R^2 + \omega^2(L - M_{12})^2}} \sin(\omega t - \phi_1) + \frac{1}{2} i_2 \tag{5.23}$$

where

$$\phi_1 = \tan^{-1} \frac{\omega(L - M_{12})}{R} . \tag{5.24}$$

Equations 5.22 and 5.23 show that the currents flowing through the figure-eight-shaped null-flux coils 1 and 2 consist of two parts: the first part results from the vertical displacement; the second part, from the lateral displacement. At the vertical null-flux position ($E_1 = E_2$ and $E_3 = E_4$), both i_1 and i_2 equal half of i_3. In this case, there still exists a null-flux guidance force so long as i_2 exists. This force does not exist in a conventional side-wall null-flux suspension system, in which all magnetic forces vanish at the vertical null-flux position even though there exists a lateral displacement; in a cross-connected, null-flux coil system, magnetic forces disappear only at both lateral and vertical equilibrium positions.

Substituting Equations 5.19, 5.22, and 5.23 into Equations 5.12 through 5.14 and taking the integral with respect to time over a period, one can determine the time-averaged forces in terms of dynamic circuit parameters. These forces can be grouped according to physical insight and the positions on which the forces act, as shown in Figure 5.5. The time-averaged null-flux levitation force, F_z, between a pair of SCMs and a pair of cross-connected figure-eight-shaped null-flux coils is

$$F_z = F_{z11} + F_{z12} + F_{z22} + F_{z21}, \tag{5.25}$$

where F_{z11} and F_{z22} are the null-flux levitation forces from the interaction between the SCMs and the left- and right-hand-side null-flux coils, respectively, when the two coils are not cross-connected. These forces are given by

$$F_{z11} = -\frac{I_s^2}{4} \frac{v^2}{v^2 + v_{c1}^2} \frac{M_{p1} - M_{p2}}{L - M_{12}} \left(\frac{\partial M_{p1}}{\partial z} - \frac{\partial M_{p2}}{\partial z} \right) \tag{5.26}$$

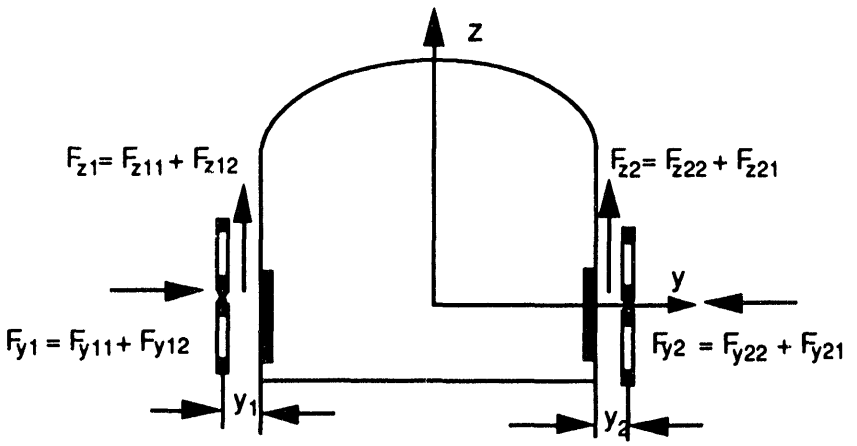

FIGURE 5.5 Cross-Sectional View of the Side-Wall Null-Flux Suspension System

and

$$F_{z22} = -\frac{I_s^2}{4}\frac{v^2}{v^2 + v_{c1}^2}\frac{M_{p3} - M_{p4}}{L - M_{12}}\left(\frac{\partial M_{p3}}{\partial z} - \frac{\partial M_{p4}}{\partial z}\right). \tag{5.27}$$

F_{z12} and F_{z21} are the additional levitation forces produced by the left- and right-hand-side, figure-eight-shaped null-flux coils resulting from the cross-connection:

$$F_{z12} = -\frac{I_s^2}{8}\frac{v^2}{v^2 + v_{c2}^2}\frac{(M_{p1} + M_{p2}) - (M_{p3} + M_{p4})}{L + M_{12}} \times \left(\frac{\partial M_{p1}}{\partial z} + \frac{\partial M_{p2}}{\partial z}\right) \tag{5.28}$$

and

$$F_{z21} = \frac{I_s^2}{8}\frac{v^2}{v^2 + v_{c2}^2}\frac{(M_{p1} + M_{p2}) - (M_{p3} + M_{p4})}{L + M_{12}} \times \left(\frac{\partial M_{p3}}{\partial z} + \frac{\partial M_{p4}}{\partial z}\right). \tag{5.29}$$

F_{z21} and F_{z12} are very small because the derivatives of the mutual inductances M_{s1} and M_{s2} with respect to vertical displacements have opposite signs, and so do those of M_{s3} and M_{s4}. The last terms of Equations 5.28 and 5.29 are small. Consequently, F_{z11} and F_{z22} are the dominant terms. Similarly, one can express the magnetic drag as follows:

$$F_x = F_{x11} + F_{x12} + F_{x22} + F_{x21}, \tag{5.30}$$

where F_{x11} and F_{x22} are the magnetic drag produced by the left- and right-hand-side, figure-eight-shaped null-flux coils when they are not cross-connected:

$$F_{x11} = -\frac{I_s^2}{4}\frac{vv_{c1}}{v^2 + v_{c1}^2}\frac{\pi/\tau(M_{p1} - M_{p2})^2}{L - M_{12}} \tag{5.31}$$

and

$$F_{x22} = -\frac{I_s^2}{4}\frac{vv_{c1}}{v^2 + v_{c1}^2}\frac{\pi/\tau(M_{p3} - M_{p4})^2}{L - M_{12}}, \tag{5.32}$$

and F_{x12} (= F_{x21}) is the additional drag resulting from the cross-connection:

$$F_{x12} = -\frac{I_s^2}{16}\frac{vv_{c2}}{v^2 + v_{c2}^2}\frac{\pi/\tau[(M_{p1} + M_{p2}) - (M_{p3} + M_{p4})]^2}{L + M_{12}}. \tag{5.33}$$

Because the magnetic drag in the left-hand side, $F_{x11} + F_{x12}$, is not equal to the drag in the right-hand side, $F_{x22} + F_{x21}$, when a lateral displacement occurs, dynamic instability may exist in the yaw modes. The guidance force can also be expressed as:

$$F_y = F_{y11} + F_{y12} + F_{y22} + F_{y21}, \tag{5.34}$$

where F_{y11} and F_{y22} are the guidance forces produced by the figure-eight-shaped null-flux coils on the left- and right-hand sides, respectively, when the two coils are not cross-connected:

$$F_{y11} = -\frac{I_s^2}{4}\frac{v^2}{v^2 + v_{c1}^2}\frac{(M_{p1} - M_{p2})}{L - M_{12}}\left(\frac{\partial M_{p1}}{\partial y_1} - \frac{\partial M_{p2}}{\partial y_1}\right) \tag{5.35}$$

and

$$F_{y22} = -\frac{I_s^2}{4}\frac{v^2}{v^2 + v_{c1}^2}\frac{(M_{p3} - M_{p4})}{L - M_{12}}\left(\frac{\partial M_{p3}}{\partial y_2} - \frac{\partial M_{p4}}{\partial y_2}\right). \tag{5.36}$$

F_{y12} and F_{y21} are the guidance forces resulting from the cross-connection; they are the major guidance forces, depending upon the lateral displacement and following the principle of null-flux suspension. F_{y12} and F_{y21} are given by

$$F_{y12} = -\frac{\Gamma_s^2}{8}\frac{v^2}{v^2 + v_{c2}^2}\frac{(M_{p1} + M_{p2} - M_{p3} - M_{p4})}{L + M_{12}} \times \left(\frac{\partial M_{p1}}{\partial y_1} + \frac{\partial M_{p2}}{\partial y_1}\right) \tag{5.37}$$

and

$$F_{y21} = \frac{\Gamma_s^2}{8}\frac{v^2}{v^2 + v_{c2}^2}\frac{(M_{p1} + M_{p2} - M_{p3} - M_{p4})}{L + M_{12}} \times \left(\frac{\partial M_{p3}}{\partial y_2} + \frac{\partial M_{p4}}{\partial y_2}\right). \tag{5.38}$$

In Equations 5.26 through 5.38, v_{c1} and v_{c2} are the characteristic speeds, which are defined as the speeds at which the magnetic drags F_{x11}, F_{x22}, and F_{x12}, F_{x21} approach their peaks, respectively. As a result of cross-connection, two major drag forces exist: one associated with vertical displacement and characterized by v_{c1}, and another associated with lateral displacement and characterized by v_{c2}. They are

$$v_{c1} = \frac{\tau R}{\pi(L - M_{12})} \tag{5.39}$$

and

$$v_{c2} = \frac{\tau R}{\pi(L + M_{12})}. \tag{5.40}$$

Until now, all magnetic forces for the cross-connected null-flux suspension system have been derived in terms of dynamic circuit parameters on the basis of harmonic approximation. These relations are straightforward and easy to use, because they are not a function of time. One need only determine the mutual inductances between one SCM and one loop of the null-flux coil at a fixed longitudinal coordinate, or at a plane transverse to the motion, and then determine the derivatives of the mutual inductance with respect to the lateral and vertical displacements.

5.4 Example And Discussion

To better understand the performance of the cross-connected figure-eight-shaped null-flux coil suspension system, it is helpful to consider a numerical example. Table 5.1 lists the dimensions and other parameters used in the example, which are similar to those used in a paper by Tanaka.[3]

TABLE 5.1 Data Used for the Example

Parameter	Specification
Superconducting Magnet	
Length (m)	1.7
Height (m)	0.5
Current (kA)	700
Figure-eight-shaped null-flux coil	
Length (m)	0.55
Height/loop (m)	0.31
Cross-section/conductor (cm^2)	1
Number of turns	36
Vertical space between the two loop centers (m)	0.42
Conductivity of Al ($m^{-1}\Omega^{-1}$)	3×10^7
Resistance/loop R (mΩ)	20.64
Inductance/loop L (mH)	0.88
Mutual inductance between upper and lower loops (mH)	-65.8

Assuming a pole pitch of 2 m for the SCM and a vehicle speed of 138 m/s, one obtains v_{c1} = 13.9 m/s and v_{c2} = 16.1 m/s. The time constant of the null-flux coil is about 42.6 ms.

Figure 5.6 shows the dependence of the null-flux lift force components on the vertical displacement, with a lateral displacement of -5 cm and an effective air gap of 20 cm. One can see that the lift forces F_{z11} and F_{z22} are dominant. As expected, the lift components, F_{z12} and F_{z21}, that arise because of the cross-connection, are relatively small. Note that F_{z11} is much larger than F_{z22} because the lateral displacement of -5 cm makes the air gap on the left-hand side decrease to 15 cm and that on the right-hand side increase to 25 cm. Clearly, such a large force difference between two null-flux coils could lead to a rolling motion. The cross-connection between the two figure-eight-shaped coils may reduce such rolling motion slightly, because F_{z12} is negative and F_{z21} is positive. The dimensions of the figure-eight-shaped null-flux coil and SCM may be designed to increase $F_{z12}$and F_{z21} and to improve vehicle stability. The lateral displacement could be encountered while making a turn with the center of curvature to the right. The induced roll is in the correct direction for passenger comfort.

The guidance force as a function of vertical displacement at a lateral displacement of -5 cm is illustrated in Figure 5.7. One can see that a guidance force of about 5 kN ($F_{y12} + F_{y21}$), resulting from the cross-connection, is obtained at zero vertical displacement. The main advantage of the cross-connected null-flux coil suspension system over a conventional null-flux suspension system is that the former provides null-flux guidance for a large range of vertical displacements, including the vertical null-flux position. The guidance forces F_{y11} and F_{y22}, resulting from the

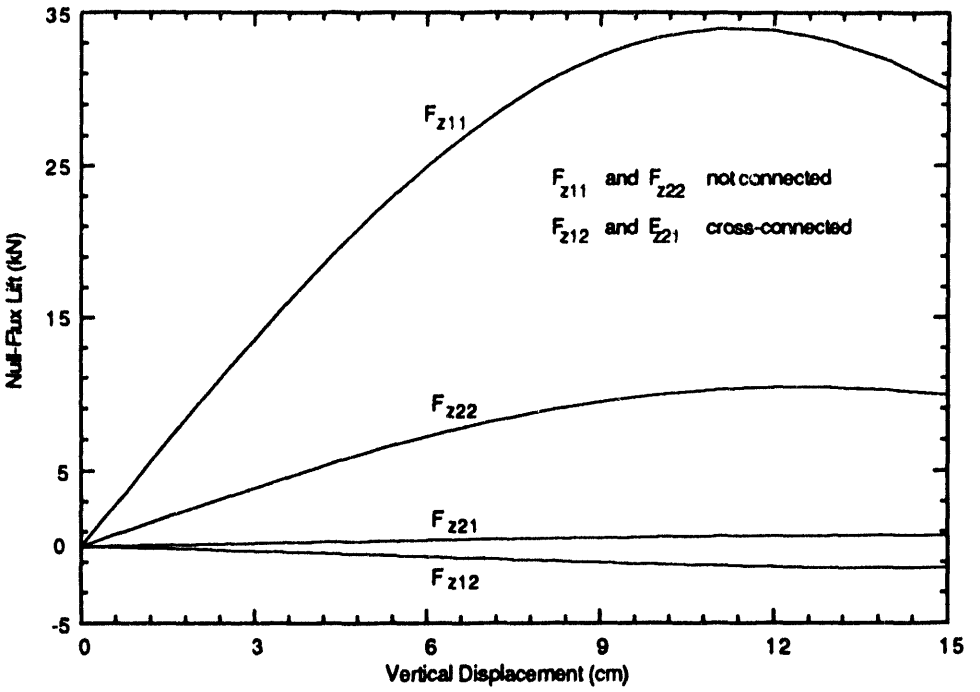

FIGURE 5.6 Null-Flux Force Components as a Function of Vertical Displacement (Speed: 138 m/s; Effective Gap: 20 cm; Lateral Shift: 5 cm) (See Table 5.1 for Other Parameters)

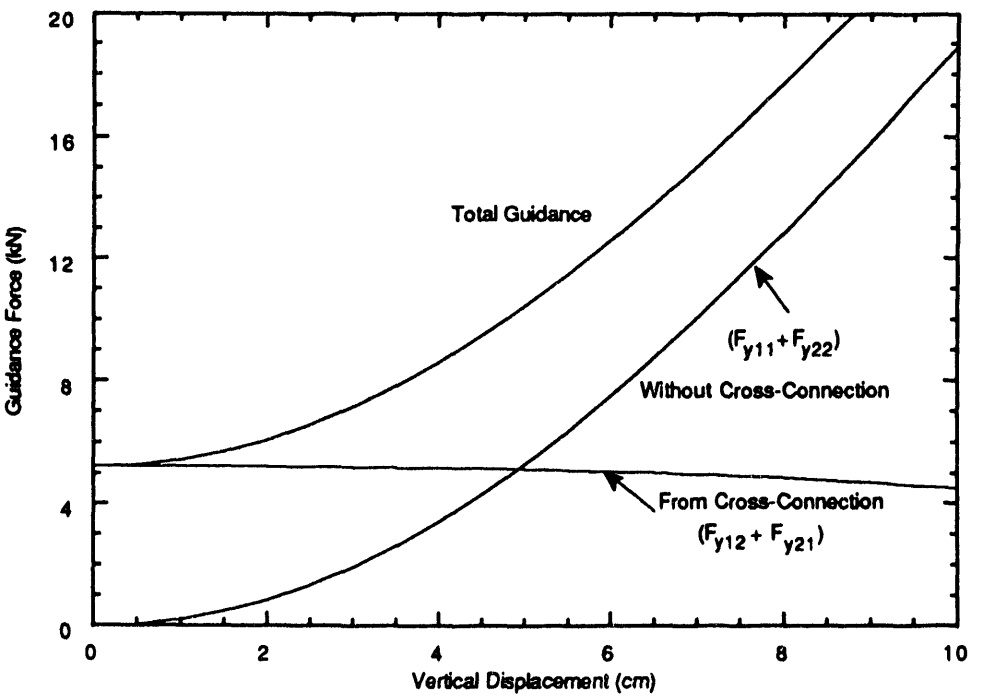

FIGURE 5.7 Guidance Force Components vs. Vertical Displacement (See Table 5.1 and Figure 5.6 for Other Parameters)

difference of air gap without cross-connection, depend upon the vertical displacement. They are relatively small at a small vertical displacement and increase rapidly at a large vertical displacement. Both guidance forces reach the same value at a vertical displacement of about 5 cm. Because a maglev vehicle usually operates at a relatively small vertical displacement, such as 2 to 4 cm, one can conclude that the guidance forces resulting from the cross-connection are dominant for normal maglev operations.

Total lift and guidance forces, lift-to-drag ratio, and guidance-to-drag ratio as a function of vertical displacement at a lateral displacement of 5 cm are illustrated in Figure 5.8. The lift-to-drag ratio has a maximum value of 140 at about 2 cm vertical displacement, while the maximum value of the guidance-to-drag ratio appears at a zero vertical displacement.

Figure 5.9 shows the dependence of the lift-to-drag ratio on vertical displacement, with lateral displacement as a parameter. The lift-to-drag ratio decreases monotonically as the lateral displacement increases, regardless of the vertical displacement. On the other hand, for a fixed value of lateral displacement, the ratio goes through a maximum value as the vertical displacement increases. That is, at small vertical displacements, as the vertical displacement approaches zero the drag force increases in magnitude relative to the lift force (also see Figure 5.8). Only in the case where the lateral displacement is zero (Figure 5.9) does the drag force decrease relative to the lift

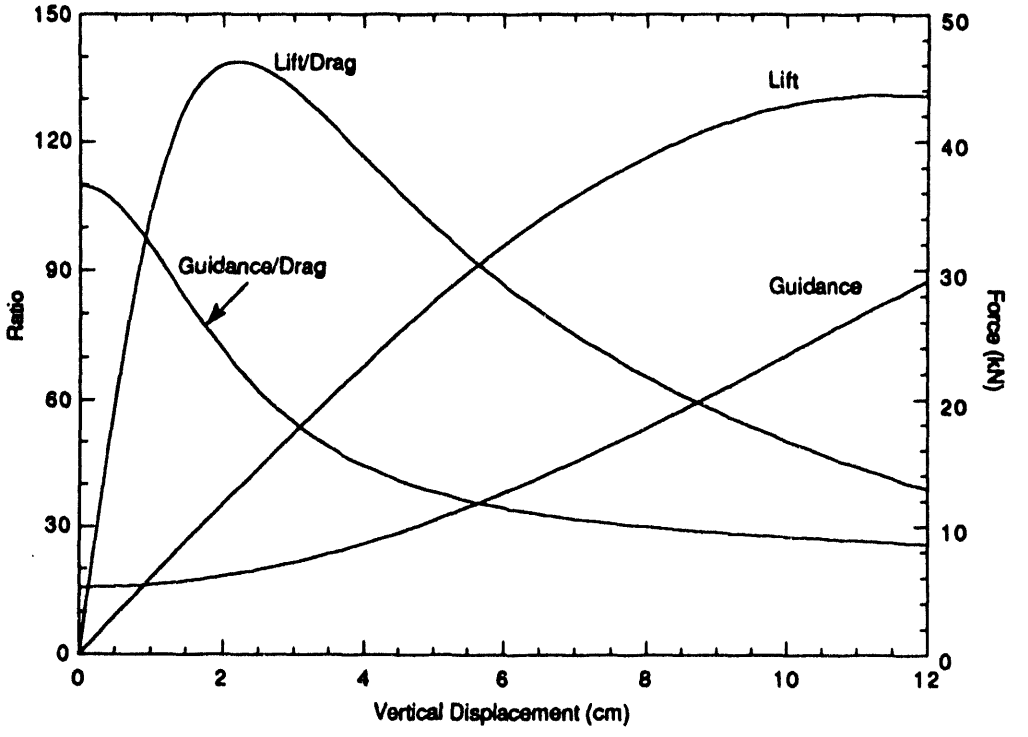

FIGURE 5.8 Total Lift, Guidance, Lift/Drag, and Guidance/Drag as Functions of Vertical Displacement (See Table 5.1 and Figure 5.6 for Other Parameter)

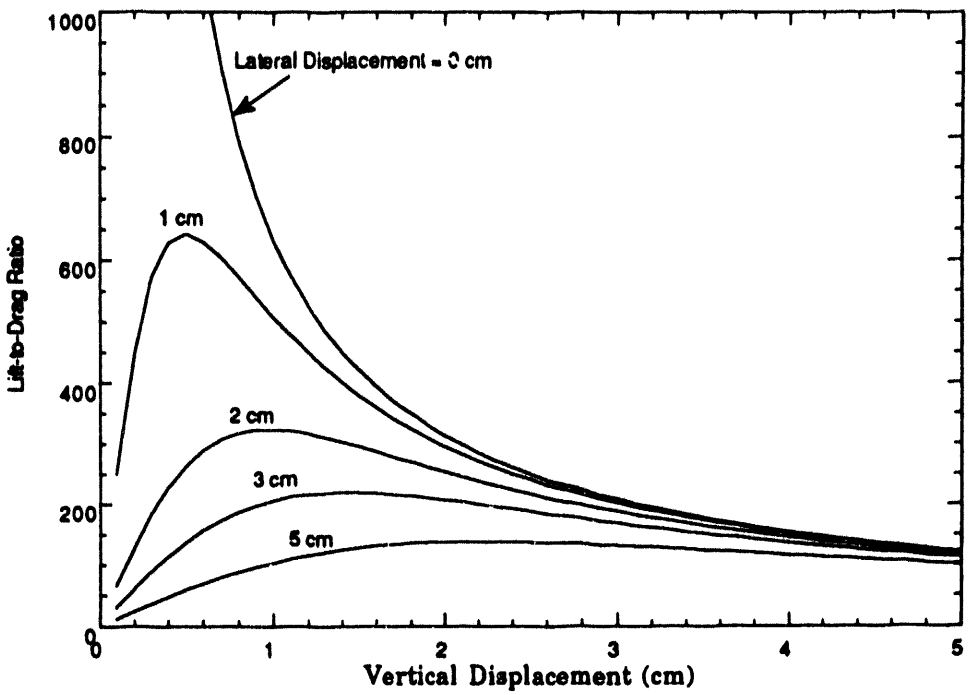

FIGURE 5.9 Lift-to-Drag Ratio Profile as a Function of Vertical Displacement, with Lateral Offset as a Parameter (Speed: 138 m/s; Effective Gap: 20 cm)

force, as the vertical displacement approaches zero or lift-to-drag ratio approaches infinite. This is in contrast to the case where no cross-connection exists. In the latter case, the drag force diminishes in magnitude relative to the lift force as the vertical displacement approaches zero, regardless of the lateral displacement.

Guidance force as a function of lateral displacement, with vertical displacement as a parameter, is shown in Figure 5.10. Both the guidance force and lateral stiffness increase as the vertical displacement increases. Maximum guidance forces are about 13 kN for a zero vertical displacement and about 20 kN for a 3-cm vertical displacement.

Figure 5.11 shows the dependence of lift and guidance forces acting on each SCM on lateral displacement at a vertical displacement of 3 cm. A large change in lift can be observed as the maglev vehicle is displaced laterally, while the guidance force changes are rather small. This implies that the lateral stiffnesses of the two forces are very different. Figure 5.12 shows the dependence of lift, guidance, and drag forces on lateral displacement, where all forces are minimal at the lateral equilibrium and increase as the lateral displacement increases. In particular, the drag force increases faster than the other two forces.

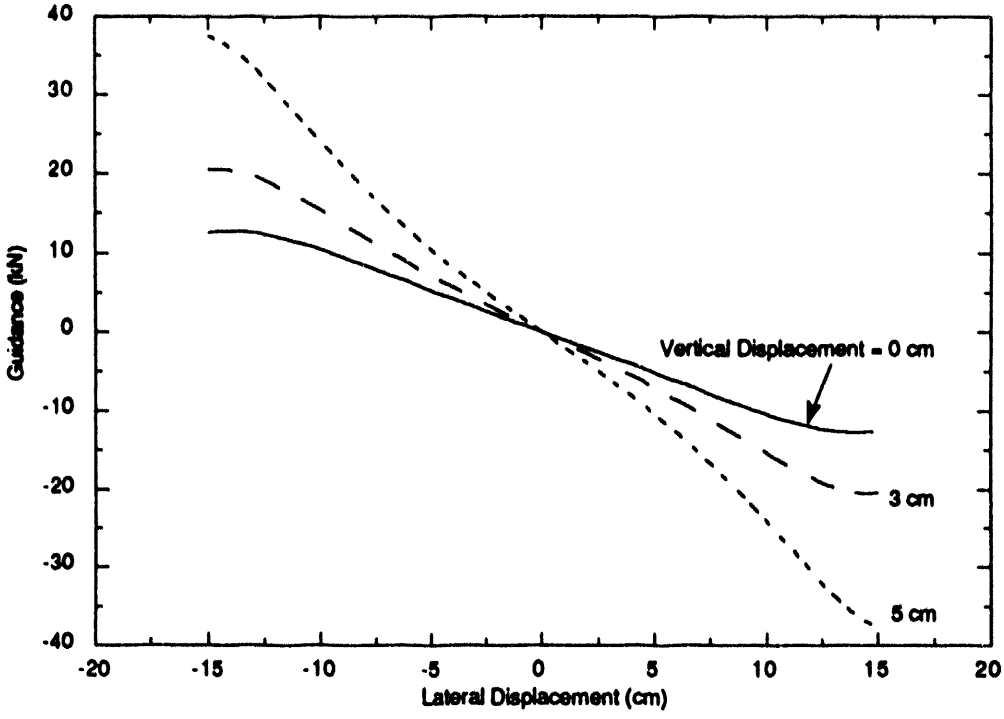

FIGURE 5.10 Total Guidance Force vs. Lateral Displacement, with Vertical Displacement as a Parameter (Speed: 138 m/s; Effective Gap: 20 cm) (Ref. Table 5.1)

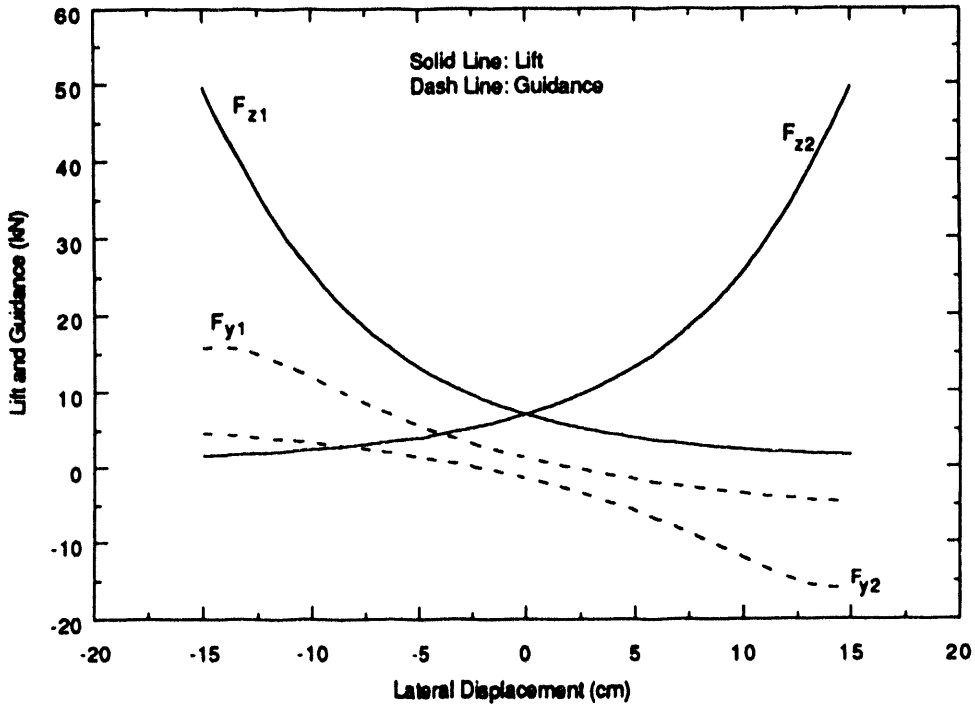

FIGURE 5.11 Lift and Guidance Force Acting on Left- and Right-Hand-Side SCMs as a Function of Lateral Displacement (Speed: 138 m/s; Effective Gap: 20 cm; Vertical Offset: 3 cm)

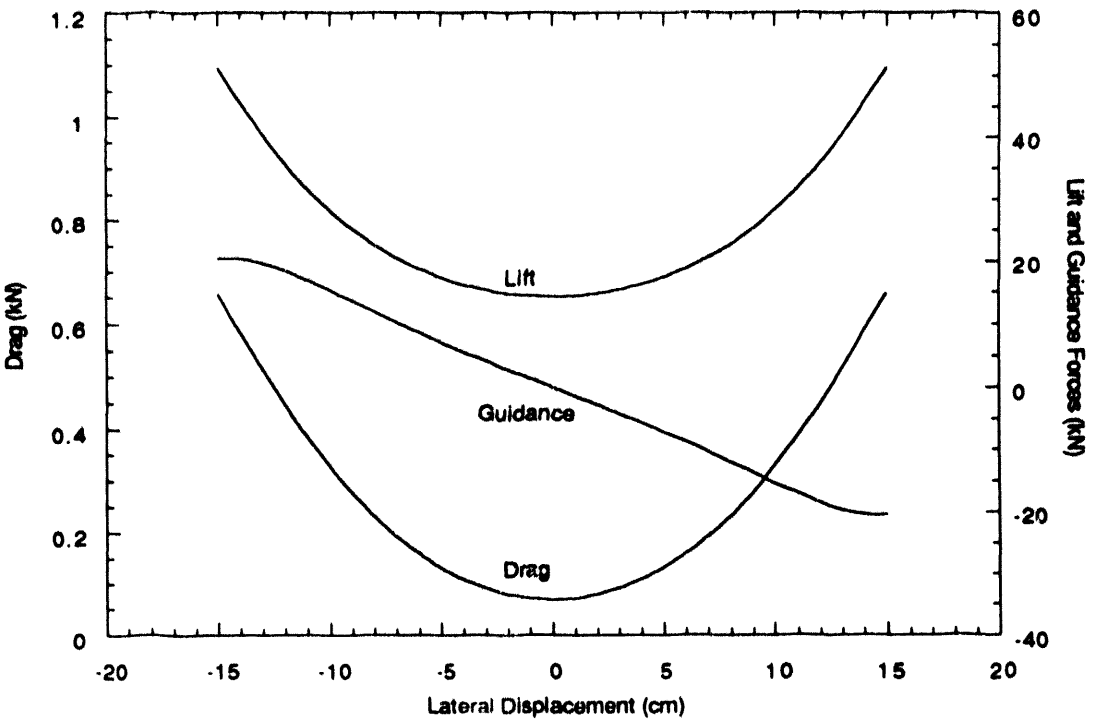

FIGURE 5.12 Lift, Guidance, and Drag Forces as a Function of Lateral Displacement

Assuming a coil pitch of 0.7 m for the figure-eight-shaped null-flux coil, and a pole pitch of 2.1 m for the SCMs aboard the vehicle, one obtains a pitch ratio (SCM pole pitch over coil pitch) of 3. Thus, the total lift force from the interaction between a pair of SCMs and two rows of cross-connected, figure-eight-shaped null-flux coils would be three times greater than that discussed above. According to Figure 5.8, the lift force acting on a pair of SCMs at a vertical displacement of 3 cm is about 51 kN. Twelve such SCMs can lift 31 metric tons at a vertical displacement of 3 cm and 21.5 metric tons at a vertical displacement of 2 cm. The guidance force associated with the twelve-SCM vehicle at a lateral displacement of 5 cm is about 13 metric tons for a 3-cm vertical displacement and 11 metric tons for a 2-cm vertical displacement.

5.5 Conclusions

A simple dynamic circuit model for the cross-connected, figure-eight-shaped null-flux coil suspension system has been developed. The model can be used for the determination of both transient and steady-state performance of the cross-connected, null-flux coil levitation and guidance system. The closed-form expressions for the magnetic force components are obtained on the basis of a harmonic approximation. These simple relations are useful for vehicle dynamic stability studies. Numerical results show that a cross-connected, null-flux suspension system has many advantages over the conventional null-flux coil levitation system. In particular, such a system can

provide null-flux guidance at any vertical displacement. On the other hand, in contrast to the non cross-connected system, there is only one point where the drag force goes to zero; namely, when both the lateral and vertical displacements are zero.

5.6 References

1. Fujiwara, S. and T. Fujimoto, 1989, "Characteristics of the Combined Levitation and Guidance System Using Ground Coils on the Side Wall of the Guideway," Proceedings of the International Conference on Maglev '89, July, pp. 241-244.

2. Fujie, J., 1991, "Current Status of Superconducting Maglev System," Journal of the International Superconductivity Technology Center, Vol. 4, No. 4, pp. 40-43.

3. Tanaka, H., 1991, "Change in the Coil Distribution of Electrodynamic Suspension System," Proceedings of the International Symposium on Magnetic Suspension Technology, NASA Hampton, Va., Aug. 19-23, pp. 813-825.

4. He, J.L. and D.M. Rote, 1992, "Computer Model Simulation of Null-Flux Magnetic Suspension and Guidance," Selected Proceedings of the Sixth World Conference on Transport Research, Vol. IV, June 29 - July 3, pp. 3087-3097.

5. He, J.L., D.M. Rote, and H.T. Coffey, 1991, "Computation of Magnetic Suspension of Maglev System Using Dynamic Circuit Theory," Proceedings of the International Symposium on Magnetic Suspension Technology, Hampton, Va., NASA Conference Publication 3152, Aug. 19-23, pp. 919-938.

6 Analysis of the Combined Null-Flux Coil Propulsion, Levitation, and Guidance System

This chapter presents an analysis of a Japanese maglev system that uses only one set of coils in the guideway for combined propulsive, levitational, and guidance functions. Our preliminary study, which uses the dynamic circuit approach, indicates that the system appears very promising.

6.1 Introduction

The updated Japanese EDS maglev system invented by Fujiwara et al. uses a combined propulsion and null-flux suspension concept, in which two rows of figure-eight-shaped null-flux coils are mounted on the side walls of the guideway and are cross-connected.[1-3] The coils on each side wall are connected in a three-phase configuration and energized by a power supply. Four groups of superconducting magnets aboard the vehicle interact with these null-flux coils on the guideway to generate propulsive, null-flux levitational, and null-flux guidance forces. The concept has many potential advantages over existing EDS maglev systems. In particular, it requires only one set of guideway coils to perform the three functions, which could greatly reduce guideway costs.

To date, the system has not been studied in sufficient detail to determine if it really works and performs well. In this chapter, the dynamic circuit approach is used to investigate the system and predict its performance. The use of dynamic circuit theory, in combination with numerical analysis, to deal with the null-flux EDS maglev system has been discussed in previous papers.[4-6] This discussion emphasizes the combined functions of propulsion, levitation, and guidance and the coupling effects among these functions. Simple closed-form formulas for the magnetic forces are obtained on the basis of a harmonic approximation. For the purpose of proving the concept and obtaining physical insight, only the fundamental wave in the longitudinal direction (direction of motion) is considered. However, to ensure that the analysis is accurate, a numerical approach is also applied to the lateral and vertical motions.

6.2 The Dynamic Circuit Model

To study the combined propulsion, levitation, and guidance system, it is necessary to consider a complete motor section (an energized guideway block). In a long-stator propulsive system, the energized block length is generally longer than that of the vehicle magnet system. One may divide the block length into two sections: one that couples with the magnet system of the vehicle and another that comprises the balance of the block. Letting n_b be the total number of poles in the block, n_m the number of poles that couple with the vehicle magnet system, and t the pole pitch of the vehicle magnet system, one can express the length of the energized block and the length of the vehicle magnet system as $n_b t$ and $n_m t$, respectively. In a three-phase system, each pole interacts with three figure-eight-shaped guideway coils, so that each figure-eight-shaped

null-flux coil is in different phase. Figure 6.1 depicts the combined propulsion, levitation, and guidance system. Two rows of figure-eight-shaped coils on opposite sides are cross-connected to form a null-flux guidance system, and the coils in the same row are connected in series to form three-phase propulsion windings. Thus, the three functions of propulsion, levitation, and guidance are expected to be achieved with one set of figure-eight-shaped guideway coils.

As is discussed in Section 5.2.1 and in Reference 4, a figure-eight-shaped coil interacting with an SCM can be represented by an equivalent circuit having two branches connected in parallel. Each branch has a resistance R, a self-inductance L, and an induced voltage E. At the null-flux position, there is no circulating current or magnetic force because the induced voltages in each branch are equal. A circulating current flows through the branches, and a net force is generated, if a vertical displacement exists between the SCM and the null-flux coil. Similarly, as discussed in Section 5.2.2, two cross-connected, figure-eight-shaped coils can be represented by a circuit containing four branches connected in parallel, each of which represents a single loop of the figure-eight-shaped coils.[4] Null-flux lift and guidance forces are generated when circulating currents exist. By applying the information provided in Reference 4, one can represent one phase of the combined system shown in Figure 6.1 by an equivalent circuit, as shown in Figure 6.2. In Figure 6.2, R and L_e are the resistance and the equivalent inductance of a loop of the figure-eight-shaped coil and $\mathbf{E}_1$, $\mathbf{E}_2$, $\mathbf{E}_3$, and $\mathbf{E}_4$ represent the phasor voltages induced in the loop. The terms $\mathbf{E}_1$, $\mathbf{E}_2$, $\mathbf{E}_3$, and $\mathbf{E}_4$ are also called the "armature voltages" or "induced voltages." The terms n_b and n_m are used to modify the circuit for phase representation. The equivalent circuit consists of two parts: the left part, representing the figure-eight-shaped coils per phase that couple with the magnet system of the vehicle, and the right part, representing the remaining guideway coils per phase that do not couple with the magnet system of the vehicle. The system can be viewed as four linear synchronous motors operating in parallel. (That is, the upper loops of the figure-eight-shaped coils form one motor on each side, and the lower loops of the coils form another motor on each side.) The terms $\mathbf{I}_1$, $\mathbf{I}_2$ $\mathbf{I}_3$, and $\mathbf{I}_4$ are the phasor currents flowing in each loop of the figure-eight-shaped coils. They are also the currents flowing in four different motors because the loop coils belonging to the same phase are connected in series. The sum of $\mathbf{I}_1$, $\mathbf{I}_2$, $\mathbf{I}_3$, and $\mathbf{I}_4$ is the phase current that produces propulsive force, and the differences between $\mathbf{I}_1$ and $\mathbf{I}_2$ and between $\mathbf{I}_3$ and $\mathbf{I}_4$ generate null-flux lift. The null-flux guidance force is generated from the current difference between the sum of $\mathbf{I}_1$ and $\mathbf{I}_2$ and the sum of $\mathbf{I}_3$ and $\mathbf{I}_4$.

To determine the currents flowing in each branch, one can use the Thevenin equivalent circuit technique to simplify Figure 6.2. Thus, a simple, equivalent-circuit model for the combined system is formed, as shown in Figure 6.3, where R_{ph} and X_{ph} are the resistance and reactance for each equivalent phase and E_{ph} and V_{ph} are the induced and applied phase voltages, respectively. They are

$$R_{ph} = \frac{1}{4} n_b R, \tag{6.1}$$

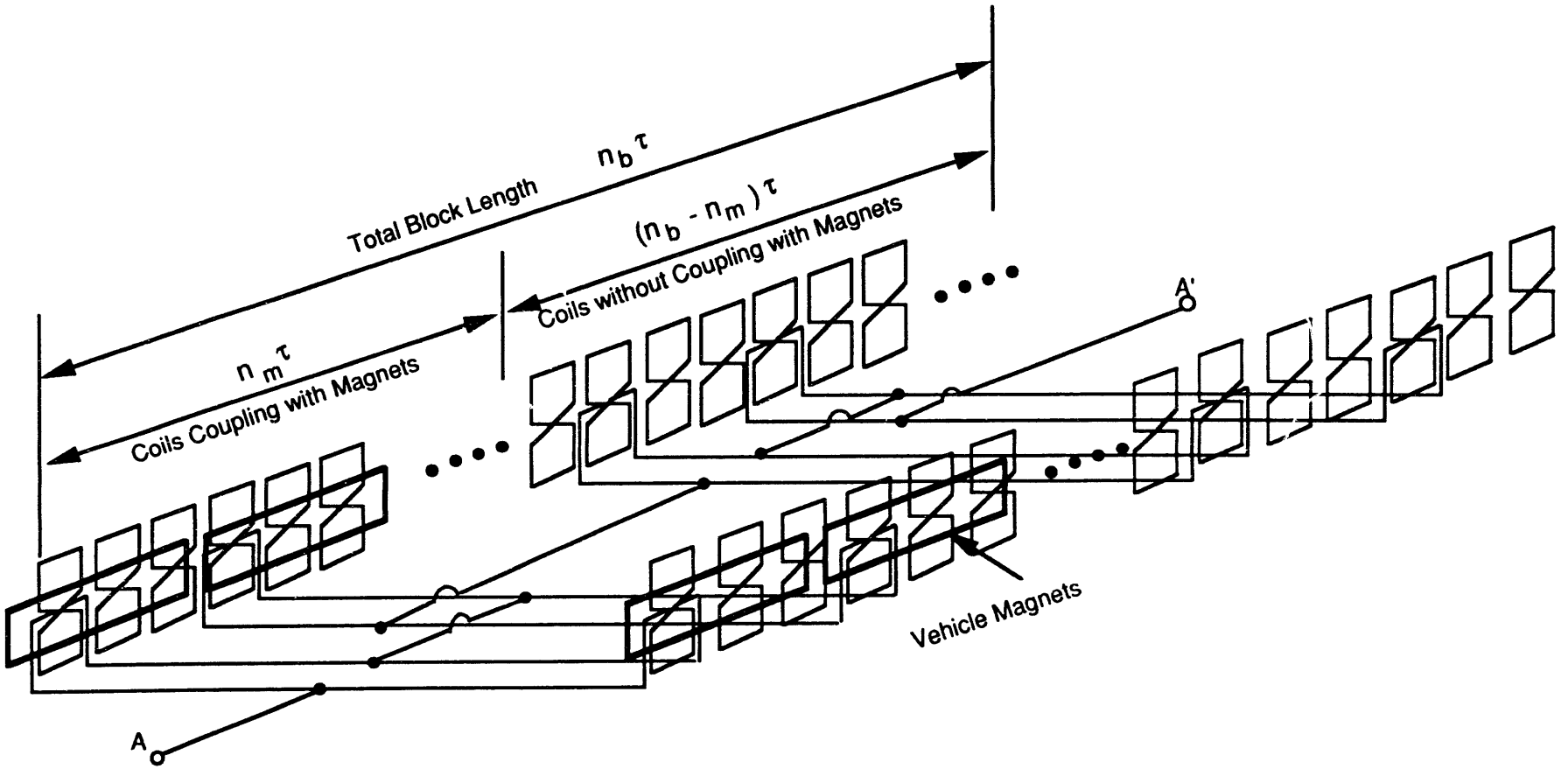

FIGURE 6.1 A Sketch of the Combined Propulsion, Levitation, and Guidance System

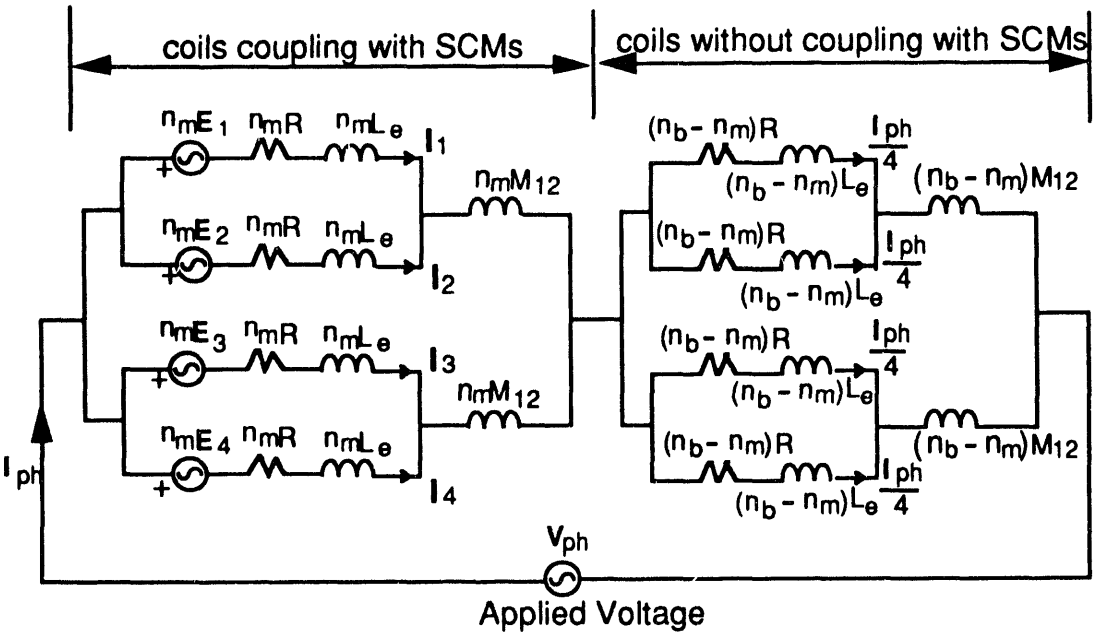

FIGURE 6.2 One-Phase Circuit Diagram of the Combined System

$$x_{ph} = \frac{1}{4} n_b x'_e, \qquad (6.2)$$

and

$$\mathbf{E}_{ph} = \frac{n_m}{4} (\mathbf{E}_1 + \mathbf{E}_2 + \mathbf{E}_3 + \mathbf{E}_4), \qquad (6.3)$$

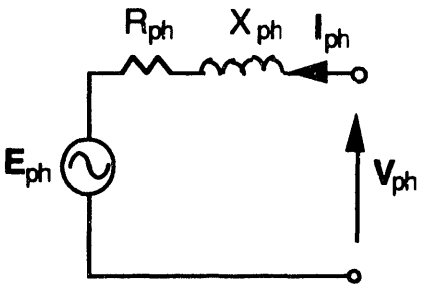

FIGURE 6.3 Equivalent Circuit

where $x'_e = \omega (L + M_{12} - M_{ab})$ of which M_{12} is the mutual inductance between the upper and lower loops and M_{ab} is the mutual inductance between the two longitudinal neighboring loops that belong to different phases. (M_{12} and M_{ab} are negative because the two loops are in parallel.) Note that $\mathbf{E}_1$, $\mathbf{E}_2$, $\mathbf{E}_3$, and $\mathbf{E}_4$ are in phase, although their amplitudes may differ, because the two cross-connected figure-eight-shaped coils experience the same SCM phase as the vehicle moves forward. Thus, one can conclude from Equation 6.3 that $\mathbf{E}_{ph}$ is in phase with $\mathbf{E}_1$, $\mathbf{E}_2$, $\mathbf{E}_3$, and $\mathbf{E}_4$. By taking the applied voltage $\mathbf{V}_{ph}$ as a reference phasor, one can introduce a power angle δ by which the induced voltage $\mathbf{E}_{ph}$ lags $\mathbf{V}_{ph}$. Thus, Equation 6.3 may be rewritten as

$$\mathbf{E}_{ph} = E_{ph} e^{-j\delta} = \frac{n_1}{4} (\mathbf{E}_1 + \mathbf{E}_2 + \mathbf{E}_3 + \mathbf{E}_4)\, e^{-j\delta}. \qquad (6.4)$$

The root mean square (rms) value of the induced voltage may also be expressed in terms of the mutual inductance between the moving SCM and the loop coil

$$\mathbf{E}_i = \frac{1}{\sqrt{2}} I_s \omega \mathbf{M}_{si} \qquad i=1,4\ . \tag{6.5}$$

The flux linking the figure-eight-shaped coils lags the induced voltage by 90°. Dividing the flux by the SCM current (which is assumed to be constant), one can express the mutual inductances and their derivatives in phasor notation

$$\mathbf{M}_{si} = -jM_{si}e^{-j\delta}, \tag{6.6}$$

$$\frac{\partial \mathbf{M}_{si}}{\partial x} = \beta M_{si}e^{-j\delta}, \tag{6.7}$$

$$\frac{\partial \mathbf{M}_{si}}{\partial y} = -j\frac{\partial M_{si}}{\partial y}e^{-j\delta}, \tag{6.8}$$

and

$$\frac{\partial \mathbf{M}_{si}}{\partial z} = -j\frac{\partial M_{si}}{\partial z}e^{-j\delta}, \tag{6.9}$$

where $\beta = \pi/\tau$ and M_{si} (i = 1,4) are functions of y and z, depending upon vertical and lateral vehicle motions, as shown in Figure 6.4.

The currents flowing in each branch of the circuit are then determined from Figures 6.2 and 6.3 as follows:

$$\mathbf{I}_{ph} = \frac{\mathbf{V}_{ph} - \mathbf{E}_{ph}}{R_{ph} + jx_{ph}}, \tag{6.10}$$

$$\mathbf{I}_1 = \frac{\mathbf{I}_{ph}}{4} + \frac{(\mathbf{E}_3 + \mathbf{E}_4) - (\mathbf{E}_2 + \mathbf{E}_1)}{4(R + jx_e')} + \frac{\mathbf{E}_2 - \mathbf{E}_1}{2(R + jx_e)}, \tag{6.11}$$

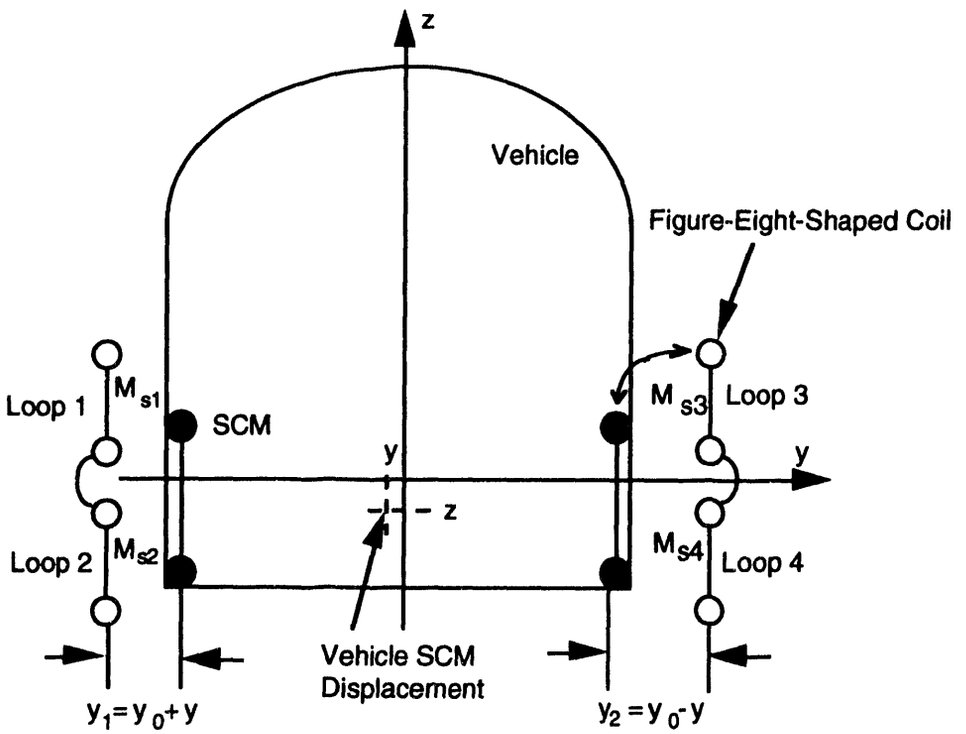

FIGURE 6.4 Vehicle Magnet and the Figure-Eight-Shaped Coil Relations (cross section)

$$\mathbf{I}_2 = \frac{\mathbf{I}_{ph}}{4} + \frac{(\mathbf{E}_3 + \mathbf{E}_4) - (\mathbf{E}_2 + \mathbf{E}_1)}{4(R + jx_e')} - \frac{\mathbf{E}_2 - \mathbf{E}_1}{2(R + jx_e)}, \tag{6.12}$$

$$\mathbf{I}_3 = \frac{\mathbf{I}_{ph}}{4} - \frac{(\mathbf{E}_3 + \mathbf{E}_4) - (\mathbf{E}_2 + \mathbf{E}_1)}{4(R + jx_e')} + \frac{\mathbf{E}_4 - \mathbf{E}_3}{2(R + jx_e)}, \tag{6.13}$$

and

$$\mathbf{I}_4 = \frac{\mathbf{I}_{ph}}{4} - \frac{(\mathbf{E}_3 + \mathbf{E}_4) - (\mathbf{E}_2 + \mathbf{E}_1)}{4(R + jx_e')} - \frac{\mathbf{E}_4 - \mathbf{E}_3}{2(R + jx_e)}. \tag{6.14}$$

Equations 6.11 through 6.14 show that each current contains three terms: The first term is associated with the applied voltage, the second term deals with the lateral motion, and the third term results from vertical motion. Subtracting Equation 6.12 from 6.11 and Equation 6.14 from 6.13, one obtains the currents circulating in the figure-eight-shaped coils as

$$\mathbf{I}_1 - \mathbf{I}_2 = \frac{\mathbf{E}_2 - \mathbf{E}_1}{(R + jx_e)} \tag{6.15}$$

and

$$\mathbf{I}_3 - \mathbf{I}_4 = \frac{\mathbf{E}_4 - \mathbf{E}_3}{(R + jx_e)}. \tag{6.16}$$

These internal circulating currents, which depend upon the vertical displacement to produce null-flux lift, are generally not affected by the propulsive and guidance currents. By adding Equations 6.11 to 6.14, one obtains the propulsive current, I_{ph}, resulting from the applied voltage. This implies that the propulsive force is not affected by the levitational and guidance currents. Similarly, one can also show that the null-flux guidance current is independent of the propulsive and levitational currents:

$$(\mathbf{I}_1 + \mathbf{I}_2) - (\mathbf{I}_3 + \mathbf{I}_4) = \frac{(\mathbf{E}_3 + \mathbf{E}_4) - (\mathbf{E}_2 + \mathbf{E}_1)}{2(R + jx_e)}. \tag{6.17}$$

The lateral displacement generates the voltage difference between the figure-eight-shaped coils on the two sides and produces the null-flux guidance force. It can be concluded from the above relations that the propulsive, levitational, and guidance currents of the combined system are independent from the viewpoint of the null-flux principle. However, it will be shown that small force couplings, those that do not follow the null-flux principle, do exist among the three functions.

6.3 The Propulsive Force

The propulsive force can be readily determined from the equivalent circuit shown in Figures 6.2 and 6.3. The total complex power, **S**, delivered to the combined system is

$$\mathbf{S} = P + jQ = \mathbf{V}_{ph}\mathbf{I}_{ph}^{*}, \tag{6.18}$$

where the real power is

$$P = 3\mathrm{Re}\left\{\mathbf{V}_{ph}\mathbf{I}_{ph}^{*}\right\} = 3\,V_{ph}\frac{R_{ph}\left(V_{ph} - E_{ph}\cos\delta\right) + x_{ph}E_{ph}\sin\delta}{R_{ph}^{2} + x_{ph}^{2}} \tag{6.19}$$

and the reactive power is

$$Q = 3\mathrm{Im}\left\{\mathbf{V}_{ph}\mathbf{I}_{ph}^{*}\right\} = 3\,V_{ph}\frac{x_{ph}\left(V_{ph} - E_{ph}\cos\delta\right) - R_{ph}E_{ph}\sin\delta}{R_{ph}^{2} + x_{ph}^{2}} \,. \tag{6.20}$$

The power factor of the combined system can be determined from Equations 6.19 and 6.20. Because the resistance of the system is much smaller than the reactance, it is a good approximation to neglect the resistance R. Thus, the real power absorbed from the electric power system is also the power delivered to the load. The converted mechanical power can then be obtained from Equation 6.19:

$$P = \mathrm{Re}\left\{\mathbf{E}_{ph}\mathbf{I}_{ph}^{*}\right\} = 3\frac{n_m}{n_b}\frac{V_{ph}(E_1 + E_2 + E_3 + E_4)}{x_e'}\sin\delta \,. \tag{6.21}$$

Equation 6.21 shows that the propulsive power of the combined system is given by the sum of the powers of the four individual linear motors, which have induced voltages of E_1, E_2, E_3, and E_4. The propulsive power is independent of internal circulating currents that generate null-flux levitational and guidance forces. Finally, the propulsive force is obtained in terms of the mutual inductances from Equations 6.5 and 6.21:

$$F_p = \frac{P}{v} = \frac{3}{\sqrt{2}}\frac{n_m}{n_b}\frac{M_{s1} + M_{s2} + M_{s3} + M_{s4}}{L + M_{12} - M_{ab}}\frac{V_{ph}I_s}{v}\sin\delta \,. \tag{6.22}$$

The simple relation shown in Equation 6.22 relates the propulsive force of the combined system to the system parameters. It is important to note that, for a given vehicle speed v, the propulsive force depends upon several major factors: (1) the ratio of the length of the vehicle magnet system to the length of the energized block, (2) the sum of the coupling coefficients between vehicle magnets and the guideway coils, (3) the applied voltage, and (4) the current flowing in the superconducting coils. Figures 6.5 and 6.6 show the dependence of the coupling coefficients on the vertical and lateral displacements, respectively. The sum of the four coupling coefficients is rather insensitive to the lateral and vertical motions of the vehicle. For the system indicated in Table 6.1, the calculated coupling sum coefficient is 1.4%, and the maximum thrust is

TABLE 6.1 Data Used for Numerical Example

Item	Value
Superconducting magnet	
Length (m)	1.5
Height (m)	0.5
Pole pitch (m)	1.6
Current (kN)	700
Figure-eight-shaped coil	
Length (m)	0.4
Height/loop (m)	0.3
Turns	42
Cross-section/turn (cm^2)	1
Space between two loops (between two conductor centers) (cm)	12
Vehicle information	
Magnet system length (m)	32
No. of magnets	40
Required propulsive force (kN)	200
Energized block length (m) (n_m = 20, n_b = 70)	112
Load angle	30°
Some predicted results	
Required phase voltage (kV)	9.9
Induced phase voltage (kV)	7.8
Phase current (kA)	1.2
Power factor (%)	77.6
Lift force at 2-cm vertical displacement (kN)	664
Guidance force at 4-cm lateral displacement (kN)	326

obtained at a power angle of 90°. Assuming a vehicle speed of 500 km/h (139 m/s), a magnet current of 700 kA, and a power angle of 30°, one obtains the following relation:

$$F_p = 75 \frac{n_m}{n_b} V_{ph} .$$

If one assumes a required propulsive force of 200 kN, the required phase voltage is 2.7 kV for $n_m/n_b = 1$, 5.3 kV for $n_m/n_b = 0.5$, and 10.7 kV for $n_m/n_b = 0.25$. In order to keep the applied phase voltage within 10 kV, this gives an energized block length of about 100 m for a vehicle having a 20- to 30-m-long magnet system.

6.4 The Levitational Force

The levitational force F_L is obtained from Equations 6.1 through 6.14 as

$$F_L = 3n_m I_s \mathrm{Re}\left\{\sum_1^4 \mathbf{I}_i \frac{\partial \mathbf{M}_{si}^*}{\partial z}\right\} = F_{LL} + F_{LP} + F_{LG}. \tag{6.23}$$

The force consists of three components: F_{LL}, resulting from the vertical displacement and following the null-flux principle; F_{LP}, resulting from the applied voltage; and F_{LG}, resulting from the lateral displacement. The term F_{LL}, in terms of mutual inductances and their derivatives, is given by

$$F_{LL} = \frac{3}{2\sqrt{2}} n_m I_s^2 \left\{ \frac{(M_{s2} - M_{s1})}{L_e}\left(\frac{\partial M_{s1}}{\partial z} - \frac{\partial M_{s2}}{\partial z}\right) + \frac{(M_{s4} - M_{s3})}{L_e}\left(\frac{\partial M_{s3}}{\partial z} - \frac{\partial M_{s4}}{\partial z}\right)\right\}. \tag{6.24}$$

For a vertical displacement of $z < 0$, $M_{s2} > M_{s1}$, $M_{s4} > M_{s3}$, the derivatives of M_{s1} and M_{s3} are positive and those of M_{s2} and M_{s4} are negative, but their amplitudes are of the same order, as shown in Figures 6.5 through 6.8. A positive null-flux lift is induced at a negative vertical displacement, independent of the lateral displacement.

The second term of the levitation force, F_{LP}, is given by

$$F_{LP} = 3I_s n_m \frac{V_{ph}\cos\delta - E_{ph}}{4x_{ph}}\left[\frac{\partial M_{s1}}{\partial z} + \frac{\partial M_{s2}}{\partial z} + \frac{\partial M_{s3}}{\partial z} + \frac{\partial M_{s4}}{\partial z}\right]. \tag{6.25}$$

This term depends upon the propulsive current flowing through the power source. It is also a function of vertical displacement. At zero vertical displacement, the sum of the mutual derivatives with respect to the vertical displacement is always zero, independent of the lateral displacement. In this case, F_{LP} disappears, independent of the propulsive current. Under normal operating conditions, a negative vertical displacement always exists. In this case, the sum of the mutual inductance derivatives (with respect to the vertical displacement) is positive, as shown in Figures 6.7 and 6.8. It follows that $F_{LP} > 0$ for $V_{ph}\cos\delta > E_{ph}$, which represents a lagging internal power factor, and $F_{LP} < 0$ for $V_{ph}\cos\delta < E_{ph}$, which represents a leading internal power factor. This lift-force component also can be viewed as a result of the edge effect between the upper and lower linear motors, which operate in parallel.

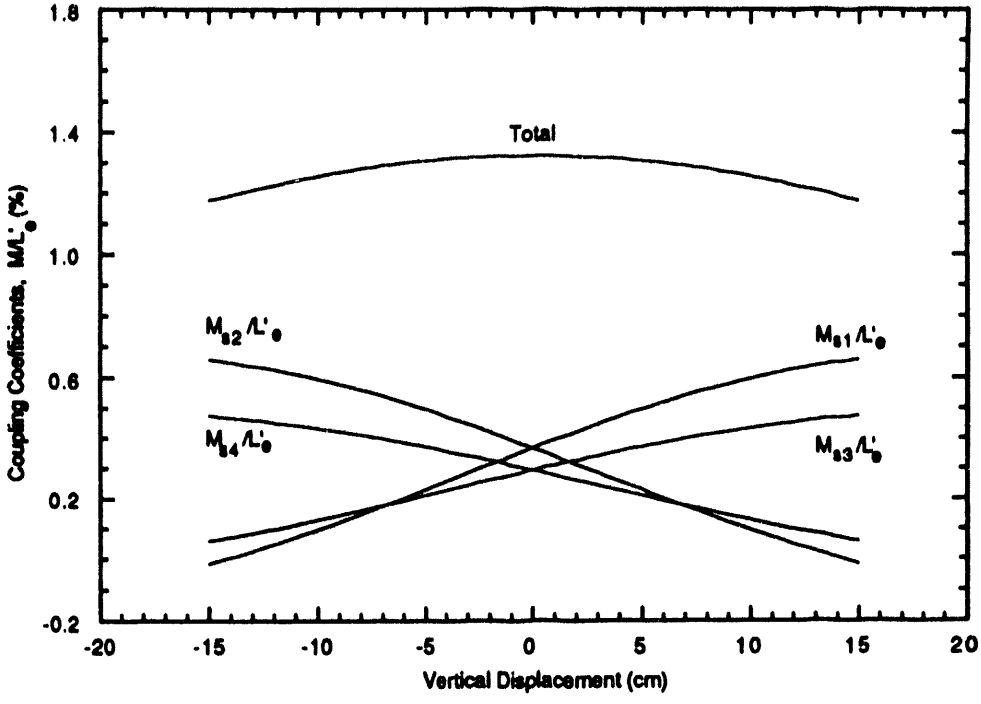

FIGURE 6.5 Coupling Coefficients as a Function of Vertical Displacement at a Lateral Displacement of -4 cm

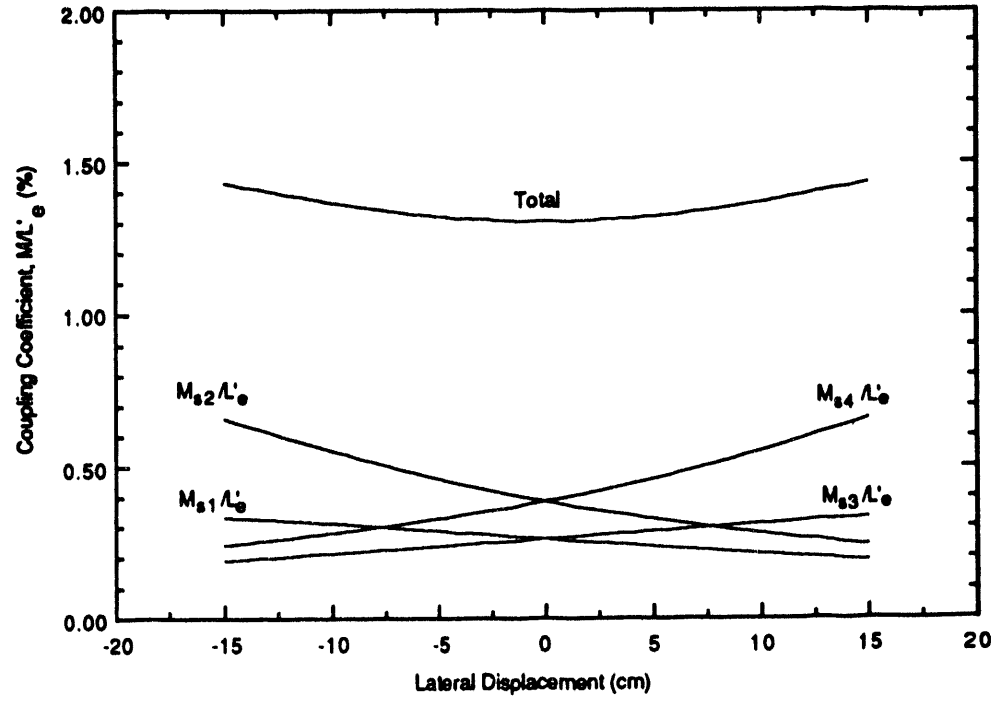

FIGURE 6.6 Coupling Coefficients as a Function of Lateral Displacement with a Vertical Displacement of -3 cm

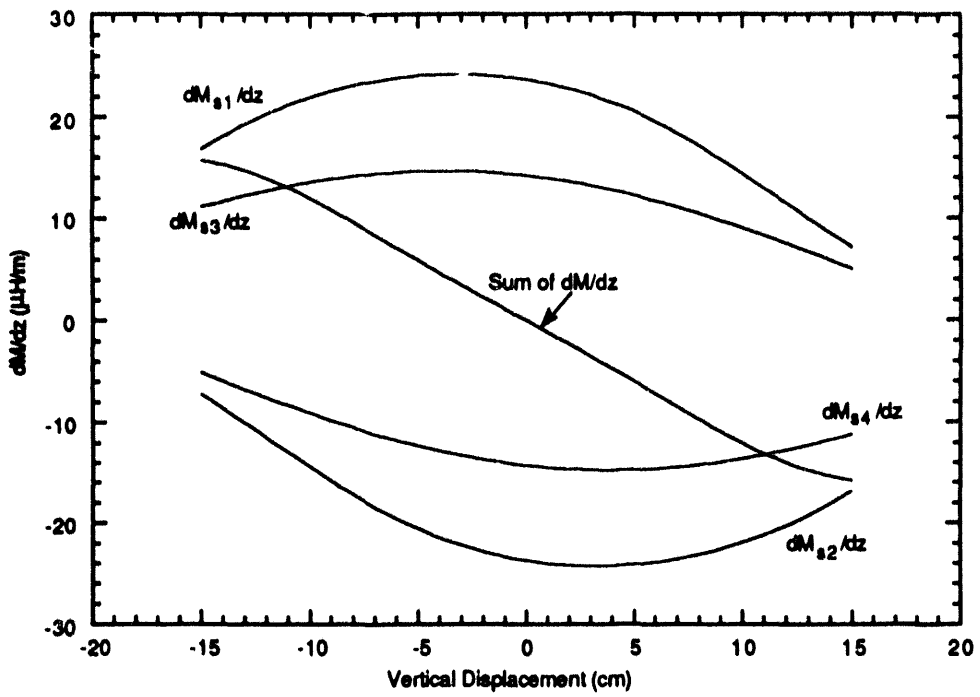

FIGURE 6.7 Derivative of Mutual Inductance with Respect to Vertical Displacement as a Function of Vertical Displacement at a Lateral Displacement of -4 cm

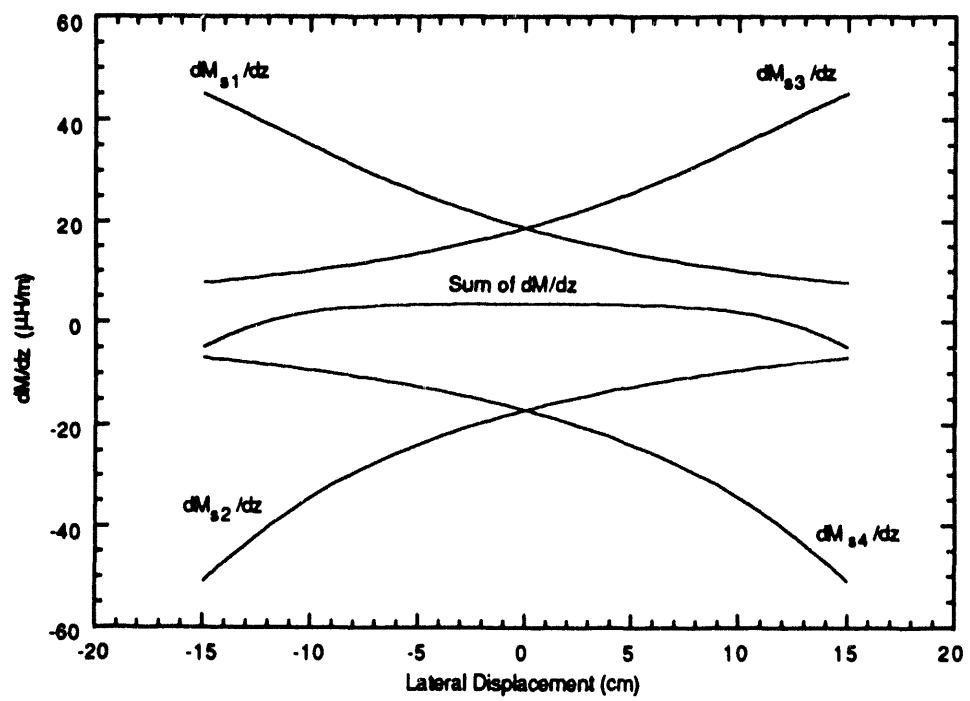

FIGURE 6.8 Derivative of Mutual Inductance with Respect to Vertical Displacement as a Function of Lateral Displacement at a Vertical Displacement of -3 cm

The third term of the levitational force, F_{LG} results from the vehicle's lateral displacement

$$F_{LG} = \frac{3}{4\sqrt{2}}\, n_m I_s^2 \left[\frac{(M_{s3} + M_{s4}) - (M_{s1} + M_{s2})}{L_e'}\right]\left[\left(\frac{\partial M_{s1}}{\partial z} + \frac{\partial M_{s2}}{\partial z}\right) - \left(\frac{\partial M_{s3}}{\partial z} + \frac{\partial M_{s4}}{\partial z}\right)\right]. \quad (6.26)$$

This term is very small because the derivatives of mutual inductances (M_{s1} and M_{s2}, with respect to vertical displacement) have opposite signs. M_{s3} and M_{s4} also have opposite signs as shown in Figures 6.5 through 6.8. F_{LG} may be positive or negative, depending upon the lateral displacement.

Figure 6.9 shows the levitational force components as a function of displacement at a lateral displacement of -4 cm. Clearly, F_{LL} is dominant and F_{LG} is negligible. The term F_{LP} is small at a small vertical displacement. In this computation, the required propulsive force is assumed to be 200 kN, the SCM current is 700 kA, the total number of vehicle SCMs is 40 (corresponding to $n_m = 20$), and the total energized block length is $n_b t = 112$ m. Other detailed information is given in Table 6.1. As shown in Figure 6.9, a vehicle of 60 to 70 metric tons can be levitated at a vertical displacement of about 2 cm (around 700 kN).

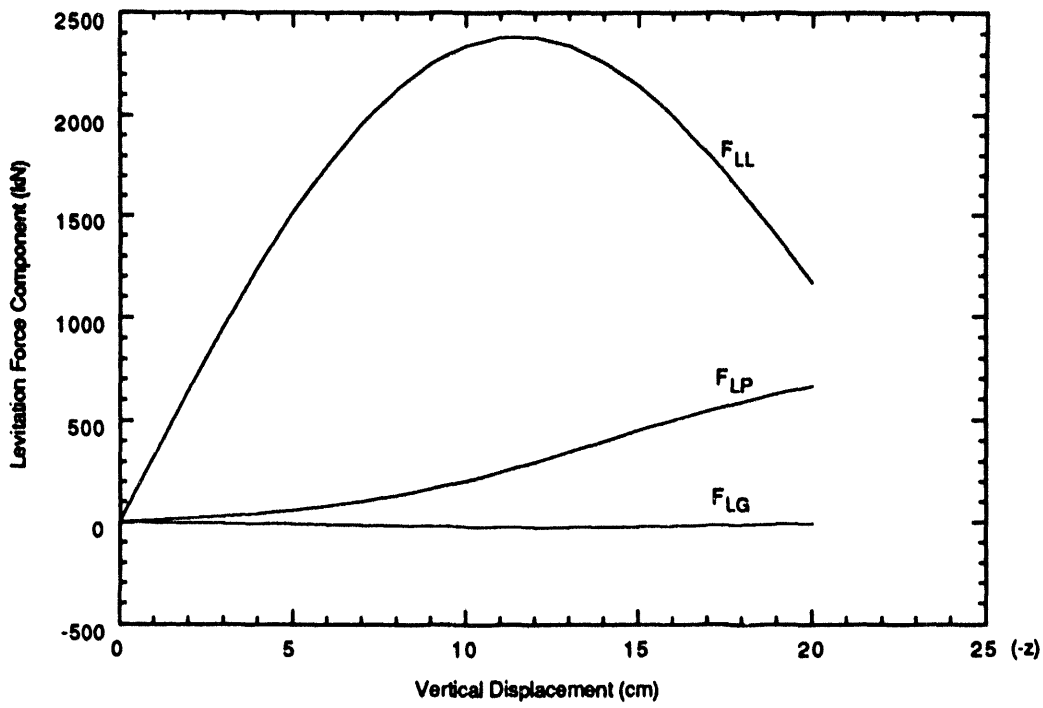

FIGURE 6.9 Levitation Force Components as a Function of Vertical Displacement at a Lateral Displacement of -4 cm

6.5 The Guidance Force

An approach similar to that described in Section 6.4 can be used to determine the guidance force. However, the guidance force depends upon two different air gaps, requiring the introduction of two coordinate systems. By letting y_0 be the equivalent air gap, the distance from the center of the SCM to the center of the figure-eight-shaped coil, one can define $y_1 = y_0 + y$ and $y_2 = y_0 - y$, as shown in Figure 6.4. Therefore, the guidance force can be expressed as:

$$F_G = 3n_m I_s \mathrm{Re}\left\{ I_1 \frac{\partial M_{s1}^*}{\partial y_1} + I_2 \frac{\partial M_{s2}^*}{\partial y_1} + I_3 \frac{\partial M_{s3}^*}{\partial y_2} + I_4 \frac{\partial M_{s4}^*}{\partial y_2} \right\} = F_{GG} + F_{GP} + F_{GL}, \qquad (6.27)$$

where F_{GG} denotes the guidance force resulting from the lateral displacement. This term follows the null-flux principle and is a dominant part of the guidance force. It is given by

$$F_{GG} = \frac{3}{4\sqrt{2}} n_m I_s^2 \left[\frac{(M_{s3} + M_{s4}) - (M_{s1} + M_{s2})}{L_e'} \right] \left[\left(\frac{\partial M_{s1}}{\partial y_1} + \frac{\partial M_{s2}}{\partial y_1} \right) - \left(\frac{\partial M_{s3}}{\partial y_2} + \frac{\partial M_{s4}}{\partial y_2} \right) \right], \qquad (6.28)$$

and F_{GP} is the guidance force component due to the propulsive current,

$$F_{GP} = 3 I_s n_m \frac{V_{ph}\cos\delta - E_{ph}}{4 x_{ph}} \left[\frac{\partial M_{s1}}{\partial y_1} + \frac{\partial M_{s2}}{\partial y_1} + \frac{\partial M_{s3}}{\partial y_2} + \frac{\partial M_{s4}}{\partial y_2} \right]. \qquad (6.29)$$

F_{GP} is an unstable force, according to the data in Figures 6.5, 6.6, 6.10, and 6.11, in which the sum of the mutual inductance derivatives, with respect to lateral displacement, is negative for a negative lateral displacement. This implies that the force is negative for a lagging internal power factor ($V_{ph}\cos\delta > E_{ph}$). In other words, a negative lateral displacement leads to a negative guidance force because the propulsive motors operate in such a way that the vehicle SCMs are attracted by the air gap traveling wave with a load angle δ between 0° to 90°. As the vehicle shifts to one side and the air gap on this side decreases, the attractive force increases naturally, as described by Equation 6.29. The last term of the guidance force results from the vertical displacement. It couples with the null-flux lift and is given by

$$F_{GL} = \frac{3}{2\sqrt{2}} n_m I_s^2 \left\{ \frac{(M_{s2} - M_{s1})}{L_e'} \left(\frac{\partial M_{s1}}{\partial y_1} - \frac{\partial M_{s2}}{\partial y_1} \right) + \frac{(M_{s4} - M_{s3})}{L_e'} \left(\frac{\partial M_{s3}}{\partial y_2} - \frac{\partial M_{s4}}{\partial y_2} \right) \right\}. \qquad (6.30)$$

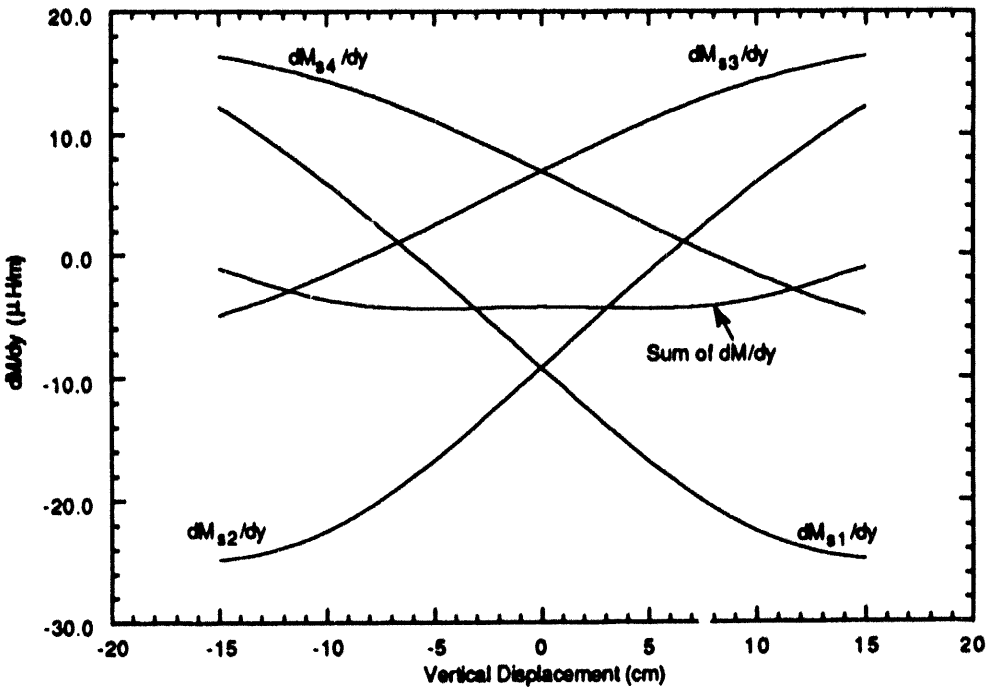

FIGURE 6.10 Derivative of Mutual Inductance with Respect to Lateral Displacement as a Function of Vertical Displacement at a Lateral Displacement of -4 cm

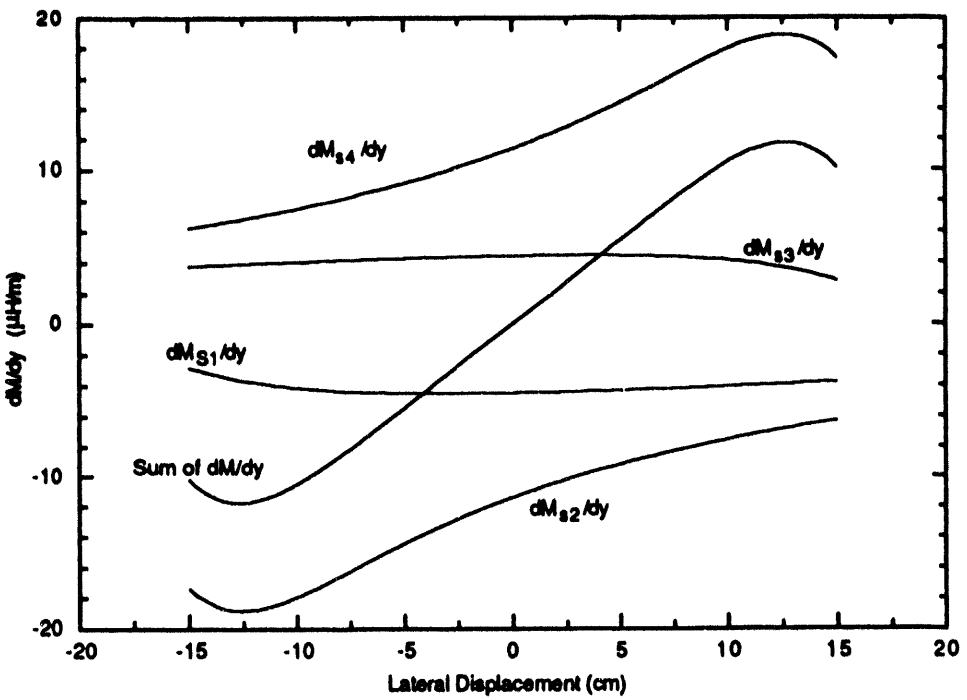

FIGURE 6.11 Derivative of Mutual Inductance with Respect to Lateral Displacement as a Function of Lateral Displacement at a Vertical Displacement of -3 cm

One can better understand Equations 6.28 through 6.30 by examining Figures 6.5, 6.6, 6.10, and 6.11. Figure 6.12 shows guidance force components plotted as a function of lateral displacement. One can see that F_{GP} is an unstable force, but it is negligible when compared with F_{GG} and F_{GL}. The term F_{GG} is dominant, and F_{GL} is relatively small, depending upon vertical displacement. The total guidance force for a vehicle having 40 SCMs ($n_m = 20$) is 159 kN for a 2-cm lateral displacement, 241 kN for a 3-cm lateral displacement, and 326 kN for a 4-cm lateral displacement.

More detailed information concerning the numerical example used above is listed in Table 6.1, which provides some other predicted results, including phase voltage, current, power factor, and block length.

6.6 Conclusions

An analytical model, in combination with a numerical approach, has been developed for a combined maglev system recently proposed in Japan. Closed-form formulas for the propulsive, levitational, and guidance magnetic forces of the system have been discussed. Preliminary results show that such a combined system can perform the three functions of propulsion, levitation, and guidance with one set of figure-eight-shaped guideway coils. The coupling effects among the three functions are small. The system has many potential advantages. Further investigation, including system optimization and computer simulations, is necessary.

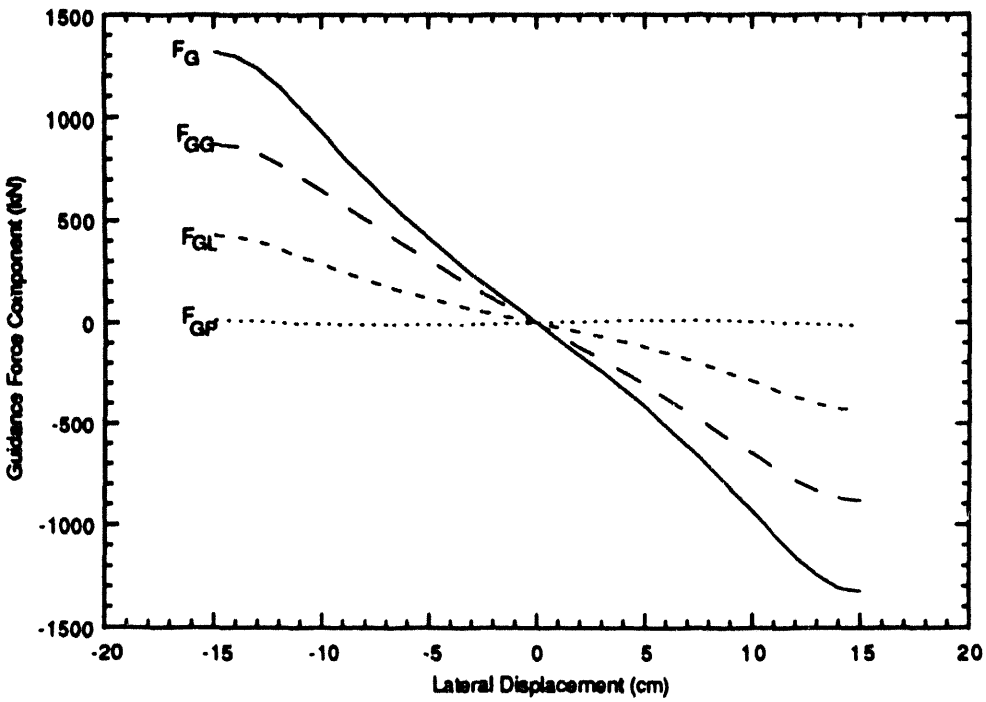

FIGURE 6.12 Guidance Force Components as a Function of Lateral Displacement with a Vertical Displacement of -3 cm

6.7 References

1. Fujiwara, S., and J. Fujie, 1988, "Levitation Propulsion Mechanism for Inductive Repulsion Type Magnetically Levitated Railway," United States Patent No. 4779538, Oct.

2. Fujiwara, S., and T. Fujimoto, 1989, "Characteristics of the Combined Levitation and Guidance System Using Ground Coils on the Side Wall of the Guideway," Proceedings International Conference on Maglev '89, July, pp. 241-244.

3. Fujiwara, S., and T. Fujimoto, 1992, "Characteristics of the Combined Levitation and Guidance TDS Maglev System," Institute of Electrical Engineers of Japan, Tokyo, Vol. 112-D, No. 5, June, pp. 459-466.

4. He, J.L., D.M. Rote, and H.T. Coffey, 1993, "Electrodynamic Forces of the Cross-Connected Figure-Eight-Shaped Null-Flux Coil Suspension System," International Conference on Maglev 93, May, pp. 64-70.

5. He, J.L., and D.M. Rote, 1992, "Computer Model Simulation of Null-Flux Magnetic Suspension and Guidance," Selected Proceedings of the Sixth World Conference on Transport Research, Vol. IV, June 29 - July 3, pp. 3087-3097.

6. He, J.L., D.M. Rote, and H.T. Coffey, 1991, "Computation of Magnetic Suspension of Maglev Systems Using Dynamic Circuit Theory," Proceeding of the International Symposium on Magnetic Suspension Technology, Hampton, Va., Aug. 19-23, NASA Conference Publication 3152, pp. 919-938.

7 Conclusions

The EDS maglev system developed in Japan has been studied in this report on the basis of dynamic circuit theory, with a special focus on magnetic suspension systems. The status of the Japanese EDS maglev system has been reviewed, and several typical versions of the figure-eight-shaped null-flux coil suspension system have been analyzed in detail, by using both transient and steady state versions of the dynamic circuit model.

The investigation has shown that the figure-eight-shaped null-flux suspension system has some important advantages over other suspension systems. In particular, it has a simple configuration, provides zero drag force at vehicle start, and maintains a very high lift-to-drag ratio during normal operation. However, the figure-eight-shaped null-flux coil suspension, without cross-connection, provides relatively little lateral guidance force. Additional guidance can be provided by alternative configurations.

A more advanced form of the figure-eight-shaped null-flux coil suspension system, with side-wall cross connection, was analyzed in Chapter 5. This configuration can provide both null-flux levitation and adequate guidance forces. Closed-form expressions for the magnetic force components were obtained on the basis of a harmonic approximation to the dynamic circuit model. These simple relations are useful for vehicle dynamic-stability studies. Study shows that such a system can provide null-flux guidance at any vertical displacement. The system is currently being tested at the Miyazaki Maglev Test Center, Japan, and is to be installed in a new maglev test track in Yamanashi Prefecture, Japan.

Another important figure-eight-shaped null-flux coil suspension system, which is discussed in Chapter 6, integrates the functions of levitation, propulsion, and guidance into a single set of guideway coils. This system has been studied recently in Japan but has undergone only very limited testing there. For the present study, an analytical model, in combination with a numerical approach, was developed. Closed-form formulas for the propulsion, levitation, and guidance magnetic forces of the system were obtained. Preliminary results show that such an integrated system can perform the combined functions of propulsion, levitation, and guidance with one set of figure-eight-shaped guideway coils. The coupling effects among the three functions are relatively small. The system has some potential advantages and is very promising.

Further investigation of the Japanese EDS maglev system is needed in the following areas: (1) optimum design of the suspension coils (including the selection of the coil pitch, coil width of the ground coils, and the pole pitch of the vehicle coils) to reduce the force pulsation and improve vehicle stability associated with space harmonics; (2) vehicle dynamic stability in connection with the magnetic damping-force; (3) real-time computer model simulations that combine the electromagnetic and electromechanical system equations; and (4) low-speed performance, with the focus on reducing the lift-off speed (now about 170–180 km/h).

Distribution for ANL/ESD-20

Internal

ANL Technical Publications Services
N. Clodi (5)
D. Weeks
B. Putnam
J.L. He (311)

External

U.S. Department of Energy Office of Scientific and Technical Information (2)
Manager, U.S. Department of Energy Chicago Field Office
ANL-E Libraries (2)
ANL-W Library

DATE

FILMED

6/15/94

END